Application of the finite element nodal model to nuclear fuel management

by

Cheng-Chi Wu

A Thesis Submitted to the
Graduate Faculty in Partial Fulfillment of the
Requirements for the Degree of
MASTER OF SCIENCE

Major: Nuclear Engineering

Iowa State University
Ames, Iowa
1983

TABLE OF CONTENTS

		Page
I.	INTRODUCTION	1
II.	THE THEORY OF FINITE ELEMENT NEUTRON DIFFUSION NODAL MODEL	3
	A. The Neutron Diffusion Equation	3
	B. The Determination of the Coefficients	6
	C. Interface Condition	19
	D. Boundary Condition	21
	E. Neutron Source Calculation	22
III.	THE APPLICATION OF FINITE ELEMENT NODAL MODEL FOR NUCLEAR FUEL MANAGEMENT	25
	A. New Group Parameter Calculation	25
	B. Power Density Calculation	30
	C. Burnup Calculation	32
	D. Boron Concentration Calculation	33
IV.	THE CALCULATION PROCEDURE	40
	A. Relaxation Method	40
	B. Convergence Criteria	41
	C. Computer Code and Calculation Procedure	42
V.	RESULTS AND DISCUSSION	45
VI.	CONCLUSION AND FURTHER STUDIES	98
VII.	REFERENCES	100
VIII.	ACKNOWLEDGMENTS	101

LIST OF FIGURES

		Page
Figure 2-1	The flux distribution over each node	5
Figure 2-2	Node geometry for diffusion coefficient evaluation	8
Figure 2-3	Assumption of flux distribution at the interface and at the boundary	20
Figure 3-1	The interpolation technique for calculation of new group parameters	29
Figure 3-2	Critical boron concentration estimation	35
Figure 3-3	Critical boron concentration as function of time after startup	37
Figure 3-4	Search for the end of core life	39
Figure 4-1	Calculation flow chart	43
Figure 5-1	The fuel loading pattern A for one-dimensional model with vacuum boundary condition	46
Figure 5-2	The comparison of the flux distribution at BOC for different convergence criteria	48
Figure 5-3	The comparison of the power distribution at BOC for different convergence criteria	49
Figure 5-4	The comparison (BNODE and DODMG) of the flux distribution at BOC	50
Figure 5-5	The comparison (BNODE and DODMG) of the power distribution at BOC	51
Figure 5-6	The comparison (BNODE and DODMG) of the flux distribution at EOC	52
Figure 5-7	The comparison (BNODE and DODMG) of the power distribution at EOC	53
Figure 5-8	The flux distribution at BOC for the loading pattern A	54
Figure 5-9	The power distribution at BOC for the loading pattern A	55

Figure 5-10	The flux distribution at 100, 200 and 300 days after startup for the loading pattern A	56
Figure 5-11	The power distribution at 100, 200 and 300 days after startup for the loading pattern A	57
Figure 5-12	The burnup distribution for 100, 200 and 300 days after startup for the loading pattern A	58
Figure 5-13	The flux distribution at EOC for the loading pattern A	60
Figure 5-14	The power distribution at EOC for the loading pattern A	61
Figure 5-15	The burnup distribution at EOC for the loading pattern A	62
Figure 5-16	The critical boron concentration after startup for the loading pattern A	63
Figure 5-17	The comparison (D(x) and D = constant) of diffusion coefficient at EOC	65
Figure 5-18	The absorption cross section Σ_{ag} at EOC	66
Figure 5-19	The fission neutron generalation probability $\nu_g \Sigma_{fg}$ at EOC	67
Figure 5-20	The comparison between uniform burnup and nonuniform burnup	68
Figure 5-21	The neutron current distribution at EOC	70
Figure 5-22	The equation balance for fast group neutron	71
Figure 5-23	The equation balance for thermal group neutron	72
Figure 5-24	The convergence of flux	73
Figure 5-25	The convergence of criticality	74
Figure 5-26	The fuel loading pattern B in one-dimensional model with albedo boundary condition	76
Figure 5-27	The flux distribution at BOC for loading pattern B	77
Figure 5-28	The power distribution at BOC for loading pattern B	78

Figure 5-29	The flux distribution at EOC for loading pattern B	79
Figure 5-30	The power distribution at EOC for loading pattern B	80
Figure 5-31	The burnup distribution at EOC for loading pattern B	81
Figure 5-32	Fuel reloading patterns C and D	84
Figure 5-33	The flux distribution at BOSC for reloading pattern C	85
Figure 5-34	The power distribution at BOSC for reloading pattern C	86
Figure 5-35	The burnup distribution at BOSC for reloading pattern C	87
Figure 5-36	The flux distribution at EOSC for reloading pattern C	88
Figure 5-37	The power distribution at EOSC for reloading pattern C	89
Figure 5-38	The burnup distribution at EOSC for reloading pattern C	90
Figure 5-39	The flux distribution at BOSC for reloading pattern D	91
Figure 5-40	The power distribution at BOSC for reloading pattern D	92
Figure 5-41	The burnup distribution at BOSC for reloading pattern D	93
Figure 5-42	The flux distribution at EOSC for reloading pattern D	94
Figure 5-43	The power distribution at EOSC for reloading pattern D	95
Figure 5-44	The burnup distribution at EOSC for reloading pattern D	96

LIST OF TABLES

		Page
Table 3-1	Example of fast neutron group cross section	26
Table 5-1	Neutron fuel data	45
Table 5-2	The multiplication factor K_∞ at EOC for each fuel element	82

I. INTRODUCTION

The prediction of the power and burnup behavior of reactor cores is very important in nuclear fuel management. When a reactor generates power, the fuel composition changes due to burnup. The way that power and burnup change with time must be known in order to assure that the reactor will operate safely throughout the life of the core.

The finite element nodal model [1] has been developed to determine flux distribution in an operating reactor. It has proved to be good method for flux calculations. However, these previous analyses do not involve power and burnup calculations. Therefore, the purpose of this research is to develop and test a one-dimensional nodal model for nuclear fuel management by considering the power and burnup of the reactor core.

In an operating reactor, there are a number of phenomena [2] that give rise to small but significant changes in some group parameters. Thus, the group parameters cannot be assumed constant over a given node. One technique of accounting for these changes is to assume that the group parameters can also be approximated by polynomials over a given node similar to the neutron flux.

The basic idea of the finite element nodal model is to present the neutron flux for a given node in terms of a polynomial. The power density at each location r is proportional to the neutron flux at that location r of a reactor. The burnup at each location r is also proportional to the power density at that location r for time T.

Therefore, the power density and burnup at time T can also be approximated by polynomials over a given node. In order to keep the reactor critical and to simplify the control calculation, chemical shim control is used in this research. With chemical shim, control is accomplished by varying the concentration of boric acid in the coolant throughout the life of the core.

The results from extensive calculations for fuel management were compared to fine mesh finite difference results. All results compared very favorably between the two methods. A large number of variables [2] affect the analytical model of the reactor for nuclear fuel management. In this research, only the variables, e.g. fuel enrichment, power distribution and multiplication factor, were considered in making fuel management.

II. THE THEORY OF FINITE ELEMENT NEUTRON DIFFUSION NODAL MODEL

A. The Neutron Diffusion Equation

The diffusion equation for neutron conservation for an energy group g is given by [3]:

$$-\nabla\cdot D_g(r)\ \nabla\phi_g(r) + \Sigma_{\tau g}(r)\ \phi_g(r) = \sum_{g'=1}^{g-1} \Sigma_{sg'g}(r)\ \phi_{g'}(r)$$

$$+ \frac{1}{K}\chi_g \sum_{g'=1}^{G} \nu_{g'}\Sigma_{fg'}(r)\ \phi_{g'}(r) \qquad (2\text{-}1)$$

where $\phi_g(r)$ = neutron flux at location r in group g,

$D_g(r)$ = neutron diffusion coefficient at location r in group g,

$\Sigma_{\tau g}(r)$ = removal cross section at location r in group g, $\Sigma_{\tau g}(r) = \Sigma_{tg}(r) - \Sigma_{sgg}(r)$,

χ_g = fission spectrum function in group g,

K = the eigenvalue of the diffusion equation,

$\nu_{g'}\Sigma_{fg'}(r)$ = neutrons per fission times fission cross section in group g′ and

$\Sigma_{sg'g}(r)$ = cross section for scattering of neutrons from group g′ to group g.

For one dimension with two neutron groups, the diffusion equation for a given node becomes

$$-\nabla \cdot D_1(x)\ \nabla\phi_1(x) + [\Sigma_{a1}(x) + \Sigma_{R1}(x)]\ \phi_1(x)$$

$$- \frac{1}{K}\ [\nu_1\Sigma_{f1}(x)\ \phi_1(x) + \nu_2\Sigma_{f2}(x)\ \phi_2(x)] = 0 \qquad (2\text{-}2)$$

$$-\nabla \cdot D_2(x)\ \nabla\phi_2(x) + \Sigma_{a2}(x)\ \phi_2(x) - \Sigma_{R1}(x)\ \phi_1(x) = 0 \qquad (2\text{-}3)$$

where $\Sigma_{R1}(x)$ is the group transfer cross section from the fast (group 1) to the thermal (group 2) group. The $\nabla \cdot D(x)\ \nabla\phi(x)$ term is equal to

$$\frac{d}{dx}\ [D(x)\ \frac{d\phi(x)}{dx}] = D(x)\frac{d^2\phi(x)}{dx^2} + \frac{dD(x)}{dx}\ \frac{d\phi(x)}{dx} \qquad (2\text{-}4)$$

Thus, Equation (2-2) and (2-3) become:

$$\frac{d^2\phi_1(x)}{dx^2} + \frac{1}{D_1(x)}\ \frac{dD_1(x)}{dx}\ \frac{d\phi_1(x)}{dx} + \frac{\frac{1}{K}\ \nu_1\Sigma_{f1}(x) - \Sigma_{a1}(x) - \Sigma_{R1}(x)}{D_1(x)}\ \phi_1(x)$$

$$+ \frac{\frac{1}{K}\ \nu_2\Sigma_{f2}(x)}{D_1(x)}\ \phi_2(x) = 0 \qquad (2\text{-}5)$$

$$\frac{d^2\phi_2(x)}{dx^2} + \frac{1}{D_2(x)}\ \frac{dD_2(x)}{dx}\ \frac{d\phi_2(x)}{dx} + \frac{\Sigma_{R1}(x)}{D_2(x)}\ \phi_1(x)$$

$$- \frac{\Sigma_{a2}(x)}{D_2(x)}\ \phi_2(x) = 0 \qquad (2\text{-}6)$$

The neutron flux and group parameters are functions of x and can be approximated by polynomials over a given node (Figure 2-1). For instance, the fluxes in two groups are approximated by

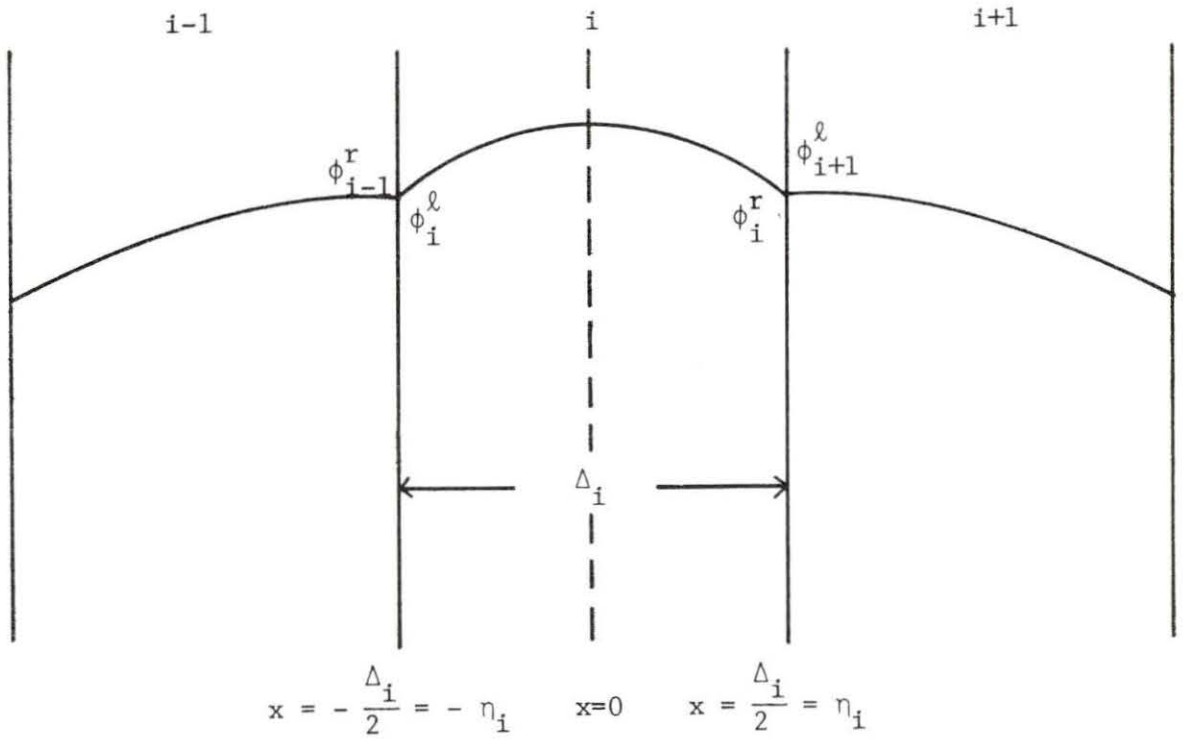

Figure 2-1. The flux distribution over each node

$$\phi_1(x) = a_o + a_1 x + a_2 x^2 + a_3 x^3 + a_4 x^4 \quad \text{fast group} \tag{2-7}$$

$$\phi_2(x) = b_o + b_1 x + b_2 x^2 + b_3 x^3 + b_4 x^4 \quad \text{thermal group} \tag{2-8}$$

Thus, the determination of the coefficients of the polynomials becomes the major concern of this method.

B. The Determination of the Coefficients

Equations (2-5) and (2-6) are rewritten as

$$\frac{d^2\phi_1(x)}{dx^2} + \frac{1}{D_1(x)} \frac{dD_1(x)}{dx} \frac{d\phi_1(x)}{dx} + \alpha_1(x)\ \phi_1(x)$$

$$+ \alpha_2(x)\ \phi_2(x) = 0 \tag{2-9}$$

$$\frac{d^2\phi_2(x)}{dx^2} + \frac{1}{D_2(x)} \frac{dD_2(x)}{dx} \frac{d\phi_2(x)}{dx} + \beta_1(x)\ \phi_1(x)$$

$$+ \beta_2(x)\ \phi_2(x) = 0 \tag{2-10}$$

where

$$\alpha_1(x) \equiv \frac{\frac{1}{K}\nu_1\Sigma_{f1}(x) - \Sigma_{a1}(x) - \Sigma_{R1}(x)}{D_1(x)} \tag{2-11}$$

$$\alpha_2(x) \equiv \frac{\frac{1}{K}\nu_2\Sigma_{f2}(x)}{D_1(x)} \tag{2-12}$$

$$\beta_1(x) \equiv \frac{\Sigma_{R1}(x)}{D_2(x)} \tag{2-13}$$

$$\beta_2(x) \equiv - \frac{\Sigma_{a2}(x)}{D_2(x)} \tag{2-14}$$

The fast neutron diffusion coefficient $D_1(x)$ over a given node can also be approximated by

$$D_1(x) = d_o + d_1 x + d_2 x^2 + d_3 x^3 + d_4 x^4 \tag{2-15}$$

The polynomial in Equation (2-15) has five unknown d_o, d_1, d_2, d_3 and d_4. Therefore, five conditions are needed to define these coefficients. These five conditions are defined as follows:

1. Evaluate $D_1(x)$ at three points, the left, center and right of a given node (Figure 2-2) as

$$D_1^{\ell} \equiv D_1(-\eta) = d_o - d_1\eta + d_2\eta^2 - d_3\eta^3 + d_4\eta^4 \tag{2-16}$$

$$D_1^{o} \equiv D_1(o) = d_o \tag{2-17}$$

$$D_1^{r} \equiv D_1(\eta) = d_o + d_1\eta + d_2\eta^2 + d_3\eta^3 + d_4\eta^4 \tag{2-18}$$

2. Evaluate the average D(x) at the left half side and the right half side of a given node as

$$\begin{aligned} D_1^{-} &\equiv \frac{1}{\eta} \int_{-\eta}^{o} (d_o + d_1 x + d_2 x^2 + d_3 x^3 + d_4 x^4)\, dx \\ &= \frac{1}{\eta} \left(d_o x + d_1 \frac{x^2}{2} + d_2 \frac{x^3}{3} + d_3 \frac{x^4}{4} + d_4 \frac{x^5}{5}\right)\Big|_{-\eta}^{o} \\ &= d_o - \frac{\eta}{2} d_1 + \frac{\eta^2}{3} d_2 - \frac{\eta^3}{4} d_3 + \frac{\eta^4}{5} d_4 \end{aligned} \tag{2-19}$$

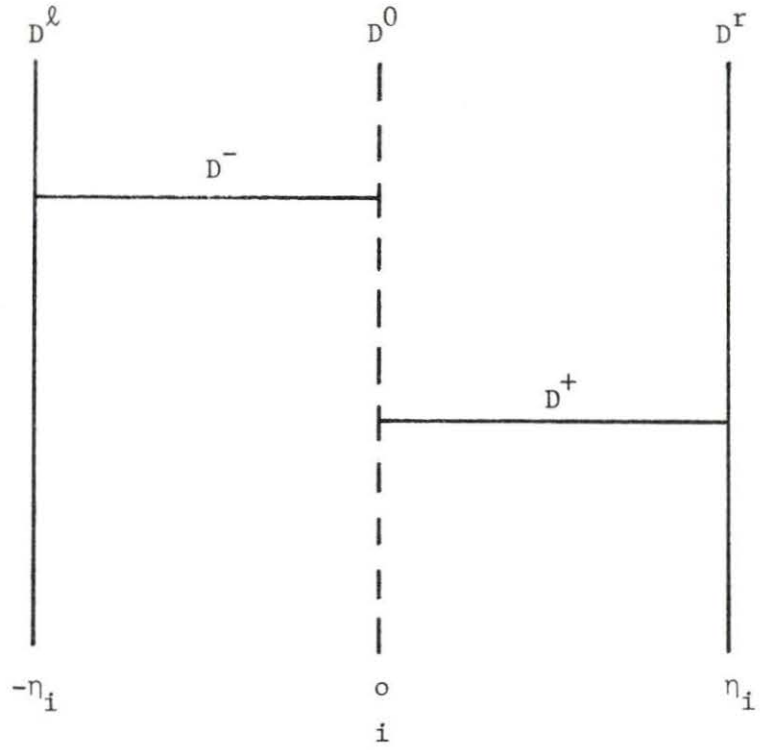

Figure 2-2. Node geometry for diffusion coefficient evaluation

$$D_1^{+} \equiv \frac{1}{\eta} \int_o^{\eta} (d_o + d_1 x + d_2 x^2 + d_3 x^3 + d_4 x^4)\, dx$$

$$= d_o + \frac{\eta}{2} d_1 + \frac{\eta^2}{3} d_2 + \frac{\eta^3}{4} d_3 + \frac{\eta^4}{5} d_4 \qquad (2\text{-}20)$$

3. The values of $D_1(x)$ at the above five conditions are known. Thus, the coefficients d_o through d_4 can be obtained by solving the simultaneous Equations (2-16) through (2-20). The results are written as follows:

$$d_o = D_1^{o} \qquad (2\text{-}21)$$

$$d_1 = \frac{1}{\eta} [2(D_1^{+} - D_1^{-}) - \frac{1}{2}(D_1^{r} - D_1^{\ell})] \qquad (2\text{-}22)$$

$$d_2 = \frac{3}{4\eta^2} [5(D_1^{+} + D_1^{-}) - (D_1^{r} + D_1^{\ell}) - 8\, D_1^{o}] \qquad (2\text{-}23)$$

$$d_3 = \frac{2}{\eta^3} [\frac{1}{2} (D_1^{r} - D_1^{\ell}) - (D_1^{+} - D_1^{-})] \qquad (2\text{-}24)$$

$$d_4 = \frac{5}{4\eta^4} [(D_1^{r} + D_1^{\ell}) - 3(D_1^{+} + D_1^{-}) + 4\, D_1^{o}] \qquad (2\text{-}25)$$

The same procedure for $D_1(x)$ is also applied to the other group parameters, $\Sigma_a(x)$, $\Sigma_R(x)$ and $\nu\Sigma_f(x)$. Thus, results similar to Equations (2-16) through (2-25) for the other group parameters can be obtained. Using the definition of $\alpha(x)$ and the above results, one can evaluate the $\alpha(x)$ at the five conditions.

$$\alpha_1^{\ell} = \frac{\frac{1}{K}\nu_1\Sigma_{f1}^{\ell} - \Sigma_{a1}^{\ell} - \Sigma_{R1}^{\ell}}{D_1^{\ell}} \tag{2-26}$$

$$\alpha_1^{o} = \frac{\frac{1}{K}\nu_1\Sigma_{f1}^{o} - \Sigma_{a1}^{o} - \Sigma_{R1}^{o}}{D_1^{o}} \tag{2-27}$$

$$\alpha_1^{r} = \frac{\frac{1}{K}\nu_1\Sigma_{f1}^{r} - \Sigma_{a1}^{r} - \Sigma_{R1}^{r}}{D_1^{r}} \tag{2-28}$$

$$\alpha_1^{-} = \frac{\frac{1}{K}\nu_1\Sigma_{f1}^{-} - \Sigma_{a1}^{-} - \Sigma_{R1}^{-}}{D_1^{-}} \tag{2-29}$$

$$\alpha_1^{+} = \frac{\frac{1}{K}\nu_1\Sigma_{f1}^{+} - \Sigma_{a1}^{+} - \Sigma_{R1}^{+}}{D_1^{+}} \tag{2-30}$$

$$\alpha_2^{\ell} = \frac{\frac{1}{K}\nu_2\Sigma_{f2}^{\ell}}{D_1^{\ell}} \tag{2-31}$$

$$\alpha_2^{o} = \frac{\frac{1}{K}\nu_2\Sigma_{f2}^{o}}{D_1^{o}} \tag{2-32}$$

$$\alpha_2^{r} = \frac{\frac{1}{K}\nu_2\Sigma_{f2}^{r}}{D_1^{r}} \tag{2-33}$$

$$\alpha_2^- = \frac{\frac{1}{K}\nu_2\Sigma_{f2}^-}{D_1^-} \tag{2-34}$$

$$\alpha_2^+ = \frac{\frac{1}{K}\nu_2\Sigma_{f2}^+}{D_1^+} \tag{2-35}$$

The first derivative of $D_1(x)$ is

$$\frac{dD_1(x)}{dx} = d_1 + 2\,d_2x + 3\,d_3x^2 + 4\,d_4x^3 \tag{2-36}$$

Using Equations (2-21) through (2-25), the following results can be obtained:

$$\frac{dD_1^{\ell}}{dx} \equiv \frac{dD_1(x)}{dx}\Big|_{x=-\eta} = d_1 - 2\,d_2\eta + 3\,d_3\eta^2 - 4\,d_4\eta^3$$

$$= \frac{1}{\eta}\left[-(D_1^r + 6\,D_1^{\ell})\right.$$

$$\left. + \frac{1}{2}(7\,D_1^+ + 23\,D_1^-) - 8\,D_1^o\right] \tag{2-37}$$

$$\frac{dD_1^o}{dx} \equiv \frac{dD_1(x)}{dx}\Big|_{x=0} = d_1$$

$$= \frac{1}{\eta}\left[2(D_1^+ - D_1^-) - \frac{1}{2}(D_1^r - D_1^{\ell})\right] \tag{2-38}$$

$$\frac{dD_1^{\,r}}{dx} \equiv \frac{dD_1(x)}{dx}\Big|_{x=\eta} = d_1 + 2\,d_2\eta + 3\,d_3\eta^2 + 4\,d_4\eta^3$$

$$= \frac{1}{\eta}\left[-\frac{1}{2}\,(23\,D_1^{\,+} + 7\,D_1^{\,-})\right.$$

$$\left. + (6\,D_1^{\,r} + D_1^{\,\ell}) + 8\,D_1^{\,o}\right] \qquad (2\text{-}39)$$

$$\frac{dD_1^{\,-}}{dx} \equiv \frac{1}{\eta}\int_{-\eta}^{o} \frac{dD_1(x)}{dx}\,dx$$

$$= \frac{1}{\eta}\int_{-\eta}^{o} (d_1 + 2\,d_2x + 3\,d_3x^2 + 4\,d_4x^3)\,dx$$

$$= d_1 - d_2\eta + d_3\eta^2 - d_4\eta^3$$

$$= \frac{1}{\eta}\,(D_1^{\,o} - D_1^{\,\ell}) \qquad (2\text{-}40)$$

$$\frac{dD_1^{\,+}}{dx} \equiv \frac{1}{\eta}\int_{o}^{\eta} \frac{dD_1(x)}{dx}\,dx$$

$$= \frac{1}{\eta}\int_{o}^{\eta} (d_1 + 2\,d_2x + 3\,d_3x^2 + 4\,d_4x^3)\,dx$$

$$= d_1 + d_2\eta + d_3\eta^3 + d_4\eta^3$$

$$= \frac{1}{\eta}\,(D_1^{\,r} - D_1^{\,o}) \qquad (2\text{-}41)$$

The first derivative of $\phi_1(x)$ is

$$\frac{d\phi_1(x)}{dx} = a_1 + 2\,a_2x + 3\,a_3x^2 + 4\,a_4x^3 \tag{2-42}$$

Applying the same procedure as D(x) to $\phi_1(x)$, the following results can also be obtained:

$$\frac{d\phi_1{}^{\ell}}{dx} \equiv \frac{d\phi_1(x)}{dx}\Big|_{x=-\eta} = \frac{1}{\eta}\left[-(\phi_1{}^{r} + 6\,\phi_1{}^{\ell}) + \frac{1}{2}(7\,\phi_1{}^{+} + 23\,\phi_1{}^{-}) - 8\,\phi_1{}^{o}\right] \tag{2-43}$$

$$\frac{d\phi_1{}^{o}}{dx} \equiv \frac{d\phi_1(x)}{dx}\Big|_{x=0} = \frac{1}{\eta}\left[2(\phi_1{}^{+} - \phi_1{}^{-}) - \frac{1}{2}(\phi_1{}^{r} - \phi_1{}^{\ell})\right] \tag{2-44}$$

$$\frac{d\phi_1{}^{r}}{dx} \equiv \frac{d\phi_1(x)}{dx}\Big|_{x=\eta} = \frac{1}{\eta}\left[-\frac{1}{2}(23\,\phi_1{}^{+} + 7\,\phi_1{}^{-}) + (6\,\phi_1{}^{r} + \phi_1{}^{\ell}) + 8\,\phi_1{}^{o}\right] \tag{2-45}$$

$$\frac{d\phi_1{}^{-}}{dx} \equiv \frac{1}{\eta}\int_{-\eta}^{o} \frac{d\phi_1(x)}{dx}\,dx = \frac{1}{\eta}(\phi_1{}^{o} - \phi_1{}^{\ell}) \tag{2-46}$$

$$\frac{d\phi_1{}^{+}}{dx} \equiv \frac{1}{\eta}\int_{o}^{\eta} \frac{d\phi_1(x)}{dx}\,dx = \frac{1}{\eta}(\phi_1{}^{r} - \phi_1{}^{o}) \tag{2-47}$$

where

$$\phi_1^{\ell} \equiv \phi_1(-\eta) = a_o - a_1\eta + a_2\eta^2 - a_3\eta^3 + a_4\eta^4 \tag{2-48}$$

$$\phi_1^{o} \equiv \phi_1(o) = a_o \tag{2-49}$$

$$\phi_1^{r} \equiv \phi_1(\eta) = a_o + a_1\eta + a_2\eta^2 + a_3\eta^3 + a_4\eta^4 \tag{2-50}$$

$$\phi_1^{-} \equiv \frac{1}{\eta}\int_{-\eta}^{o} \phi_1(x)\, dx$$

$$= a_o - \frac{\eta}{2} a_1 + \frac{\eta^2}{3} a_2 - \frac{\eta^3}{4} a_3 + \frac{\eta^4}{5} a_4 \tag{2-51}$$

$$\phi_1^{+} \equiv \frac{1}{\eta}\int_{o}^{\eta} \phi_1(x)\, dx$$

$$= a_o + \frac{\eta}{2} a_1 + \frac{\eta^2}{3} a_2 + \frac{\eta^3}{4} a_3 + \frac{\eta^4}{5} a_4 \tag{2-52}$$

Define the function $r_1(x)$ as

$$r_1(x) = \frac{1}{D_1(x)} \frac{dD_1(x)}{dx} \frac{d\phi_1(x)}{dx} + \alpha_1(x)\ \phi_1(x) \tag{2-53}$$

$$+ \alpha_2(x)\ \phi_2(x)$$

Thus, $r_1(x)$ can be evaluated by using Equations (2-7), (2-8), (2-11), (2-12), (2-15), (2-36) and (2-42). In order to keep the function $r_1(x)$ also as a fourth order polynomial, let

$$r_1(x) = C_o + C_1 x + C_2 x^2 + C_3 x^3 + C_4 x^4 \tag{2-54}$$

Applying the same procedure as $D_1(x)$, the coefficients C_o through C_4 can be evaluated as

$$C_o = r_1^{\,o} \tag{2-55}$$

$$C_1 = \frac{1}{\eta}\left[2(r_1^{\,+} - r_1^{\,-}) - \frac{1}{2}(r_1^{\,r} - r_1^{\,\ell})\right] \tag{2-56}$$

$$C_2 = \frac{3}{4\eta^2}\left[5(r_1^{\,+} + r_1^{\,-}) - (r_1^{\,r} + r_1^{\,\ell}) - 8\, r_1^{\,o}\right] \tag{2-57}$$

$$C_3 = \frac{2}{\eta^3}\left[\frac{1}{2}(r_1^{\,r} - r_1^{\,\ell}) - (r_1^{\,+} - r_1^{\,-})\right] \tag{2-58}$$

$$C_4 = \frac{5}{4\eta^4}\left[(r_1^{\,r} + r_1^{\,\ell}) - 3(r_1^{\,+} + r_1^{\,-}) + 4\, r_1^{\,o}\right] \tag{2-59}$$

where

$$r_1^{\,\ell} = \frac{1}{D_1^{\,\ell}} \frac{dD_1^{\,\ell}}{dx} \frac{d\phi_1^{\,\ell}}{dx} + \alpha_1^{\,\ell}\, \phi_1^{\,\ell} + \alpha_2^{\,\ell} \phi_2^{\,\ell} \tag{2-60}$$

$$r_1^{\,o} = \frac{1}{D_1^{\,o}} \frac{dD_1^{\,o}}{dx} \frac{d\phi_1^{\,o}}{dx} + \alpha_1^{\,o}\, \phi_1^{\,o} + \alpha_1^{\,o}\, \phi_2^{\,o} \tag{2-61}$$

$$r_1^{\,r} = \frac{1}{D_1^{\,r}} \frac{dD_1^{\,r}}{dx} \frac{d\phi_1^{\,r}}{dx} + \alpha_1^{\,r}\, \phi_1^{\,r} + \alpha_2^{\,r}\, \phi_2^{\,r} \tag{2-62}$$

$$r_1^{\,-} = \frac{1}{D_1^{\,-}} \frac{dD_1^{\,-}}{dx} \frac{d\phi_1^{\,-}}{dx} + \alpha_1^{\,-}\, \phi_1^{\,-} + \alpha_2^{\,-}\, \phi_2^{\,-} \tag{2-63}$$

$$r_1^+ = \frac{1}{D_1^+} \frac{dD_1^+}{dx} \frac{d\phi_1^+}{dx} + \alpha_1^+ \phi_1^+ + \alpha_2^+ \phi_2^+ \qquad (2\text{-}64)$$

Using Equations (2-53) and (2-54), Equation (2-9) becomes

$$\frac{d^2\phi_1(x)}{dx^2} + C_o + C_1 x + C_2 x^2 + C_3 x^3 + C_4 x^4 = 0 \qquad (2\text{-}65)$$

The coefficients C_o through C_4 are still unknown unless the coefficients of $\phi_1(x)$ are known.

Assume that the fluxes at the left and right of a given node for the fast group, ϕ_1^r and ϕ_1^ℓ, are known. Thus, the coefficients a_o and a_1 can be solved from Equation (2-48) and Equation (2-50) as

$$a_o = \frac{\phi_1^r + \phi_1^\ell}{2} - a_2\eta^2 - a_4\eta^4 \qquad (2\text{-}66)$$

$$a_1 = \frac{\phi_1^r - \phi_1^\ell}{2\eta} - a_3\eta^2 \qquad (2\text{-}67)$$

But a_2, a_3 and a_4 are still unknown. Therefore, other assumptions and techniques are needed.

The second derivative of Equation (2-7) is

$$\frac{d^2\phi_1(x)}{dx^2} = 2\,a_2 + 6\,a_3 x + 12\,a_4 x^2 \qquad (2\text{-}68)$$

Substitute Equation (2-68) into Equation (2-65). Equation (2-65) becomes equal to $g_1(x)$ instead of zero because Equations (2-7) and (2-54) are only approximations.

$$2\,a_2 + 6\,a_3x + 12\,a_4x^2 + \bar{C}_o + \bar{C}_1x + \bar{C}_2x^2 + \bar{C}_3x^3 + \bar{C}_4x^4 = g_1(x) \tag{2-69}$$

The coefficients $\bar{C}_o$ through $\bar{C}_4$ are assumed known from a previous iteration and independent of a_2, a_3 and a_4.

In order to determine the coefficients a_2, a_3 and a_4, the least-square approximation [4] is used, defined

$$E(a_2, a_3, a_4) \equiv \int_{-\eta}^{\eta} g_1^2(x)dx$$

The method is to find the coefficients a_2, a_3 and a_4 such that E is minimum. A necessary condition for E to be minimum is

$$\frac{\partial E}{\partial a_i} = 0 \qquad \text{for } i = 2, 3, 4 \tag{2-70}$$

Using Leibnitz's rule, one can equate Equation (2-70)

$$\frac{\partial}{\partial a_2} \int_{-\eta}^{\eta} g_1^2(x)dx = 2 \int_{-\eta}^{\eta} g_1(x) \frac{\partial g_1(x)}{\partial a_2} dx = 0 \tag{2-71}$$

$$\frac{\partial}{\partial a_3} \int_{-\eta}^{\eta} g_1^2(x)dx = 2 \int_{-\eta}^{\eta} g_1(x) \frac{\partial g_1(x)}{\partial a_3} dx = 0 \tag{2-72}$$

$$\frac{\partial}{\partial a_4} \int_{-\eta}^{\eta} g_1^2(x)dx = 2 \int_{-\eta}^{\eta} g_1(x) \frac{\partial g_1(x)}{\partial a_4} dx = 0 \tag{2-73}$$

From Equations (2-71) to (2-73), the coefficients a_2, a_3 and a_4 can be found.

$$a_2 = -\frac{1}{2}\bar{C}_o + \frac{3}{70}\bar{C}_4\eta^4 \tag{2-74}$$

$$a_3 = -\frac{1}{6}\bar{C}_1 - \frac{1}{10}\bar{C}_3\eta^2 \tag{2-75}$$

$$a_4 = -\frac{1}{12}\bar{C}_2 - \frac{1}{14}\bar{C}_4\eta^2 \tag{2-76}$$

where the terms on the right-hand side are also known from a previous iteration.

Define the function $r_2(x)$ as

$$r_2(x) \equiv \frac{1}{D_2(x)}\frac{dD_2(x)}{dx}\frac{d\phi_2(x)}{dx} + \beta_1(x)\,\phi_1(x) + \beta_2(x)\,\phi_2(x) \tag{2-77}$$

In order to keep the function $r_2(x)$ also as a fourth order polynomial, let

$$r_2(x) = C_o' + C_1'x + C_2'x^2 + C_3'x^3 + C_4'x^4 \tag{2-78}$$

Applying the same procedure as for $\phi_1(x)$, the coefficients of the thermal group flux $\phi_2(x)$ can be found.

$$b_o = \frac{\phi_2^{\,r} + \phi_2^{\,\ell}}{2} - b_2\eta^2 - b_4\eta^4 \tag{2-79}$$

$$b_1 = \frac{\phi_2^{\,r} - \phi_2^{\,\ell}}{2\eta} - b_3\eta^2 \tag{2-80}$$

$$b_2 = -\frac{1}{2} C_o' + \frac{3}{70} C_4' \eta^4 \tag{2-81}$$

$$b_3 = -\frac{1}{6} C_1' - \frac{1}{10} C_3' \eta^2 \tag{2-82}$$

$$b_4 = -\frac{1}{12} C_2' - \frac{1}{14} C_4' \eta^2 \tag{2-83}$$

Now the flux distribution over each node can be obtained by inserting these coefficients into Equations (2-7) and (2-8).

C. Interface Condition

The interface diffusion theory boundary conditions between two nodes (Figure 2-3) are the continuity of flux and current density across the interface [3]:

$$\phi_i^r = \phi_{i+1}^\ell \tag{2-84}$$

$$-D_i^r \left(\frac{d\phi_i^r}{dx}\right) = -D_{i+1}^\ell \left(\frac{d\phi_{i+1}^\ell}{dx}\right) \tag{2-85}$$

The first derivative of flux distribution at the interface between node i and node i+1 is

$$\frac{d\phi_i^r}{dx}\Big|_{x=\eta_i} = a_1 + 2\,a_2 x + 3\,a_3 x^2 + 4\,a_4 x^3\Big|_{x=\eta_i} \tag{2-86}$$

where the coefficients a_1 through a_4 were evaluated for node i.

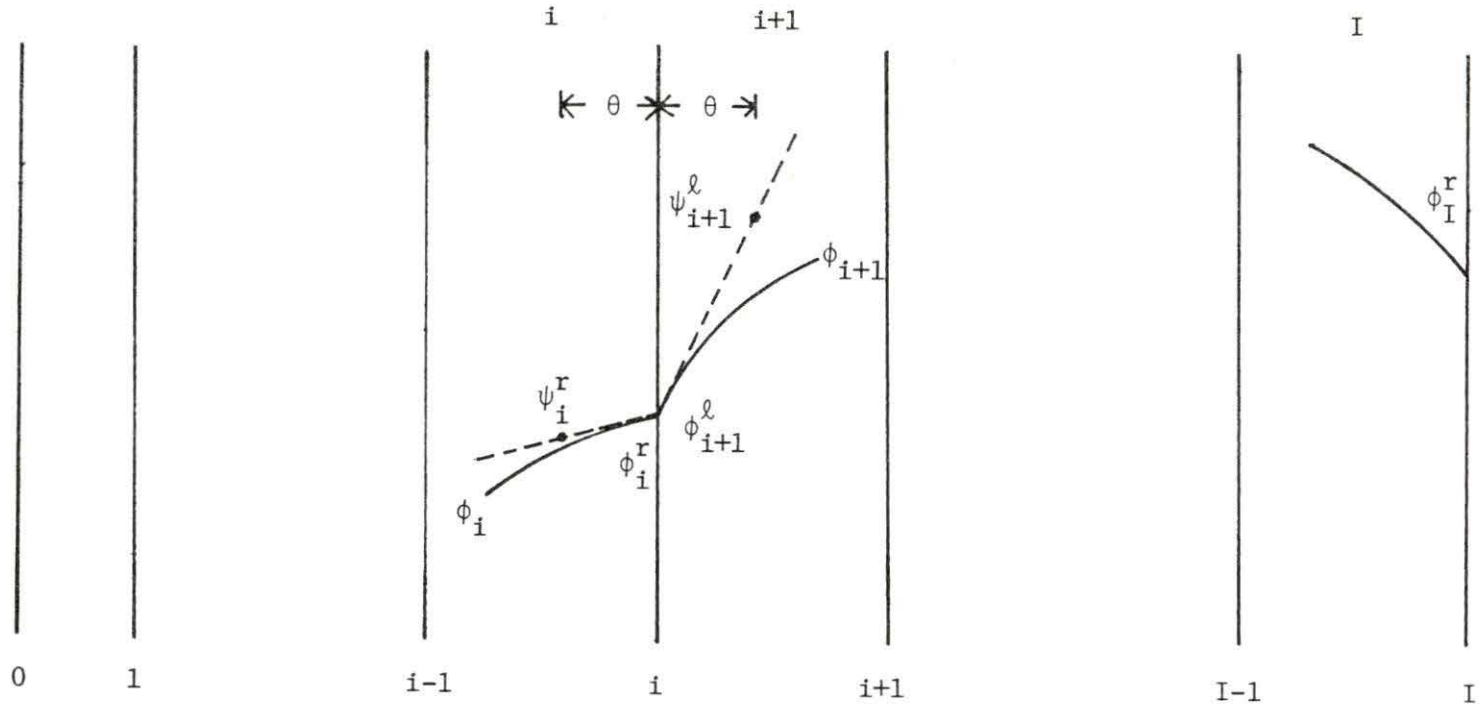

Figure 2-3. Assumption of flux distribution at the interface and at the boundary

$$\left.\frac{d\phi_{i+1}^{\ell}}{dx}\right|_{x=-\eta_{i+1}} = a_1 + 2\,a_2 x + 3\,a_3 x^2 + 4\,a_4 x^3 \Big|_{x=-\eta_{i+1}} \tag{2-87}$$

where the coefficients a_1 through a_4 were evaluated for node i+1.

In order to estimate new interface fluxes, two fictitious parameter ψ_i^r and ψ_{i+1}^{ℓ} are defined such that they satisfy the following finite difference equations at any interface:

$$\frac{\phi_i^r - \psi_i^r}{\theta} = \left.\frac{d\phi_i^r}{dx}\right|_{x=\eta_i} \tag{2-88}$$

$$\frac{\psi_{i+1}^{\ell} - \phi_{i+1}^{\ell}}{\theta} = \left.\frac{d\phi_{i+1}^{\ell}}{dx}\right|_{x=-\eta_{i+1}} \tag{2-89}$$

where θ is an arbitrarily chosen distance factor. Substitute Equations (2-88), (2-89) and (2-84) into Equation (2-85) and solve for the flux at the interface as

$$\phi_i^r = \phi_{i+1}^{\ell} = \frac{D_i^r\,\psi_i^r + D_{i+1}^{\ell}\,\psi_{i+1}^{\ell}}{D_i^r + D_{i+1}^{\ell}} \tag{2-90}$$

where ψ_i^r and ψ_{i+1}^{ℓ} are found from the previous iteration by using Equations (2-88) and (2-89).

D. Boundary Condition

The homogeneous boundary condition for the boundary node I (Figure 2-3) can be written as [5]

$$D_I^r \frac{d\phi_I^r}{dx}\Big|_{x=\eta_I} = -\tau\phi_I^r\Big|_{x=\eta_I} \tag{2-91}$$

Thus, ϕ_I^r becomes

$$\phi_I^r = -\frac{D_I^r}{\tau}\frac{d\phi_I^r}{dx}\Big|_{x=\eta_I}$$

$$= -\frac{D_I^r}{\tau}(a_1 + 2\,a_2x + 3\,a_3x^2 + 4\,a_4x^3)\Big|_{x=\eta_I} \tag{2-92}$$

where the coefficients a_1 through a_4 were evaluated for node I.

If the outer boundary is a free surface, the vacuum boundary condition can be used. For this case, τ can be expressed as

$$\tau = \frac{1}{3(0.7104)} \tag{2-93}$$

If the outer boundary is not a free surface, the albedo boundary condition can be used. For this case, τ can be expressed as

$$\tau = \frac{1}{3(0.7104)}\left(\frac{1-\alpha}{1+\alpha}\right) \tag{2-94}$$

where α is the ratio between the current out of the reflecting region to the current into the reflecting region:

$$\alpha = \frac{J_{out}}{J_{in}} \tag{2-95}$$

E. Neutron Source Calculation

For a one dimensional steady-state condition with two neutron groups, the neutron source over each node can be written as

$$S(x) = \nu_1 \Sigma_{f1}(x)\ \phi_1(x) + \nu_2 \Sigma_{f2}(x)\ \phi_2(x) \tag{2-96}$$

S(x) is also approximated by a fourth order polynomial as

$$S(x) = s_o + s_1 x + s_2 x^2 + s_3 x^3 + s_4 x^4 \tag{2-97}$$

Applying the same procedure as for $D_1(x)$, the coefficients s_o through s_4 can be obtained as

$$s_o = S^o \tag{2-98}$$

$$s_1 = \frac{1}{\eta}\left[2(S^+ - S^-) - \frac{1}{2}(S^r - S^\ell)\right] \tag{2-99}$$

$$s_2 = \frac{3}{4\eta^2}\left[5(S^+ + S^-) - (S^r + S^\ell) - 8\ S^o\right] \tag{2-100}$$

$$s_3 = \frac{2}{\eta^3}\left[\frac{1}{2}(S^r - S^\ell) - (S^+ - S^-)\right] \tag{2-101}$$

$$s_4 = \frac{5}{4\eta^4}\left[(S^r + S^\ell) - 3(S^+ + S^-) + 4\ S^o\right] \tag{2-102}$$

where

$$S^\ell \equiv S(-\eta) = \nu_1 \Sigma_{f1}^\ell \phi_1^\ell + \nu_2 \Sigma_{f2}^\ell \phi_2^\ell \tag{2-103}$$

$$S^o \equiv S(o) = \nu_1 \Sigma_{f1}^o \phi_1^o + \nu_2 \Sigma_{f2}^o \phi_2^o \tag{2-104}$$

$$S^r \equiv S(\eta) = \nu_1 \Sigma_{f1}^r \phi_1^r + \nu_2 \Sigma_{f2}^r \phi_2^r \tag{2-105}$$

$$S^- \equiv \frac{1}{\eta} \int_{-\eta}^{o} S(x)dx = \nu_1 \Sigma_{f1}^- \phi_1^- + \nu_2 \Sigma_{f2}^- \phi_2^- \tag{2-106}$$

$$S^+ \equiv \frac{1}{\eta} \int_{o}^{\eta} S(x)dx = \nu_1 \Sigma_{f1}^+ \phi_1^+ + \nu_2 \Sigma_{f2}^+ \phi_2^+ \tag{2-107}$$

The average source over a given node is

$$\bar{S} \equiv \frac{1}{2\eta} \int_{-\eta}^{\eta} S(x)dx$$

$$= \frac{1}{2\eta} \int_{-\eta}^{\eta} (s_o + s_1 x + s_2 x^2 + s_3 x^3 + s_4 x^4)dx$$

$$= s_o + \frac{s_2}{3} \eta^2 + \frac{s_4}{5} \eta^4$$

$$= \frac{1}{2} (S^+ + S^-) \tag{2-108}$$

Thus, the source over all the nodes becomes

$$S_{total} = \frac{\sum_{i=1}^{I} \bar{S}_i V_i}{\sum_{i=1}^{I} V_i} \tag{2-109}$$

where V_i is a volume of node i.

III. THE APPLICATION OF FINITE ELEMENT NODAL MODEL FOR NUCLEAR FUEL MANAGEMENT

A. New Group Parameter Calculation

In this research, the group parameters with boron concentration (0 and 1200 PPM) and burnup (13 steps from 0 to 45,000 WD/g) are tabulated functions taken from a calculated cross-section set [6]. For one type of LWR fuel, the group parameters of one neutron group are briefly shown in Table 3-1. Assume the group parameters of burnup in any burnup interval to be linear functions of burnup over the limited range in the group parameters. Thus, using an interpolation technique, the group parameters N_B of burnup B in any burnup interval B_I and B_{I+1} can be evaluated as follows (Figure 3-1):

$$\frac{N_{I+1} - N_I}{B_{I+1} - B_I} = \frac{N_{I+1} - N_B}{B_{I+1} - B}$$

where N_{I+1} = the known group parameters of burnup B_{I+1} and

N_I = the known group parameters of burnup B_I.

Therefore, N_B becomes

$$N_B = N_{I+1} + \frac{(N_{I+1} - N_I)(B - B_{I+1})}{B_{I+1} - B_I} \qquad (3\text{-}1)$$

Also assume that the relationship of the group parameters and boron concentration is linear between 0 and 1200 PPM. Using the same interpolation technique, the group parameters N_{PPM} of boron concentration PPM can be obtained as:

Table 3-1. Example of fast neutron group cross section

BORON CONCENTRATION (PPM)			Burnup step (WD/g) 0	150	500	2500	5000
		Σ_{a1}	9.1835×10^{-3}	9.1835×10^{-3}	9.1700×10^{-3}	9.1770×10^{-3}	9.2544×10^{-3}
		$K\Sigma_{f1}$	6.7497×10^{-14}	6.7497×10^{-14}	6.7256×10^{-14}	6.5611×10^{-14}	6.3455×10^{-14}
	0	$\nu\Sigma_{f1}$	5.3524×10^{-3}	5.3524×10^{-3}	5.3404×10^{-3}	5.2464×10^{-3}	5.1137×10^{-3}
		Σ_{R1}	1.7468×10^{-2}	1.7468×10^{-2}	1.7471×10^{-2}	1.7410×10^{-2}	1.7279×10^{-2}
		D_1	1.2605	1.2605	1.2607	1.2613	1.2626
		Σ_{a1}	9.4204×10^{-3}	9.4204×10^{-3}	9.4090×10^{-3}	9.4306×10^{-3}	9.5224×10^{-3}
		$K\Sigma_{f1}$	6.7386×10^{-14}	6.7386×10^{-14}	6.7187×10^{-14}	6.5748×10^{-14}	6.3848×10^{-14}
	1200	$\nu\Sigma_{f1}$	5.3441×10^{-3}	5.3441×10^{-3}	5.3358×10^{-3}	5.2593×10^{-3}	5.1478×10^{-3}
		Σ_{R1}	1.7263×10^{-2}	1.7263×10^{-2}	1.7263×10^{-2}	1.7189×10^{-2}	1.7044×10^{-2}
		D_1	1.2744	1.2744	1.2745	1.2747	1.2757

Table 3-1. (Continued)

Boron Concentration (ppm)			Burnup step (WD/g) 10,000	15,000	20,000	25,000	30,000
		Σ_{a1}	9.4312×10^{-3}	9.6134×10^{-3}	9.8023×10^{-3}	9.9744×10^{-3}	1.0124×10^{-2}
		$K\Sigma_{f1}$	5.9457×10^{-14}	5.5780×10^{-14}	5.2356×10^{-14}	4.9383×10^{-14}	4.6891×10^{-14}
	0	$\nu\Sigma_{f1}$	4.8573×10^{-3}	4.6115×10^{-3}	4.3736×10^{-3}	4.1649×10^{-3}	3.9870×10^{-3}
		Σ_{R1}	1.7029×10^{-2}	1.6801×10^{-2}	1.6582×10^{-2}	1.6385×10^{-2}	1.6214×10^{-2}
		D_1	1.2653	1.2696	1.2773	1.2858	1.2947
		Σ_{a1}	9.7134×10^{-3}	9.9043×10^{-3}	1.0098×10^{-2}	1.0275×10^{-2}	1.0430×10^{-2}
		$K\Sigma_{f1}$	6.0342×10^{-14}	5.7167×10^{-14}	5.4198×10^{-14}	5.1632×10^{-14}	4.9463×10^{-14}
	1200	$\nu\Sigma_{f1}$	4.9316×10^{-3}	4.7265×10^{-3}	4.5267×10^{-3}	4.3504×10^{-3}	4.1992×10^{-3}
		Σ_{R1}	1.6781×10^{-2}	1.6545×10^{-2}	1.6323×10^{-2}	1.6124×10^{-2}	1.5950×10^{-2}
		D_1	1.2788	1.2834	1.2909	1.2992	1.3069

Table 3-1. (Continued)

Boron Concentration (ppm)		Burnup step (WD/g) 35,000	40,000	45,000
0	Σ_{a1}	1.0256×10^{-2}	1.0375×10^{-2}	1.0483×10^{-2}
	$K\Sigma_{f1}$	4.4845×10^{-14}	4.3203×10^{-14}	4.1915×10^{-14}
	$\nu\Sigma_{f1}$	3.8292×10^{-3}	3.7193×10^{-3}	3.6241×10^{-3}
	Σ_{R1}	1.6063×10^{-2}	1.5929×10^{-2}	1.5809×10^{-2}
	D_1	1.3030	1.3099	1.3169
1200	Σ_{a1}	1.0567×10^{-2}	1.0689×10^{-2}	1.0800×10^{-2}
	$K\Sigma_{f1}$	4.7653×10^{-14}	4.6169×10^{-14}	4.4968×10^{-14}
	$\nu\Sigma_{f1}$	4.0714×10^{-3}	3.9654×10^{-3}	3.8786×10^{-3}
	Σ_{R1}	1.5797×10^{-2}	1.5661×10^{-2}	1.5540×10^{-2}
	D_1	1.3146	1.3216	1.3283

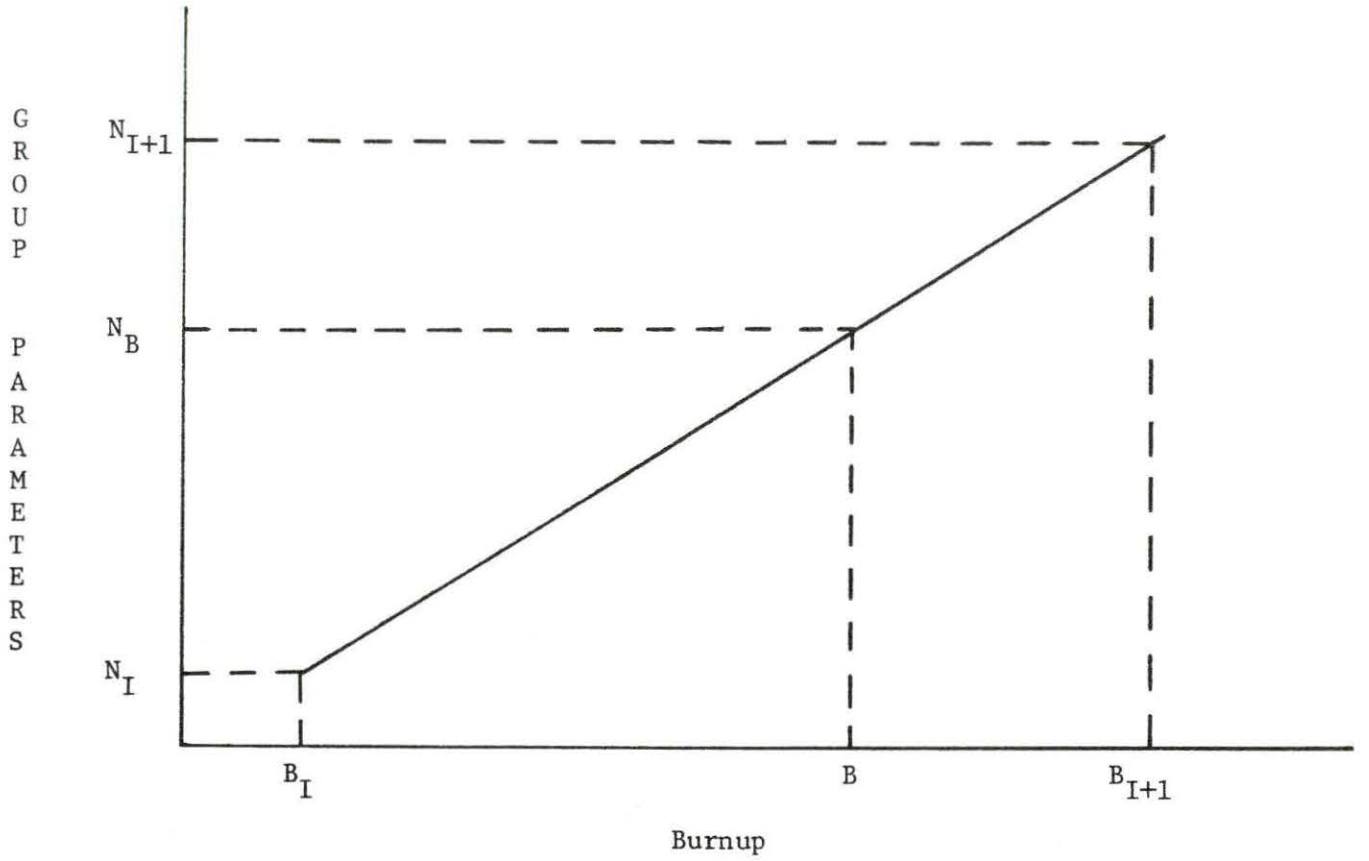

Figure 3-1. The interpolation technique for calculation of new group parameters

$$N_{PPM} = N_{1200} + \frac{(N_{1200} - N_o)(PPM - 1200)}{1200} \qquad (3\text{-}2)$$

where N_{1200} = the known group parameters of boron concentration 1200 PPM and

N_o = the known group parameters of boron concentration 0 PPM.

B. Power Density Calculation

The power density at location r of a multigroup calculation is given by [7]:

$$P(r) = \sum_g K_g \Sigma_{fg}(r)\phi_g(r) \qquad (3\text{-}3)$$

where K_g = recoverable energy (joules per fission) and

Σ_{fg} = fission cross section.

For one dimension with two neutron groups, the power density becomes

$$P(x) = K_1\Sigma_{f1}(x)\phi_1(x) + K_2\Sigma_{f2}(x)\phi_2(x) \; . \qquad (3\text{-}4)$$

P(x) is also approximated by a fourth order polynomial as

$$P(x) = p_o + p_1 x + p_2 x^2 + p_3 x^3 + p_4 x^4 \; . \qquad (3\text{-}5)$$

Applying the same procedure as for $D_1(x)$, the coefficients p_o through p_4 can be obtained as

$$p_o = P^o \qquad (3\text{-}6)$$

$$p_1 = \frac{1}{\eta}\left[2(P^+ - P^-) - \frac{1}{2}(P^r - P^\ell)\right] \tag{3-7}$$

$$p_2 = \frac{3}{4\eta^2}\left[5(P^+ + P^-) - (P^r + P^\ell) - 8\,P^o\right] \tag{3-8}$$

$$p_3 = \frac{2}{\eta^3}\left[\frac{1}{2}(P^r - P^\ell) - (P^+ - P^-)\right] \tag{3-9}$$

$$p_4 = \frac{5}{4\eta^4}\left[(P^r + P^\ell) - 3(P^+ + P^-) + 4\,P^o\right] \tag{3-10}$$

where

$$P^\ell = K_1\Sigma_{f1}^\ell\phi_1^\ell + K_2\Sigma_{f2}^\ell\phi_2^\ell \tag{3-11}$$

$$P^o = K_1\Sigma_{f1}^o\phi_1^o + K_2\Sigma_{f2}^o\phi_2^o \tag{3-12}$$

$$P^r = K_1\Sigma_{f1}^r\phi_1^r + K_2\Sigma_{f2}^r\phi_2^r \tag{3-13}$$

$$P^- = K_1\Sigma_{f1}^-\phi_1^- + K_2\Sigma_{f2}^-\phi_2^- \tag{3-14}$$

$$P^+ = K_1\Sigma_{f1}^+\phi_1^+ + K_2\Sigma_{f2}^+\phi_2^+ \tag{3-15}$$

The average power density over a given node is

$$\bar{P} = \frac{1}{2\eta}\int_{-\eta}^{\eta} P(x)\,dx \tag{3-16}$$

$$= \frac{1}{2\eta}\int_{-\eta}^{\eta}(p_o + p_1x + p_2x^2 + p_3x^3 + p_4x^4)\,dx$$

$$= p_o + \frac{p_2}{3}\eta^2 + \frac{p_4}{5}\eta^4$$

$$= \frac{1}{2} (P^{+} + P^{-})$$

C. Burnup Calculation

Assume the power density P(x) over a time interval Δt is constant. Thus, the burnup at a given time t_2 can be written as [7]:

$$B(x, t_2) = B(x, t_1) + \frac{P(x)}{\rho} \Delta t \tag{3-17}$$

where $B(x, t_1)$ = burnup at previous time t_1,

$P(x)$ = power density,

ρ = fuel density, and

Δt = $t_2 - t_1$, time interval.

$B(x, t_2)$ can also be approximated as

$$B(x, t_2) = b_o(t_2) + b_1(t_2)x + b_2(t_2)x^2 + b_3(t_2)x^3 + b_4(t_2)x^4 \ . \tag{3-18}$$

Applying the same procedure as $D_1(x)$, the coefficients $b_o(t_2)$ through $b_4(t_2)$ can also be obtained as

$$b_o(t_2) = B^{o}(t_2) \tag{3-19}$$

$$b_1(t_2) = \frac{1}{\eta} \{2[B^{+}(t_2) - B^{-}(t_2)] - \frac{1}{2}[B^{r}(t_2) - B^{\ell}(t_2)]\} \tag{3-20}$$

$$b_2(t_2) = \frac{3}{4\eta^2} \{5[B^{+}(t_2) + B^{-}(t_2)] - [B^{r}(t_2) + B^{\ell}(t_2)] - 8\, B^{o}(t_2)\} \tag{3-21}$$

$$b_3(t_2) = \frac{2}{\eta^3}\left\{\frac{1}{2}[B^r(t_2) - B^\ell(t_2)] - [B^+(t_2) - B^-(t_2)]\right\} \tag{3-22}$$

$$b_4(t_2) = \frac{5}{4\eta^4}\{[B^r(t_2) + B^\ell(t_2)] - 3[B^+(t_2) + B^-(t_2)] + 4\ B^o(t_2)\} \tag{3-23}$$

where

$$B^\ell(t_2) = B^\ell(t_1) + \frac{P^\ell}{\rho}\Delta t \tag{3-24}$$

$$B^o(t_2) = B^o(t_1) + \frac{P^o}{\rho}\Delta t \tag{3-25}$$

$$B^r(t_2) = B^r(t_1) + \frac{P^r}{\rho}\Delta t \tag{3-26}$$

$$B^-(t_2) = B^-(t_1) + \frac{P^-}{\rho}\Delta t \tag{3-27}$$

$$B^+(t_2) = B^+(t_1) + \frac{P^+}{\rho}\Delta t \tag{3-28}$$

The average burnup over a given node at time t_2 is

$$\overline{B} = \frac{1}{2\eta}\int_{-\eta}^{\eta} B(x, t_2)\,dx$$

$$= b_o(t_2) + \frac{b_2(t_2)}{3}\eta^2 + \frac{b_4(t_2)}{5}\eta^4$$

$$= \frac{1}{2}[B^+(t_2) + B^-(t_2)] \tag{3-29}$$

D. Boron Concentration Calculation

It is assumed that the reactor is controlled by a chemical shim system. Increasing the concentration of boron by 100 PPM can decrease the reactivity of the reactor about 0.01 [7]. Thus, the change in the

reactivity of the reactor resulting from a change in boron concentration can be written as

$$-\frac{100}{0.01} = \frac{\Delta PPM}{\Delta \rho} = \frac{PPM - PPM_1}{\frac{S - 1}{S}} \qquad (3\text{-}30)$$

where PPM = previous boron concentration,

PPM_1 = estimative critical boron concentration and

S = neutron source at boron concentration PPM.

Therefore, PPM_1 can be obtained from the above equation as

$$PPM_1 = PPM - 10^4\left(\frac{1}{S} - 1\right) . \qquad (3\text{-}31)$$

One cannot assume that PPM_1 is a critical boron concentration because PPM_1 is only an estimated critical boron concentration. If the reactor is not critical after using the PPM_1 calculation, a linear extrapolation technique is used to estimate the critical boron concentration (Figure 3-2):

$$\frac{S^{(P-1)} - S^{(P)}}{PPM^{(P-1)} - PPM^{(P)}} = \frac{S^{(P)} - 1.0}{PPM^{(P)} - PPM^{(P+1)}} \qquad (3\text{-}32)$$

where $PPM^{(P-1)}$ = previous boron concentration at neutron source $S^{(P-1)}$ and

$PPM^{(P)}$ = present boron concentration at neutron source $S^{(P)}$.

The boron concentration $PPM^{(P+1)}$ for the next iteration can be obtained from Equation (3-32) as

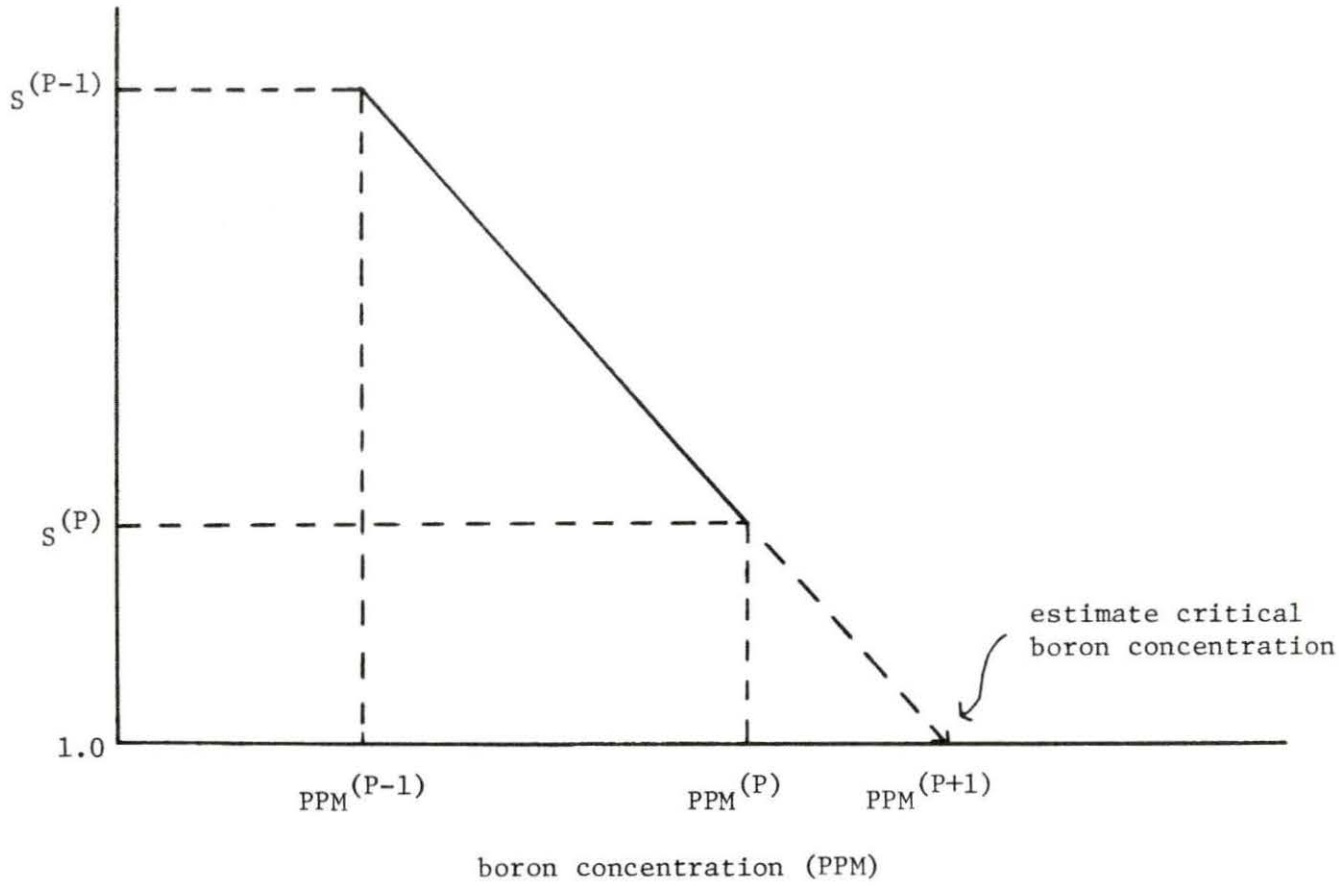

Figure 3-2. Critical boron concentration estimation

$$PPM^{(P+1)} = PPM^{(P)} - \frac{S^{(P)} - 1.0}{S^{(P-1)} - S^{(P)}} (PPM^{(P-1)} - PPM^{(P)}) \qquad (3\text{-}33)$$

Therefore, the critical boron concentration can be estimated after a number of iterations.

At startup, the reactor is necessarily fueled with more fissile material than needed to become critical, and the excess reactivity of the fuel is held down by the soluble poison. The critical boron concentration can be estimated from Equation (3-31) and the iteration technique (Equation 3-33). Once the reactor is operating in a steady state at the desired power level, as the fuel is consumed, the burnup at any given time t_2 can be evaluated from Equation (3-17). Thus, the boron concentration is reduced to keep the reactor critical and to compensate for the burnup of fuel during the time interval Δt. This critical boron concentration can also be estimated from Equation (3-31) and the iteration technique (Equation 3-33). For each time interval, the critical boron concentration is determined. A typical curve of critical boron concentration as a function of time after startup is shown in Figure 3-3 [7]. (Temperature defect and xenon effect are not included in this research.)

If the life of the core is not a multiple of Δt (assume Δt is constant), the boron concentration will become negative after the calculation of the final time interval (Figure 3-3). This negative boron concentration is not a realistic situation. In order to get a reasonable concentration at the end of the core life, another technique is used. Choose a new factor PPM_w, the boron concentration

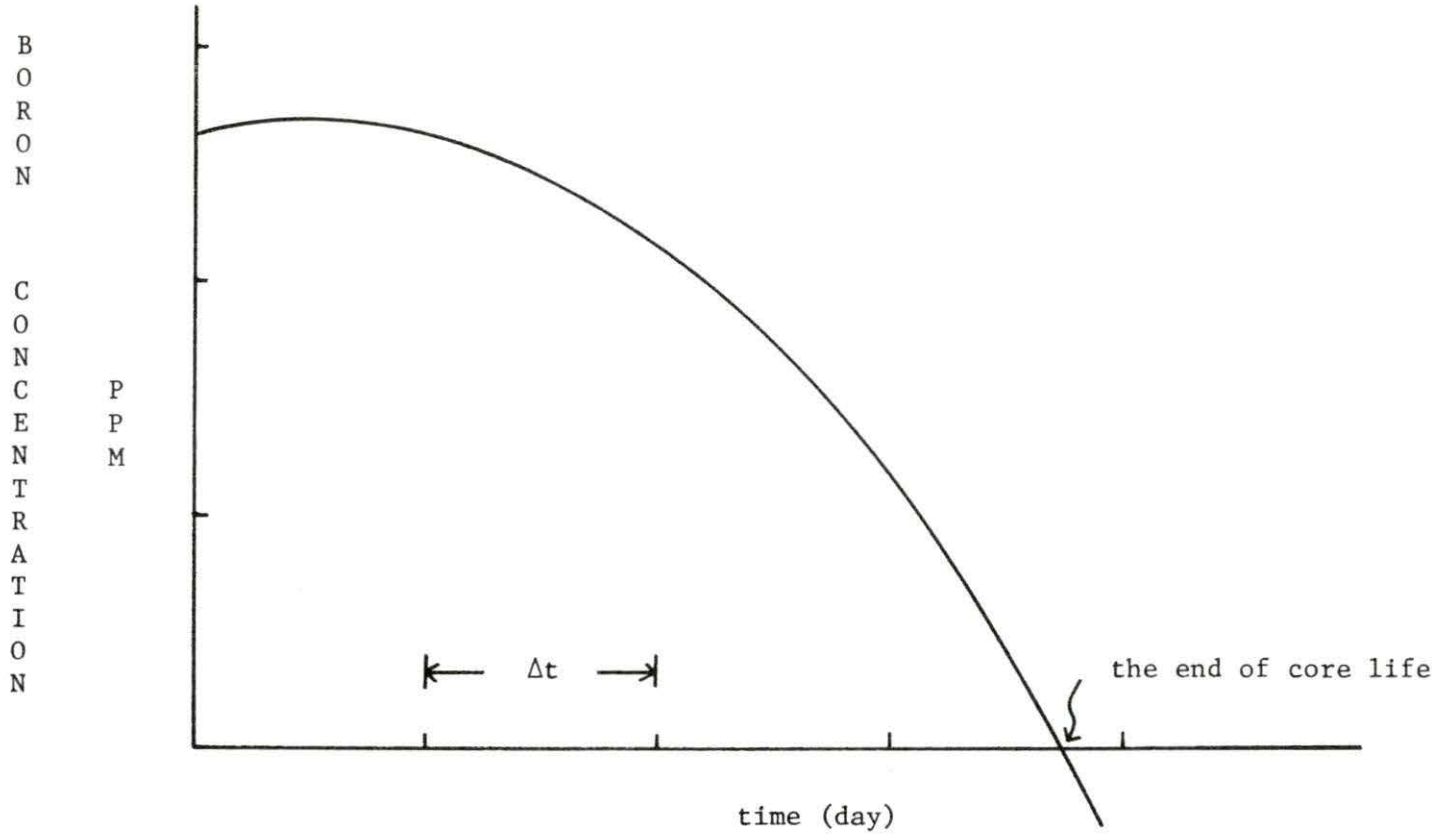

Figure 3-3. Critical boron concentration as function of time after startup

window. The time for which the critical boron concentration is within this PPM_w is defined as the end of core life. Thus, PPM_w is a criterion for searching for the end of core life. Assume the boron concentration curve in the final time interval is linear. Thus, an interpolation technique can be applied to search for the real final time interval (Figure 3-4), i.e.

$$\frac{PPM_1 - PPM_f}{\Delta t_f} = \frac{PPM_1 - PPM_2}{\Delta t} \tag{3-34}$$

where $\Delta t = t_2 - t_1$, constant time interval,

Δt_f = the real final time interval,

PPM_1 = the boron concentration at time t_1,

PPM_2 = the boron concentration at time t_2, and

$PPM_f = PPM_w/2$.

The real final time interval can be obtained from Equation (3-34):

$$\Delta t_f = \Delta t \times \frac{PPM_1 - PPM_f}{PPM_1 - PPM_2} \times A \ .$$

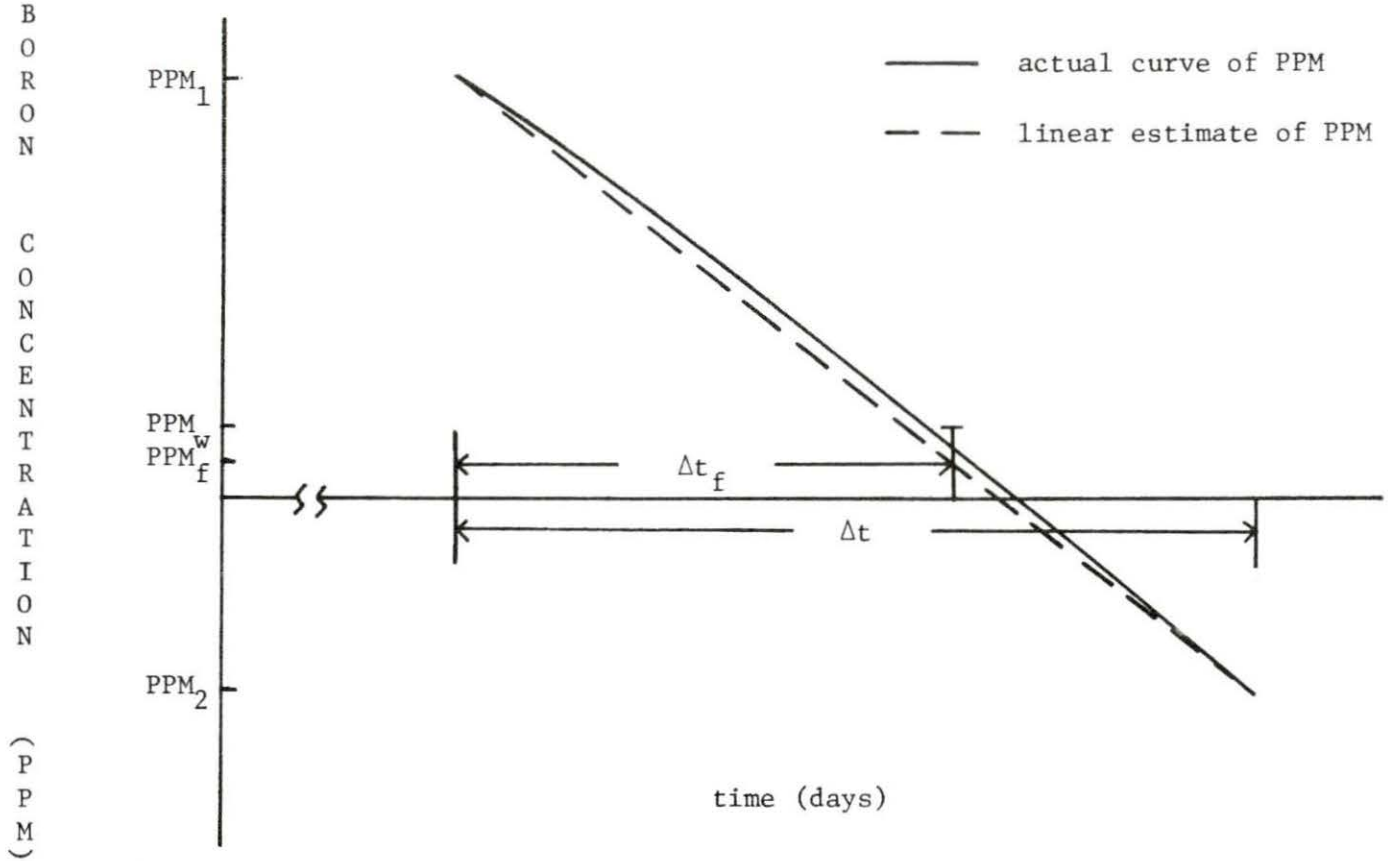

Figure 3-4. Search for the end of core life

IV. THE CALCULATION PROCEDURE

A. Relaxation Method

To enhance the speed of convergence to the final solution, a relaxation technique [4] is applied to the finite element nodal model. Let $\tilde{R}^{(P)}$ be the value calculated by the finite element nodal model. $R^{(P-1)}$ is a present value after P-1 iterations. The actual value $R^{(P)}$ for P iterations is

$$R^{(P)} = \alpha\tilde{R}^{(P)} + (1 - \alpha)\ R^{(P-1)} \tag{4-1}$$

where α is a relaxation parameter. If $\alpha = 1$, the value used for P iteration is just the value obtained from the finite element nodal model. If $\alpha \neq 1$, a relaxation technique is used to help speed convergence to the final solution.

The following parameters were used in the relaxation method that was applied to the finite element nodal model:

1. The coefficient of the flux distribution $\phi(x)$

$$a_i^{(P)} = \alpha\ \tilde{a}_i^{(P)} + (1 - \alpha)\ a_i^{(P-1)} \tag{4-2}$$

$$i = 0, 1, 2, 3, 4$$

2. The flux at interface and boundary

$$\phi^{(P)} = \alpha\ \tilde{\phi}^{(P)} + (1 - \alpha)\ \phi^{(P-1)} \tag{4-3}$$

3. The neutron source

$$S^{(P)} = \alpha \tilde{S}^{(P)} + (1 - \alpha) S^{(P-1)} \tag{4-4}$$

B. Convergence Criteria

Convergence for the flux distribution is established on the ℓ_2 norm [4]. The ℓ_2 norm for the flux distribution is

$$\varepsilon = \left|\left| 1 - \frac{\bar{\phi}^{(P-1)}}{\bar{\phi}^{(P)}} \right|\right|_2$$

$$= \left[\sum_{i=1}^{I} \left(1 - \frac{\bar{\phi}_i^{(P-1)}}{\bar{\phi}_i^{(P)}}\right)^2 \right]^{1/2} \tag{4-5}$$

where $\bar{\phi}_i$ is the average flux over each node. The convergence is established when

$$\varepsilon \leq L \tag{4-6}$$

where L is an input convergence criterion.

Convergence for criticality is established on the following equation:

$$|S_{total} - 1.0| \leq L' \qquad (4\text{-}7)$$

where 1.0 is the eigenvalue of a critical reactor and L' is an input convergence criterion for the neutron source. Therefore, the reactor is critical when a converged neutron source has been determined.

C. Computer Code and Calculation Procedure

A computer program called BNODE was developed by Dr. Rohach [8] which is a one-dimension model with two neutron groups. A flow chart of this code is shown in Figure 4-1. The procedure starts with an initial flux guess for each node. Then the procedure enters an 'inner loop' consisting of four blocks. This loop is an iteration process that yields polynomial coefficients, flux distribution and neutron source. Once the flux distribution converges, the procedure moves to the criticality convergent decision. If the reactor is not critical, the boron concentration needs to be adjusted. Owing to the change of boron concentration, new group parameters are calculated. The procedure then enters the 'inner loop' again. Once the reactor is critical, the procedure moves to the PPM_w decision. If the boron concentration is larger than the PPM_w, power density is calculated. Using this power density and a selected time interval, burnup can be evaluated. Thus, new group parameters are calculated again for the next iteration. The iterations are repeated until the boron concentration is less than the PPM window.

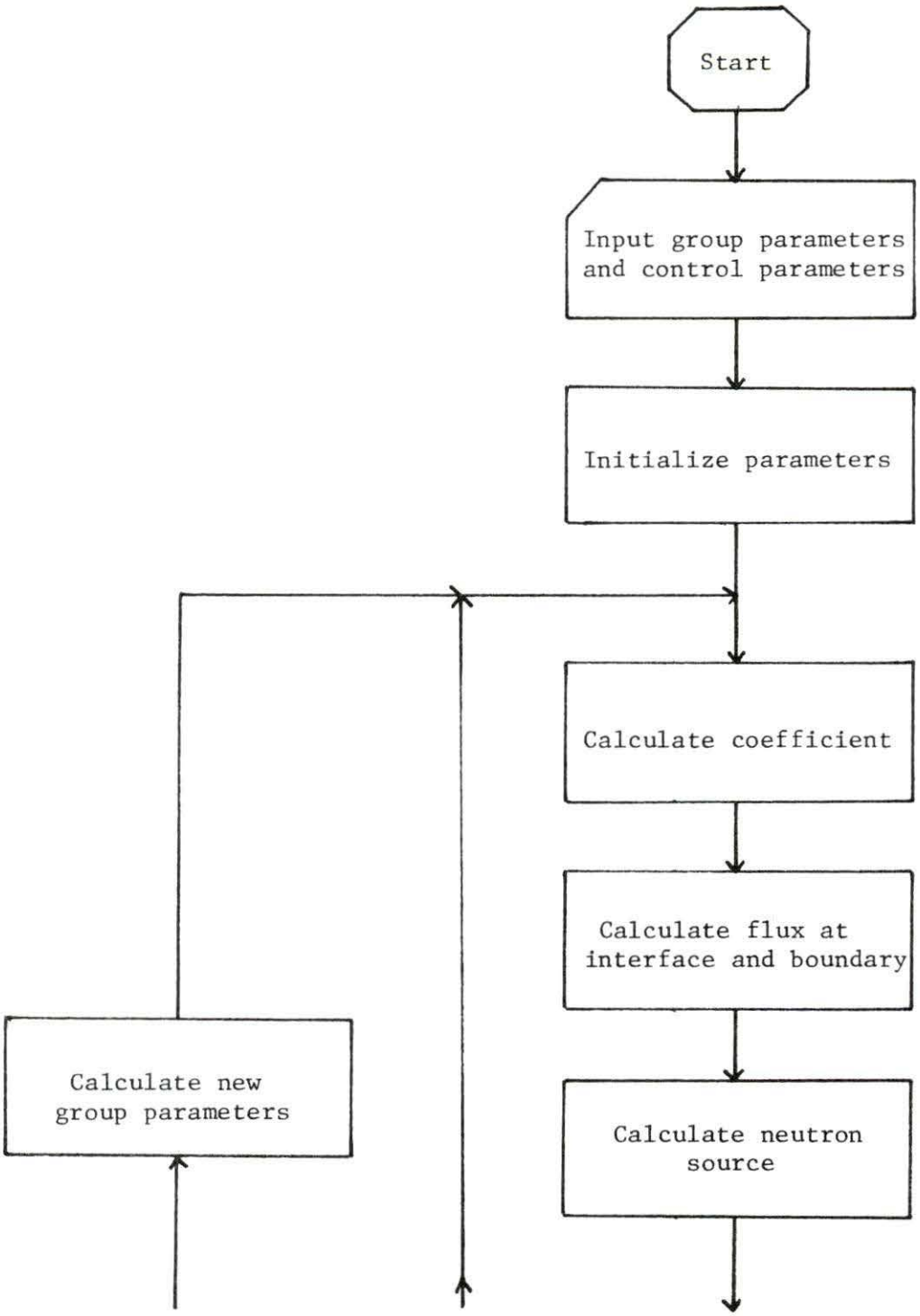

Figure 4-1. Calculation flow chart

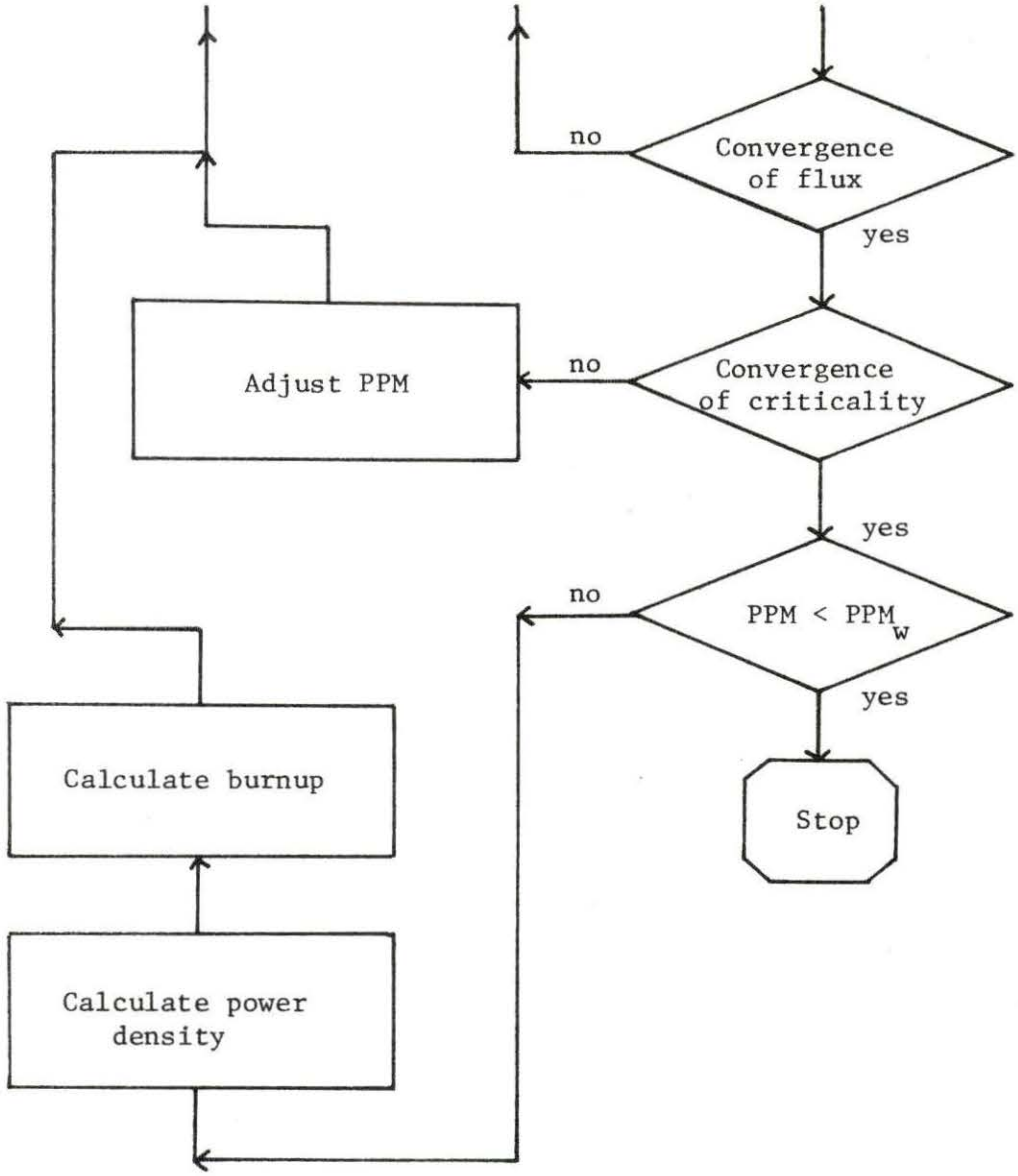

Figure 4-1. (Continued)

V. RESULTS AND DISCUSSION

Some neutron fuel data [6] are shown in Table 5-1.

Table 5-1. Neutron fuel data

Fuel	Density (g/cm^3)	Enrichment (%)
1[a]	2.541	2.38
2[a]	2.587	2.88
3[a]	2.541	2.88
4	2.725	1.87
5	2.725	2.88
6	2.725	3.52

[a]Burnable poison fuel.

A burnable poison is a large absorption cross section material which is converted into a low absorption cross section material as the result of neutron absorption. Thus, burnable poison can decrease the necessary boron concentration in the reactor that is controlled by a chemical shim. The burnable poison fuel elements are placed at selected locations in the core. The fuel loading pattern A in a one-dimensional model is shown in Figure 5-1.

A computer program DODMG has been developed [9] for finite difference approximation to one-dimension, multigroup diffusion theory. The flux and power distribution of a fine mesh (1 cm per mesh point)

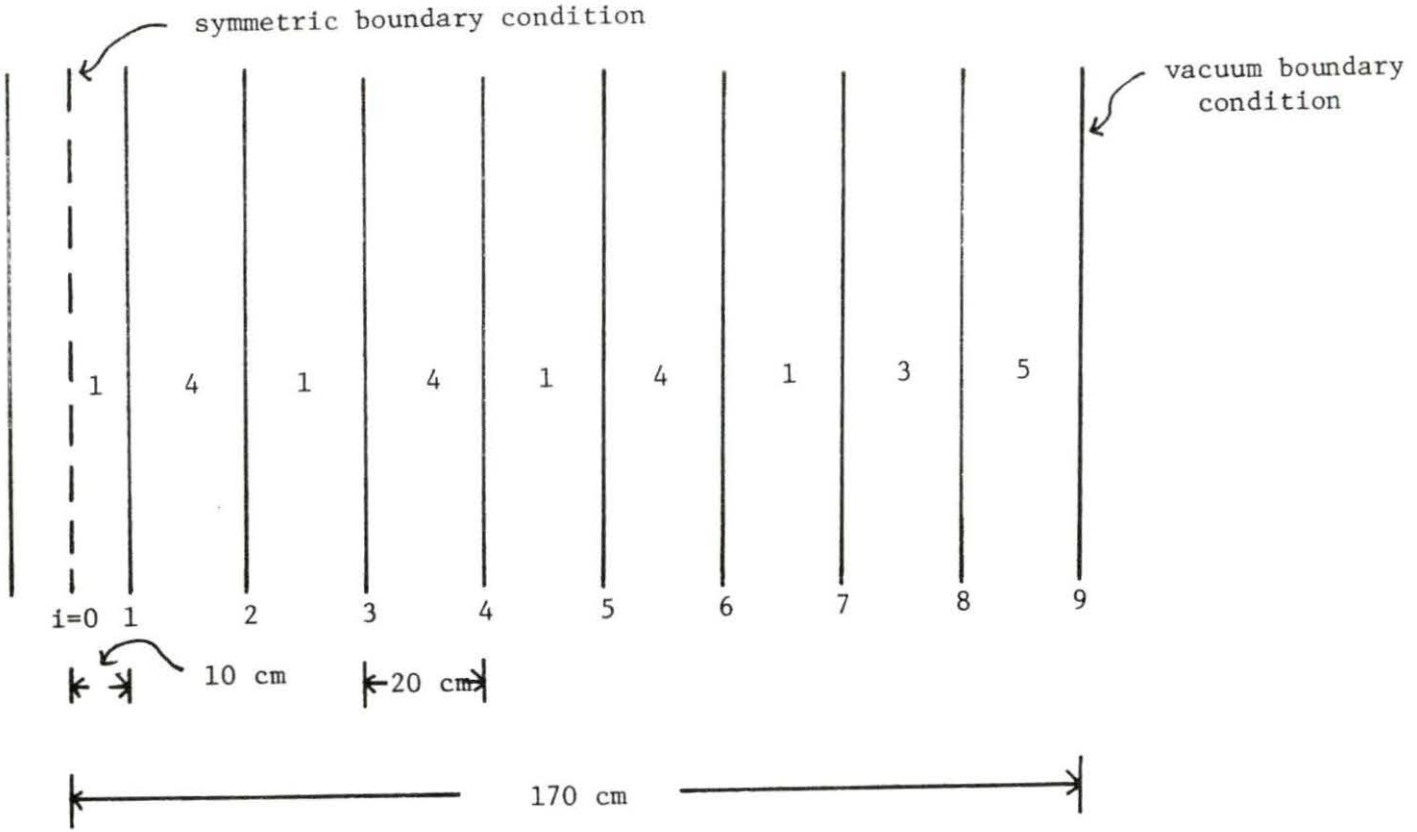

Figure 5-1. The fuel loading pattern A for one-dimensional model with vacuum boundary condition

calculation can be obtained by this code. Thus, the DODMG code can be used as a reference calculation.

Using the different convergence criteria of the BNODE code, the flux and power distribution at BOC (beginning of cycle) are shown in Figures 5-2 and 5-3. When the convergence criterion is equal to 10^{-7}, one can get results very favorably comparable to the DODMG code (Figures 5-4 and 5-5). Thus, using the same convergence criterion 10^{-7}, the flux and power distribution at EOC (end of cycle) are also obtained (Figures 5-6 and 5-7). One can observe that the results are also very good by comparing the results with the DODMG code. In order to save computer time, the convergence criterion 10^{-5} was used for following results.

The flux and power distribution at BOC are shown in Figures 5-8 and 5-9. One can note that the flux distribution shows four depressions in the locations of fuel type 1. This behavior is due to the high absorption cross section and low enrichment of burnable poison fuel. The power distribution is not continuous at the interfaces, owing to the discontinuity of $K_g \Sigma_{fg}$. The critical boron concentration at BOC is 564 PPM.

Using the time interval of 50 days and adjusting the PPM_w, the flux, power and total burnup distribution at certain times during the core life can be obtained. Figures 5-10 through 5-12 show the above distributions at 100, 200 and 300 days after startup. Thus, the change of flux, power and burnup are known during the core life. One can note that the peak is located in node 8 at 200 and 300 days. This behavior is a result of high burnup of fuel 3 at that time due to high

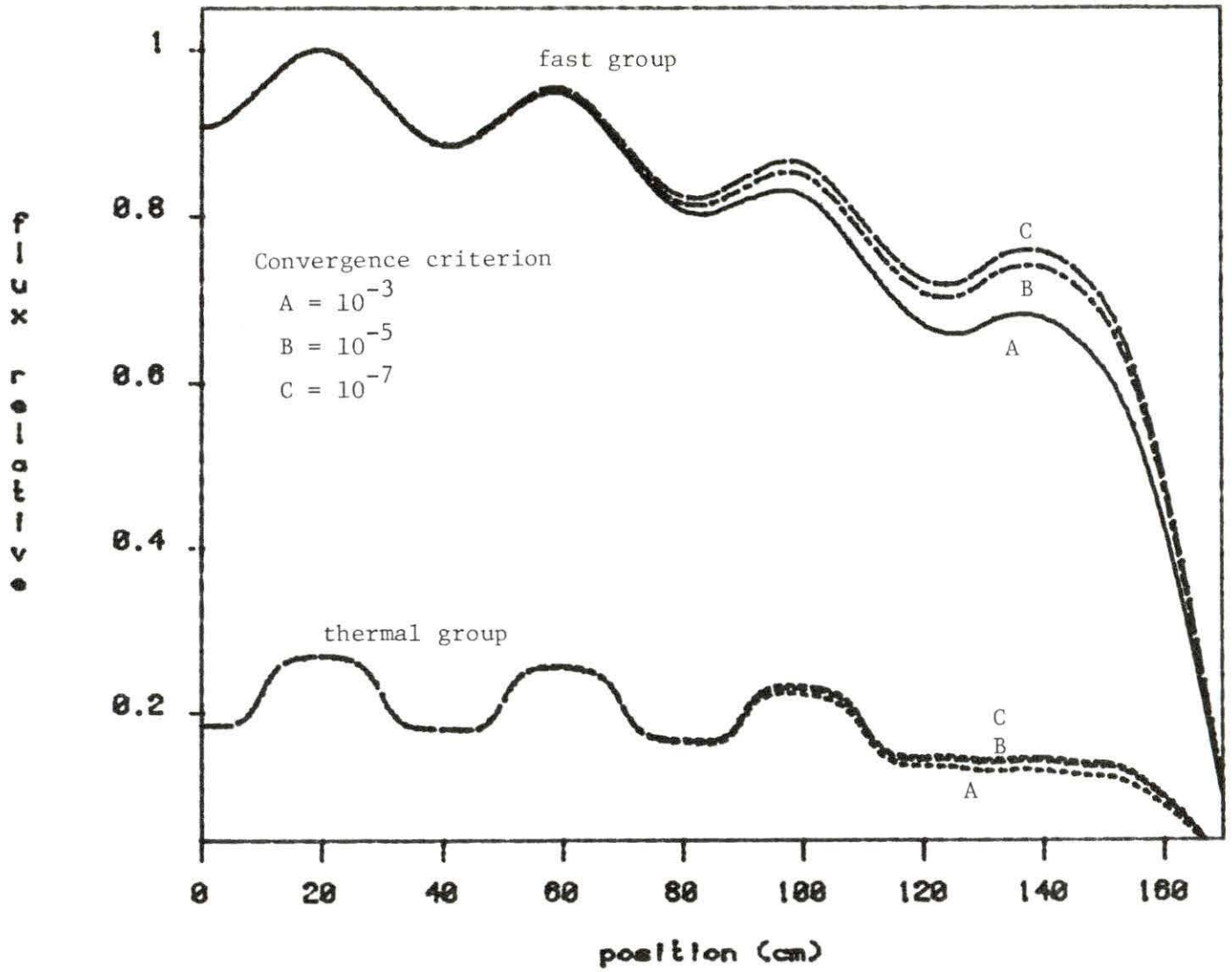

Figure 5-2. The comparison of the flux distribution at BOC for different convergence criteria

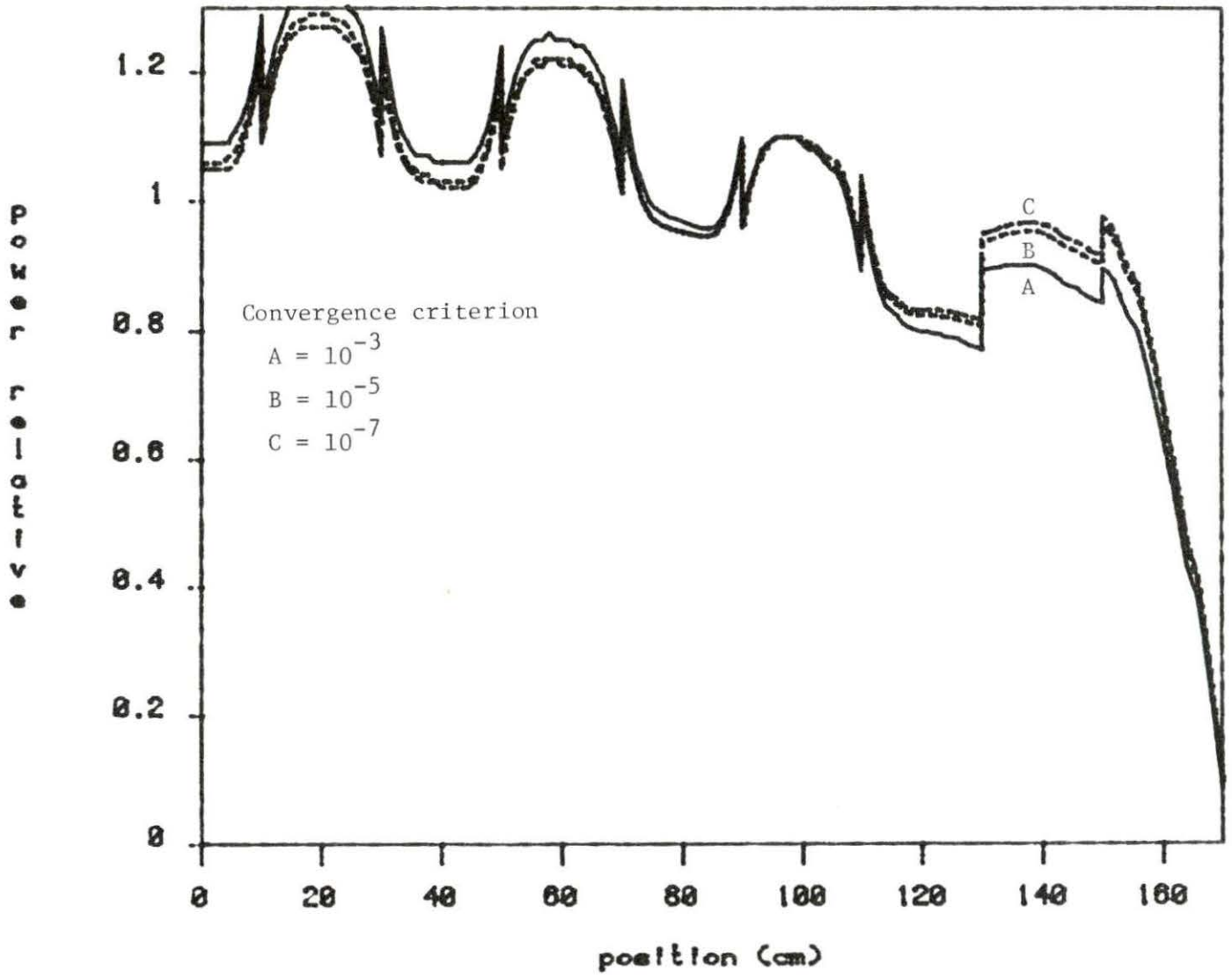

Figure 5-3. The comparison of the power distribution at BOC for different convergence criteria

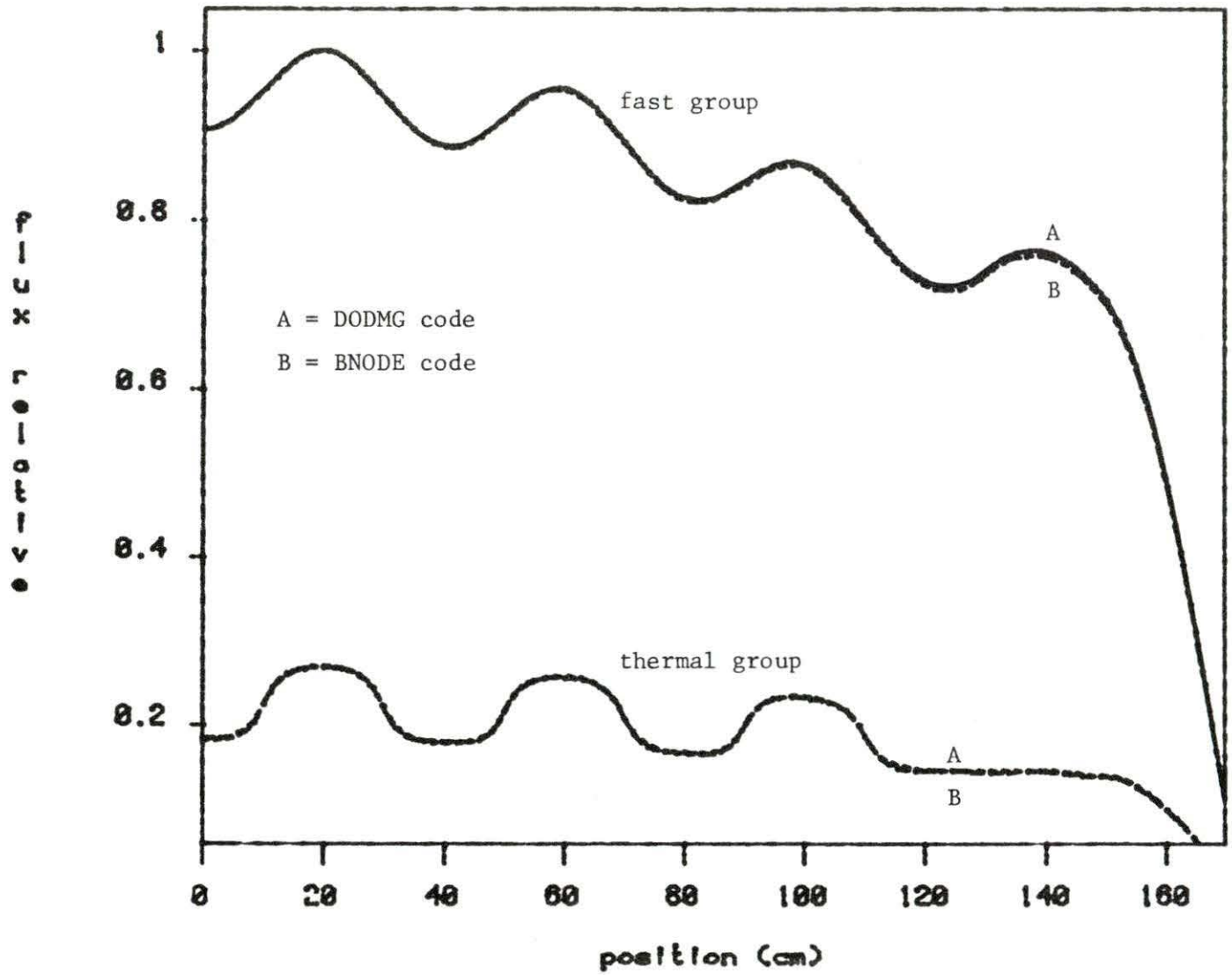

Figure 5-4. The comparison (BNODE and DODMG) of the flux distribution at BOC

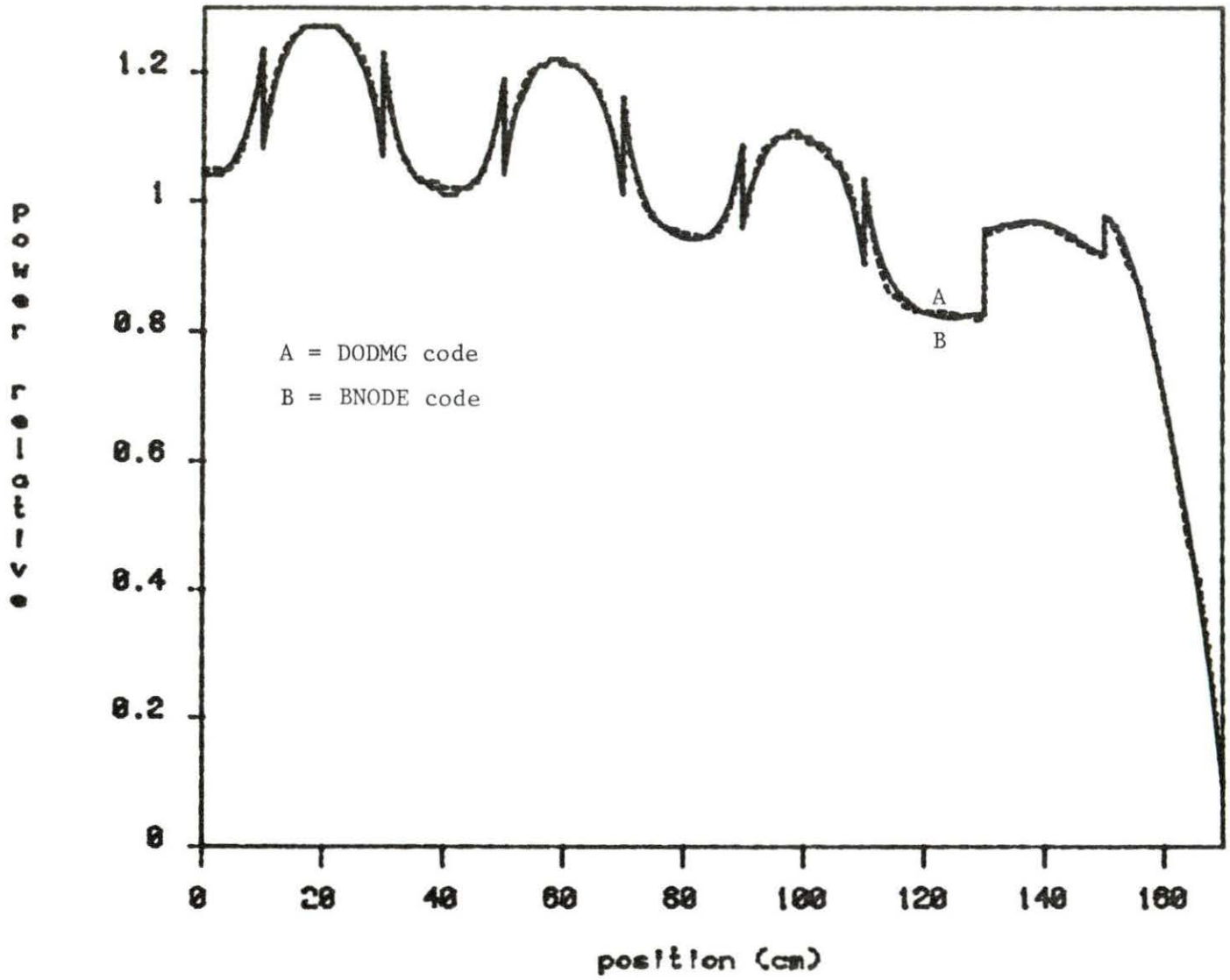

Figure 5-5. The comparison (BNODE and DODMG) of the power distribution at BOC

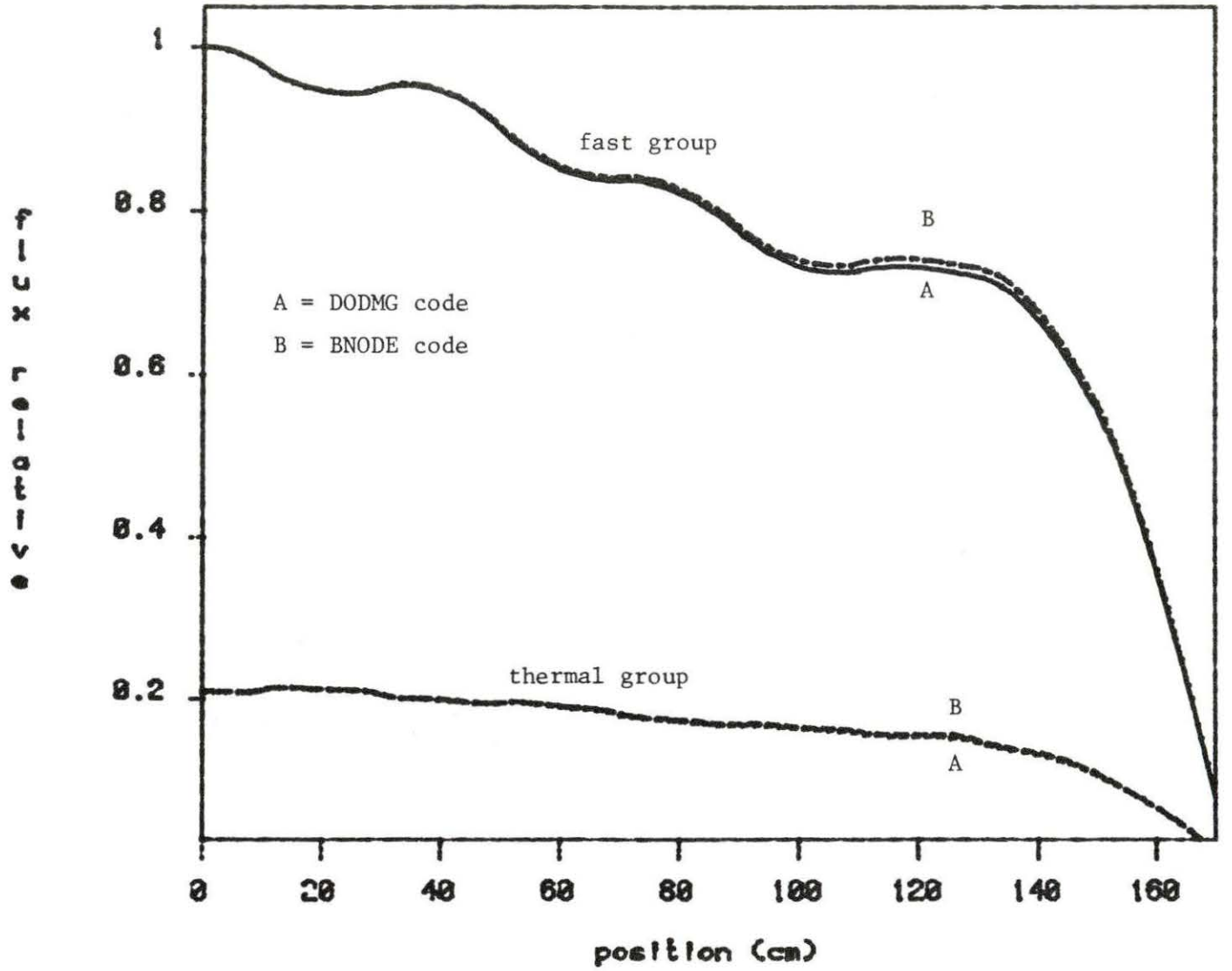

Figure 5-6. The comparison (BNODE and DODMG) of the flux distribution at EOC

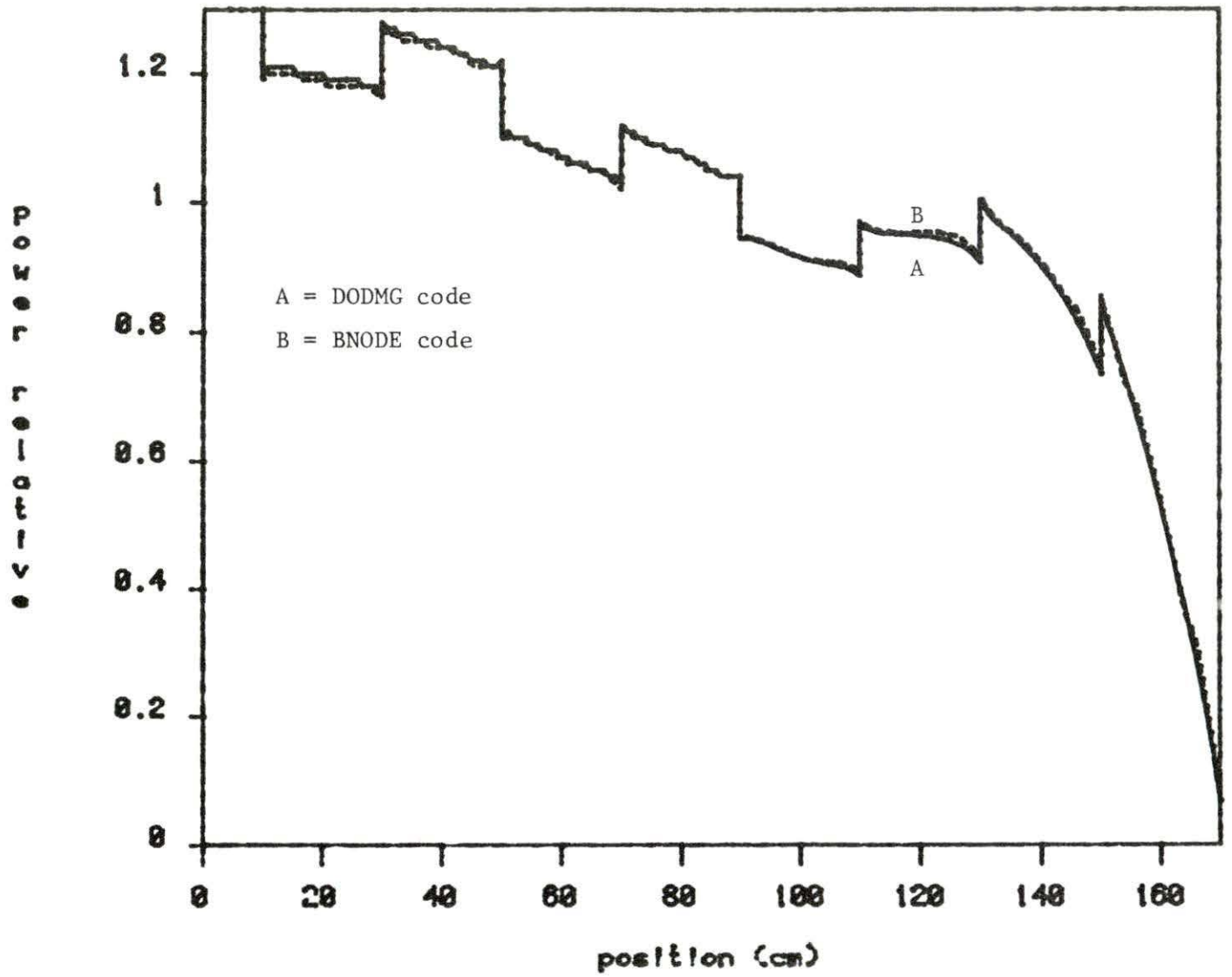

Figure 5-7. The comparison (BNODE and DODMG) of the power distribution at EOC

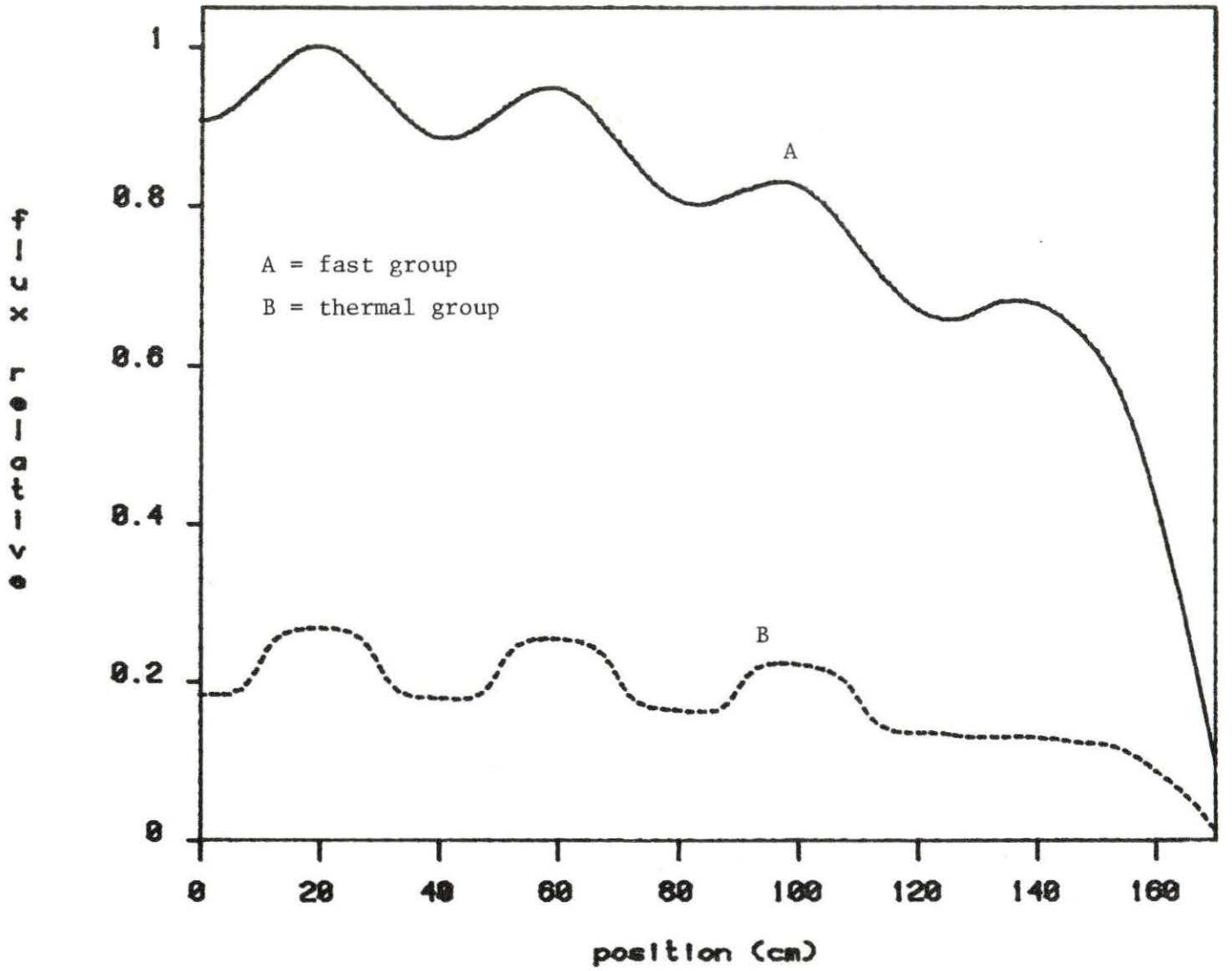

Figure 5-8. The flux distribution at BOC for the loading pattern A

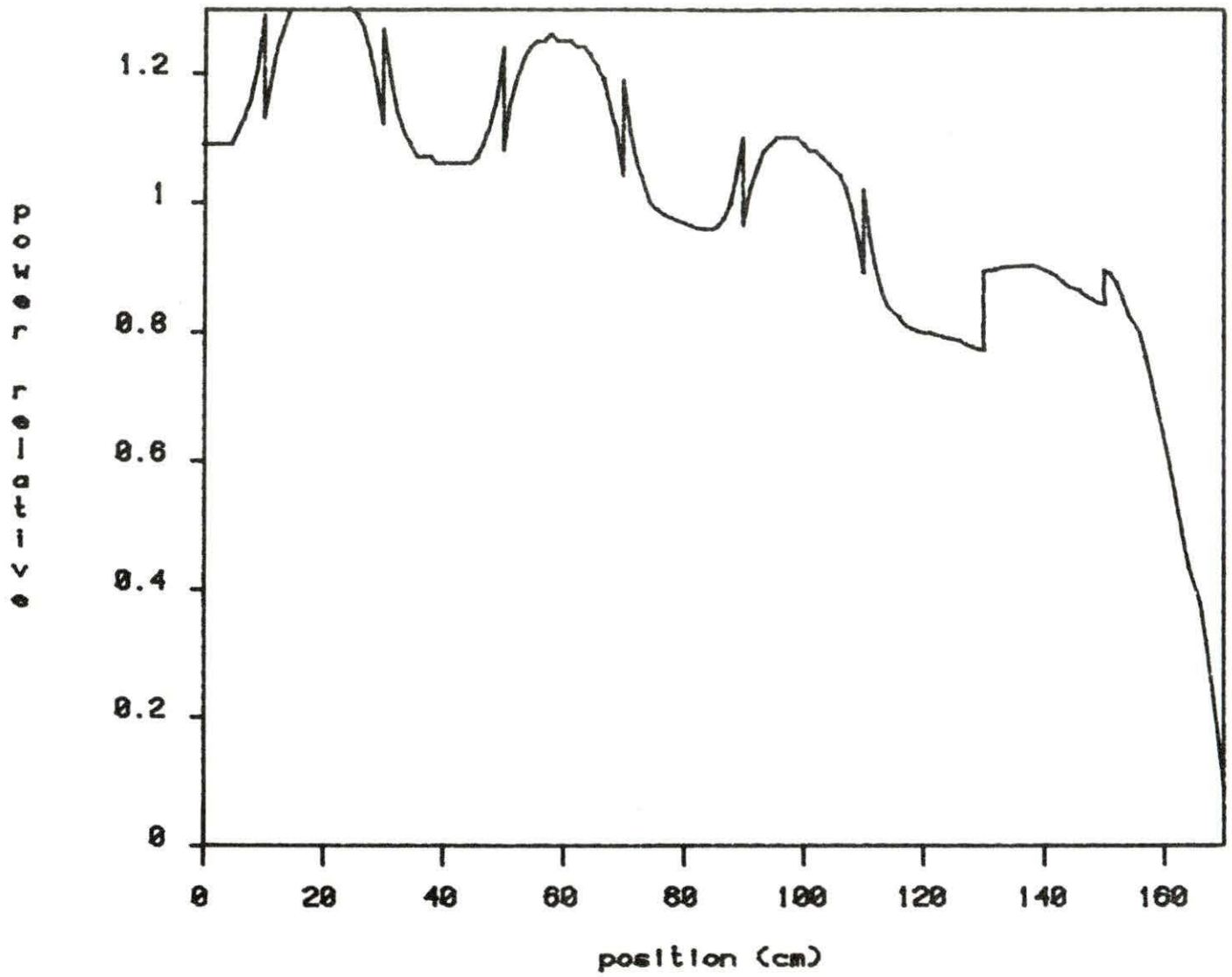

Figure 5-9. The power distribution at BOC for the loading pattern A

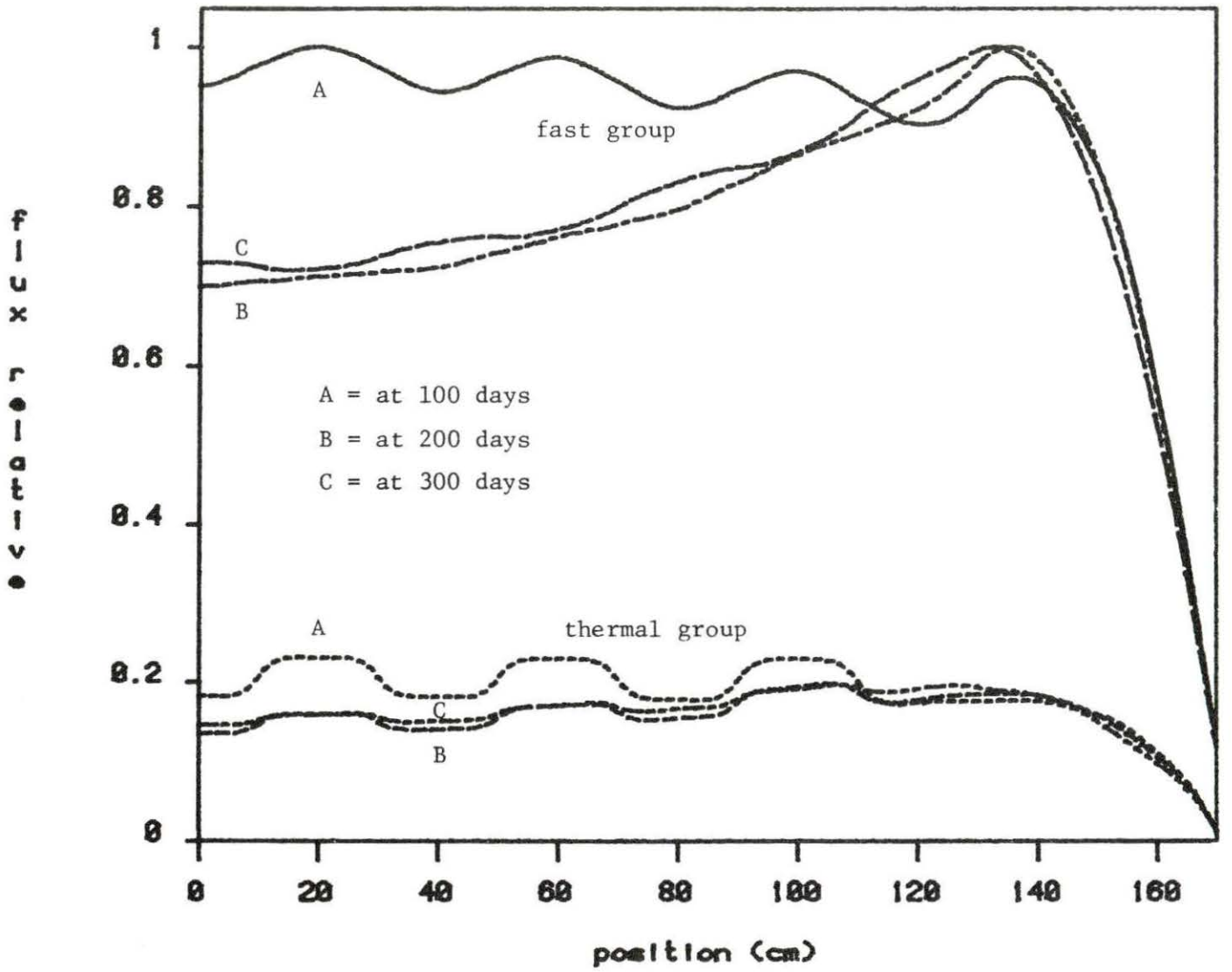

Figure 5-10. The flux distribution at 100, 200 and 300 days after startup for the loading pattern A

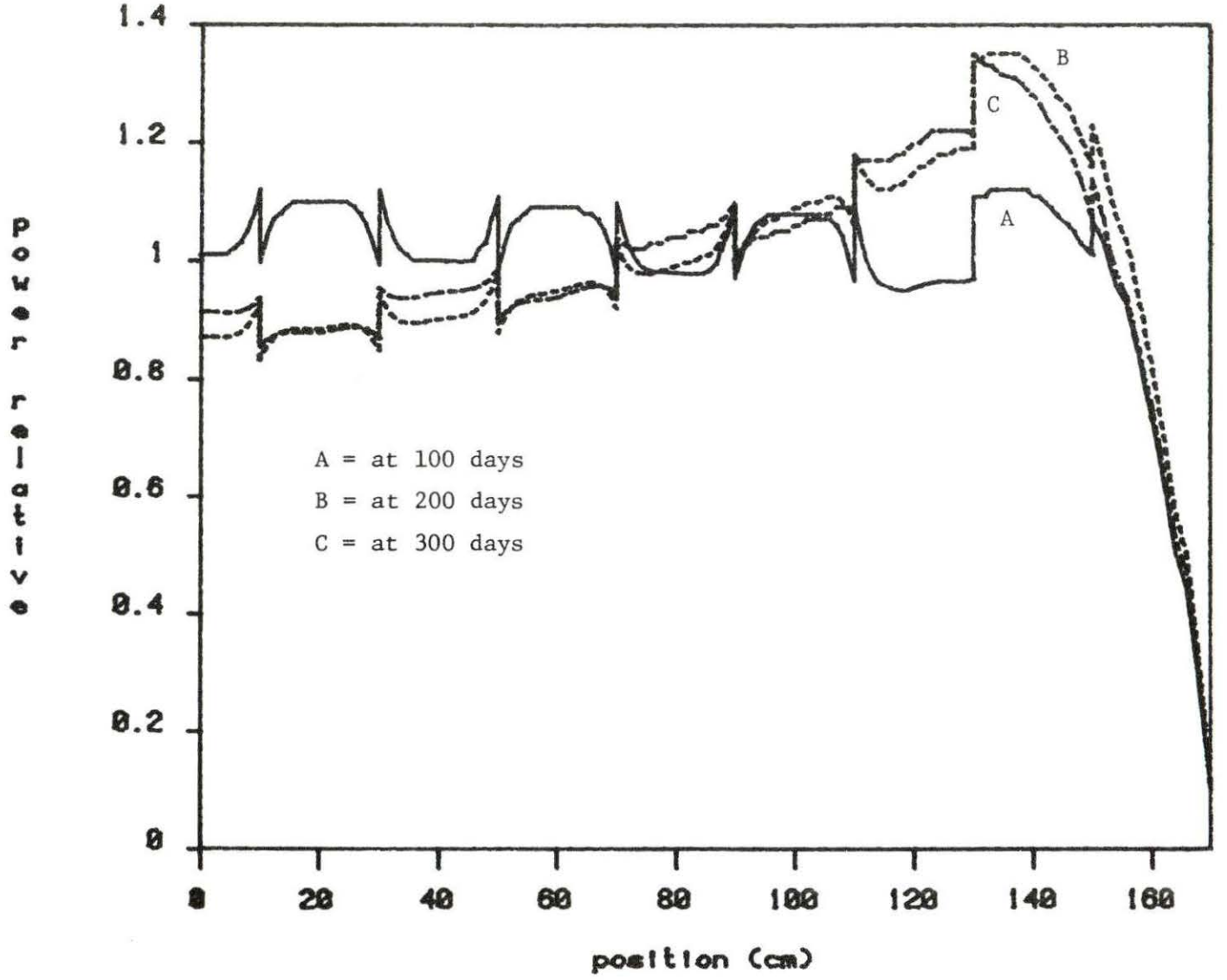

Figure 5-11. The power distribution at 100, 200 and 300 days after startup for the loading pattern A

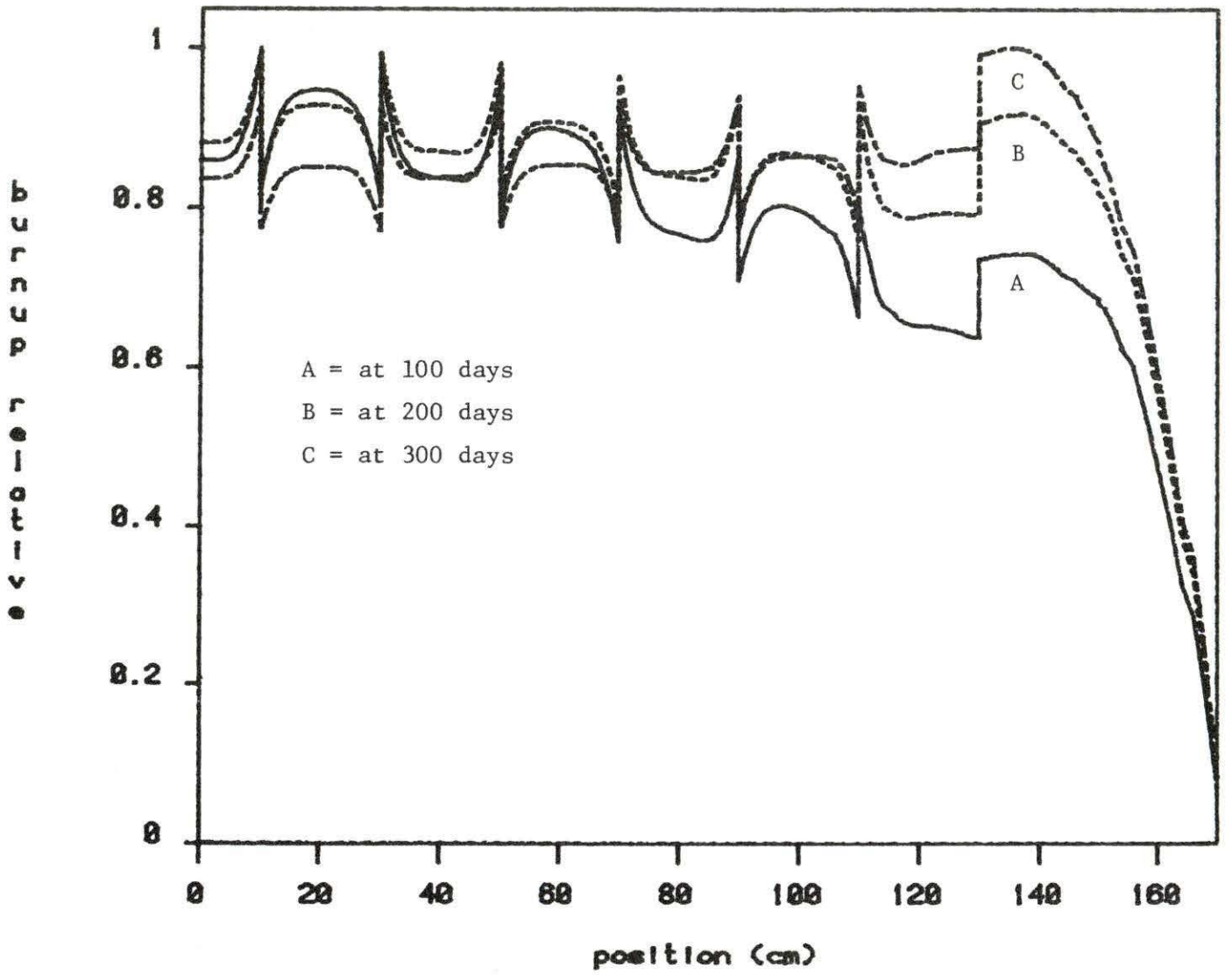

Figure 5-12. The burnup distribution for 100, 200 and 300 days after startup for the loading pattern A

enrichment, burnable poison fuel. The burnup is proportional to the power density at a certain time after startup. This behavior can also be observed in Figures 5-11 and 5-12.

The critical boron concentration reduces to 79 PPM after 400 days of burnup. This is the end of the cycle (EOC) because the critical boron concentration is less than 100 PPM, a chosen PPM_w. Figures 5-13 and 5-14 show the flux and power distribution at EOC. Both distributions are flatter than before. This is another advantage of using the burnable poison fuels at selected locations in a core. The total burnup distribution is shown in Figure 5-15. The maximum burnup is in fuel element 3 (Figure 5-1) because of the high enrichment, burnable poison fuel. The critical boron concentration as a function of time after startup is shown in Figure 5-16. The critical boron concentration increases at the beginning and then decreases until the end of the core life. This behavior shows that the converted rate (from a high-absorption cross section to a low-absorption cross section) is faster than the burnup of burnable poison fuels at the beginning. Therefore, more boron concentration is needed to keep the reactor critical.

The diffusion coefficient has been assumed to be a function of x. The assumption that the diffusion coefficient is independent of x was also made in this research. If the diffusion coefficient is not a function of x, then Equations (2-5) and (2-6) become

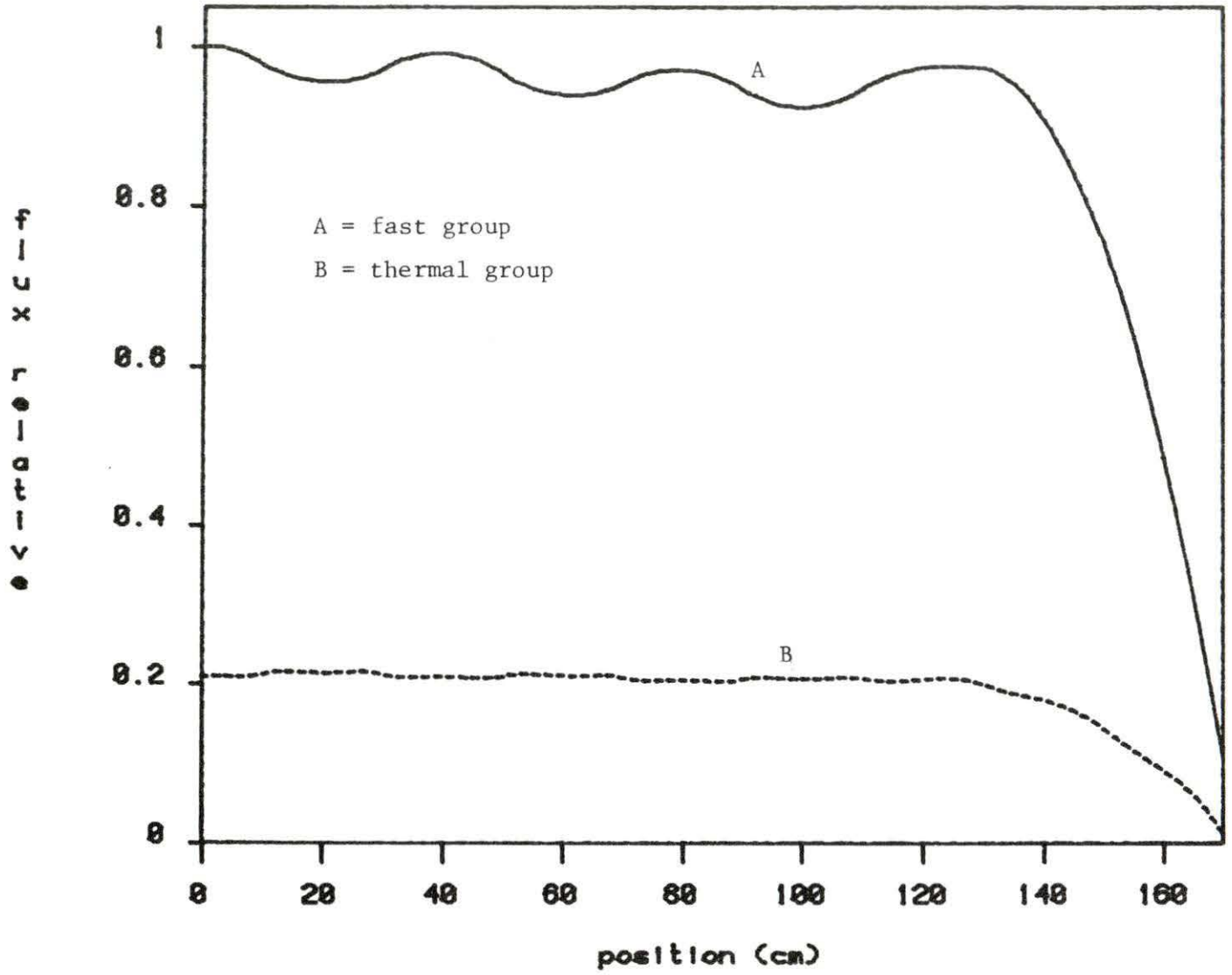

Figure 5-13. The flux distribution at EOC for the loading pattern A

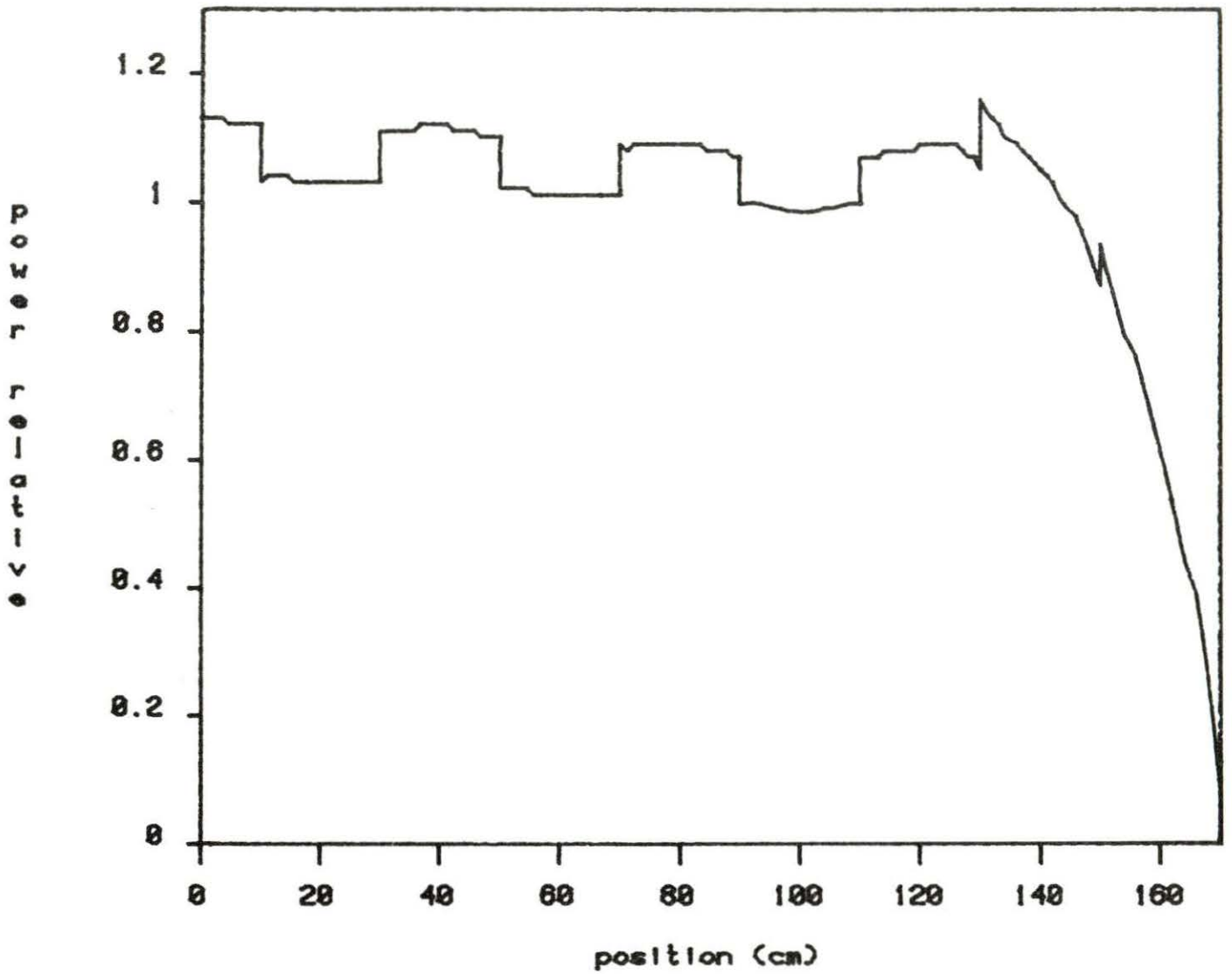

Figure 5-14. The power distribution at EOC for the loading pattern A

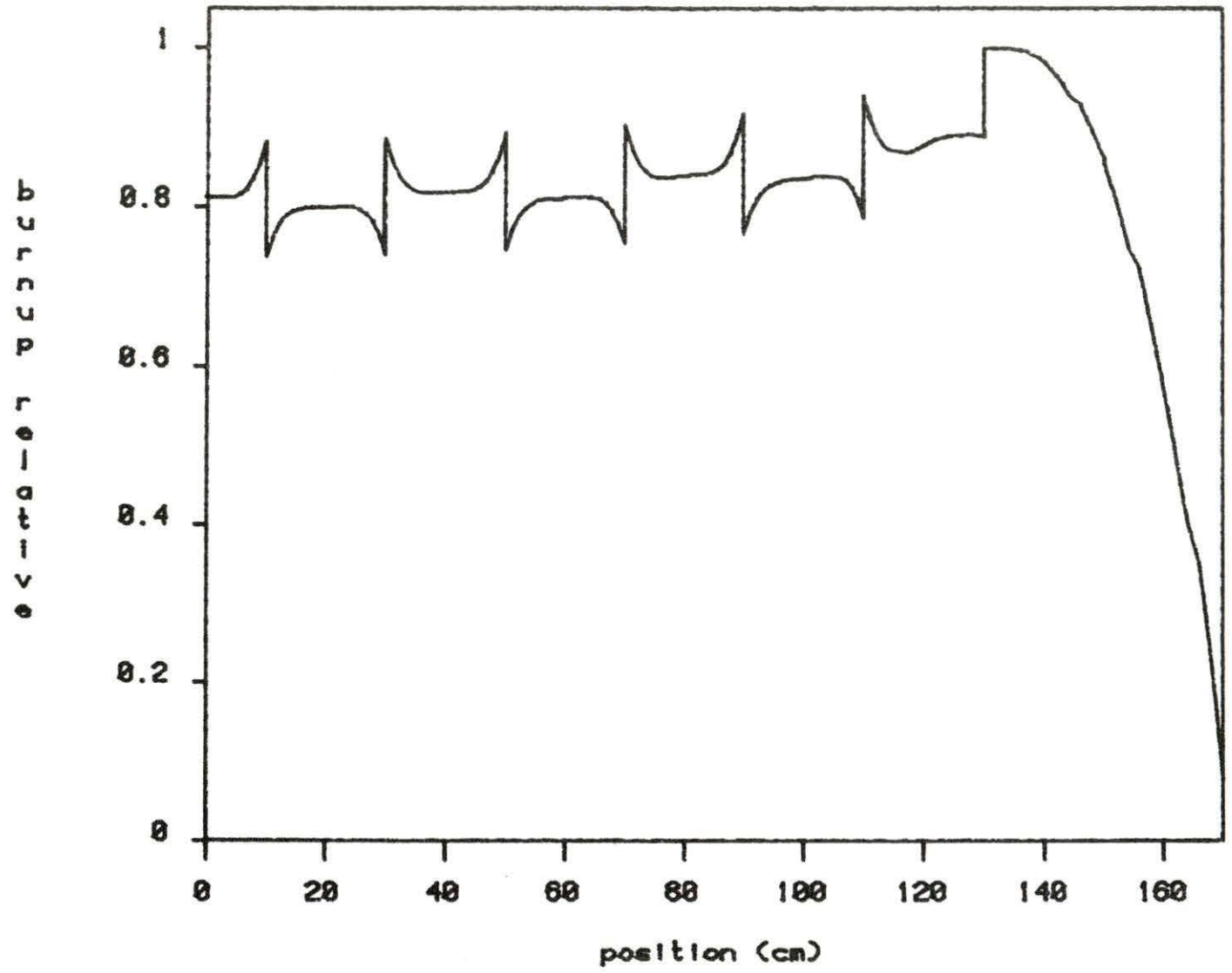

Figure 5-15. The burnup distribution at EOC for the loading pattern A

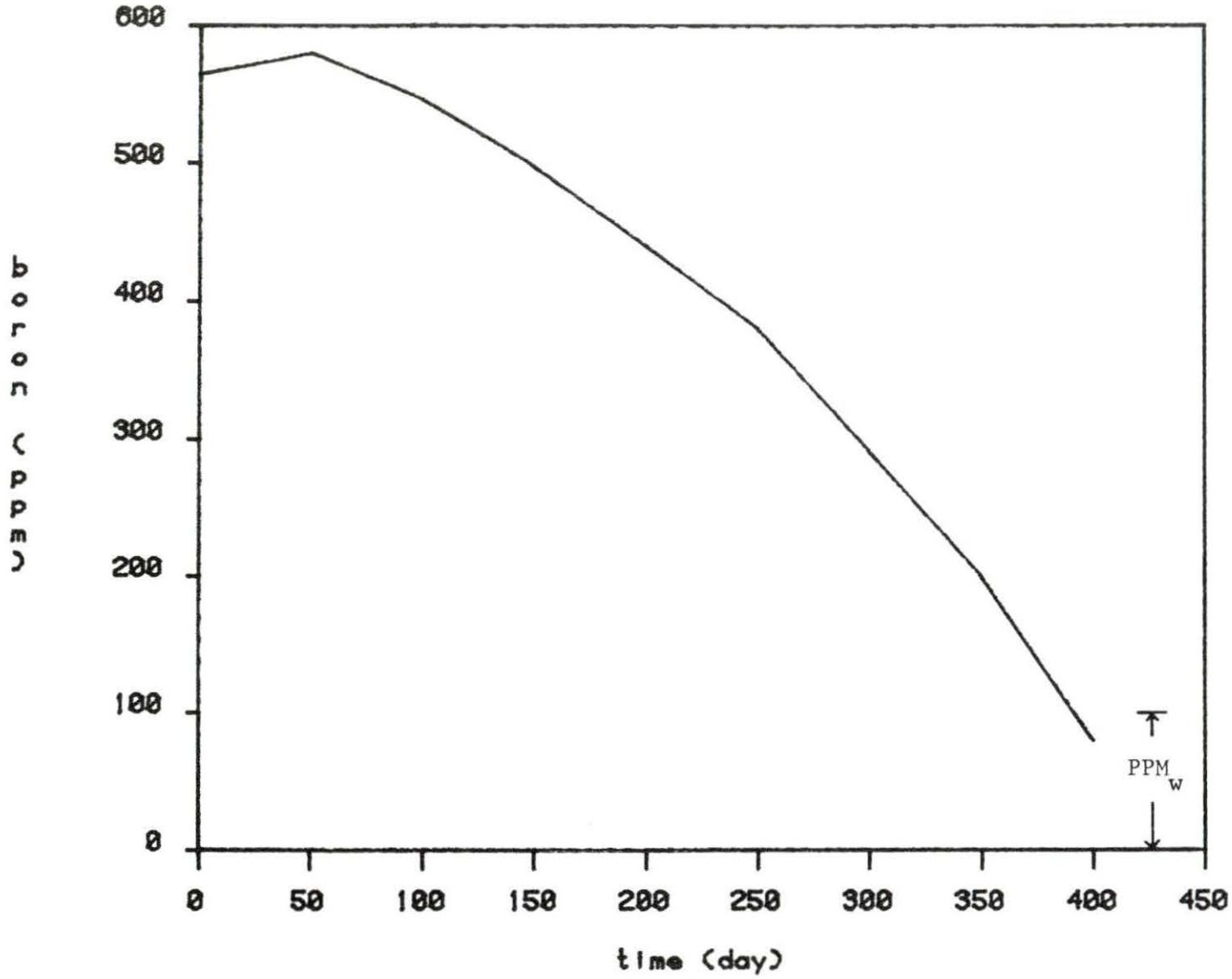

Figure 5-16. The critical boron concentration after startup for the loading pattern A

$$\frac{d^2\phi_1(x)}{dx^2} + \frac{\frac{1}{K}\nu_1\Sigma_{f1}(x) - \Sigma_{a1}(x) - \Sigma_{R1}(x)}{D_1}\phi_1(x)$$

$$+ \frac{\frac{1}{K}\nu_2\Sigma_{f2}(x)}{D_1}\phi_2(x) = 0 \qquad (5\text{-}1)$$

$$\frac{d^2\phi_2(x)}{dx^2} + \frac{\Sigma_{R1}(x)}{D_2}\phi_1(x) - \frac{\Sigma_{a2}(x)}{D_2}\phi_2(x) = 0 \qquad (5\text{-}2)$$

The comparison of these two cases for the diffusion coefficient at EOC is shown in Figure 5-17. The thermal group diffusion coefficient is identical for both cases. The fast group diffusion coefficient is almost the same for both cases. Thus, one can assume that the diffusion coefficient is not a function of x to simplify the diffusion calculation. Also note no significant differences were noted in the final results.

Figures 5-18 and 5-19 show the absorption cross section Σ_{ag} and the fission neutron generation probability $\nu_g\Sigma_{fg}$. One can observe that both are functions of x, especially at the outer region of the core.

The uniform burnup and nonuniform burnup cases were also done in this research. In the uniform burnup case, it is assumed that the average burnup (Equation 3-29) is used for each node. In the nonuniform burnup case, the burnup is a function of x (Equation 3-18) for each node. Figure 5-20 shows the comparison between the uniform burnup and the nonuniform burnup. One can note significant differences to the fuel elements which are located at the outer region of the core. Therefore, one can accumulate errors with the use of uniform burnup for

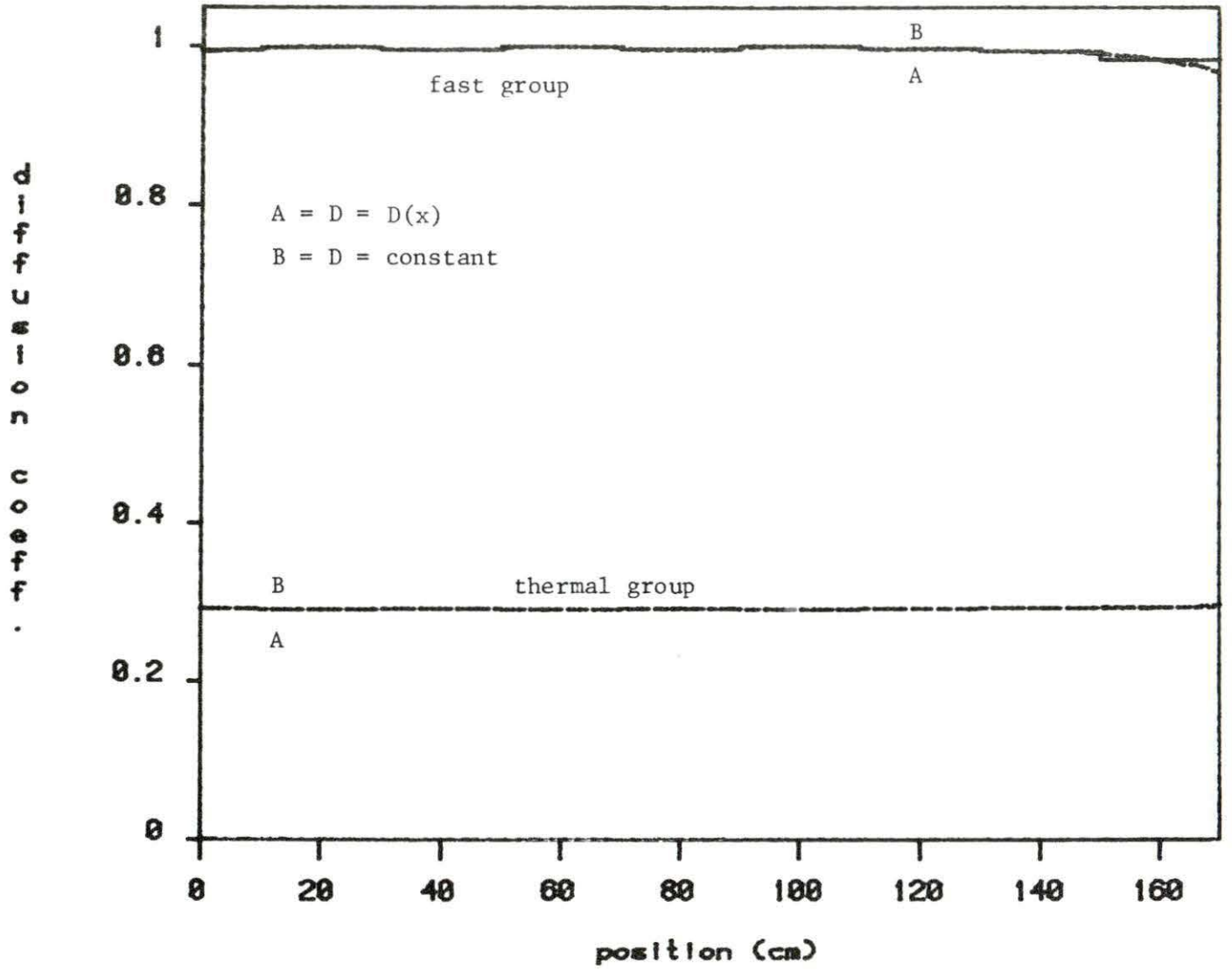

Figure 5-17. The comparison (D(x) and D = constant) of diffusion coefficient at EOC

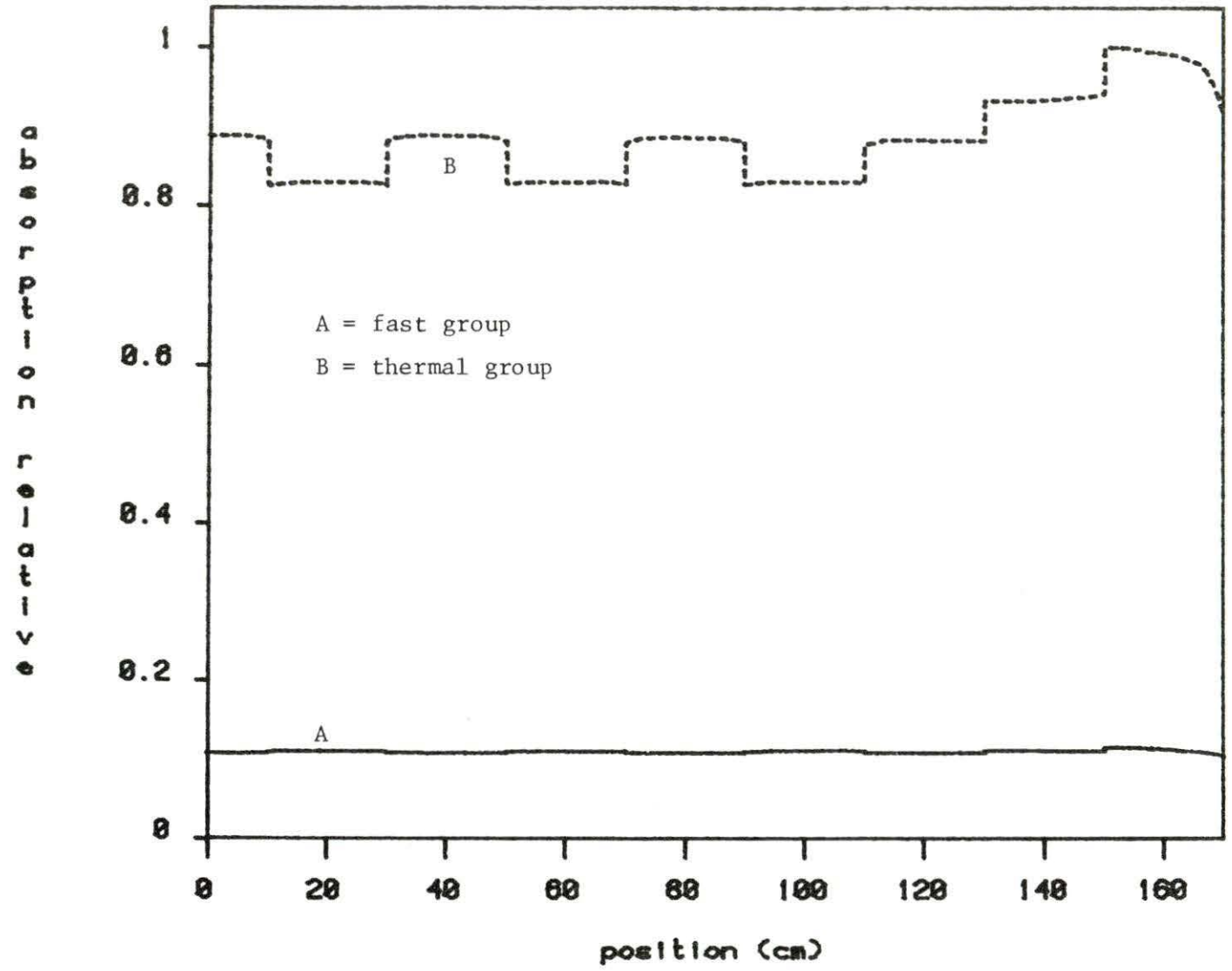

Figure 5-18. The absorption cross section Σ_{ag} at EOC

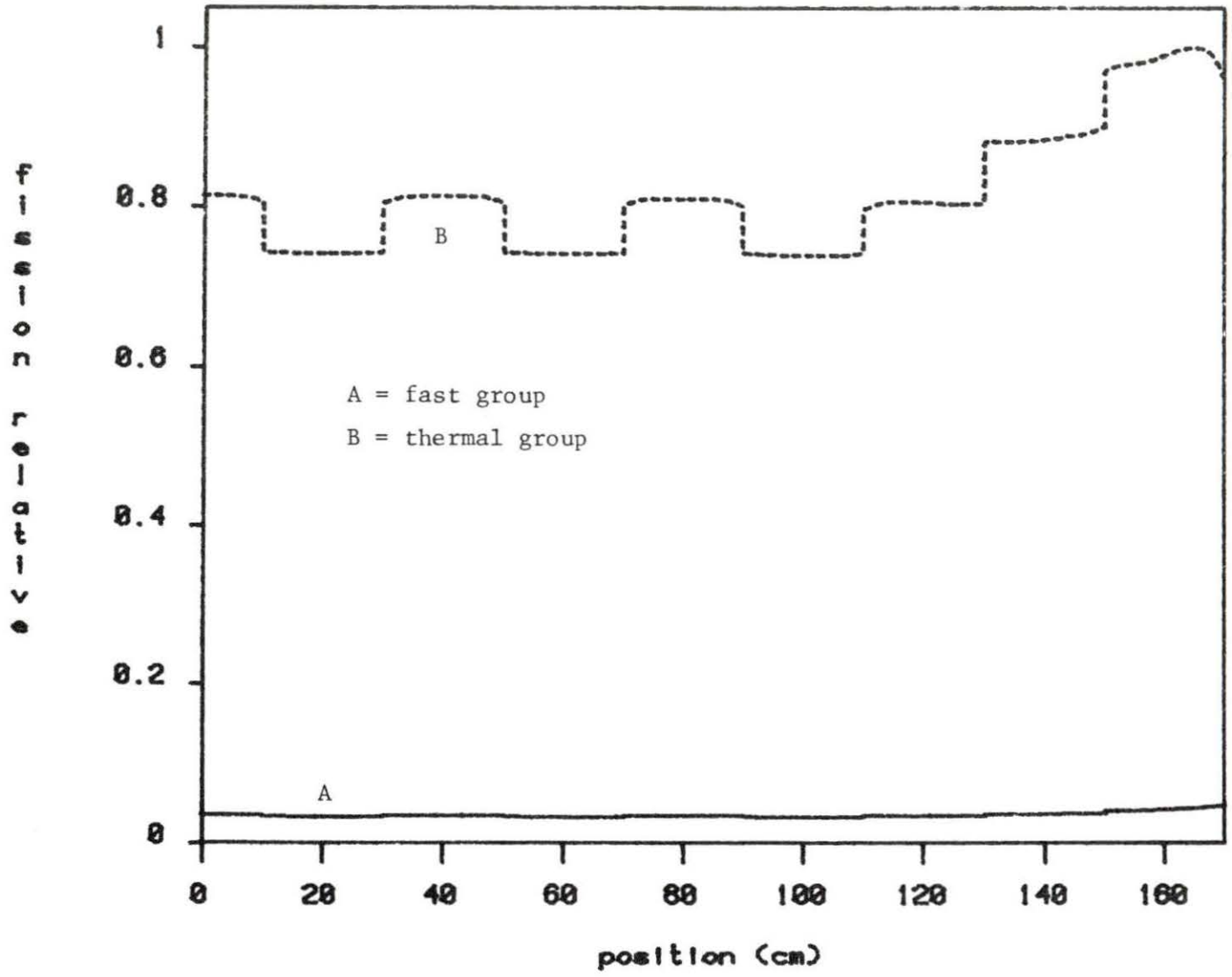

Figure 5-19. The fission neutron generalation probability $\nu_g \Sigma_{fg}$ at EOC

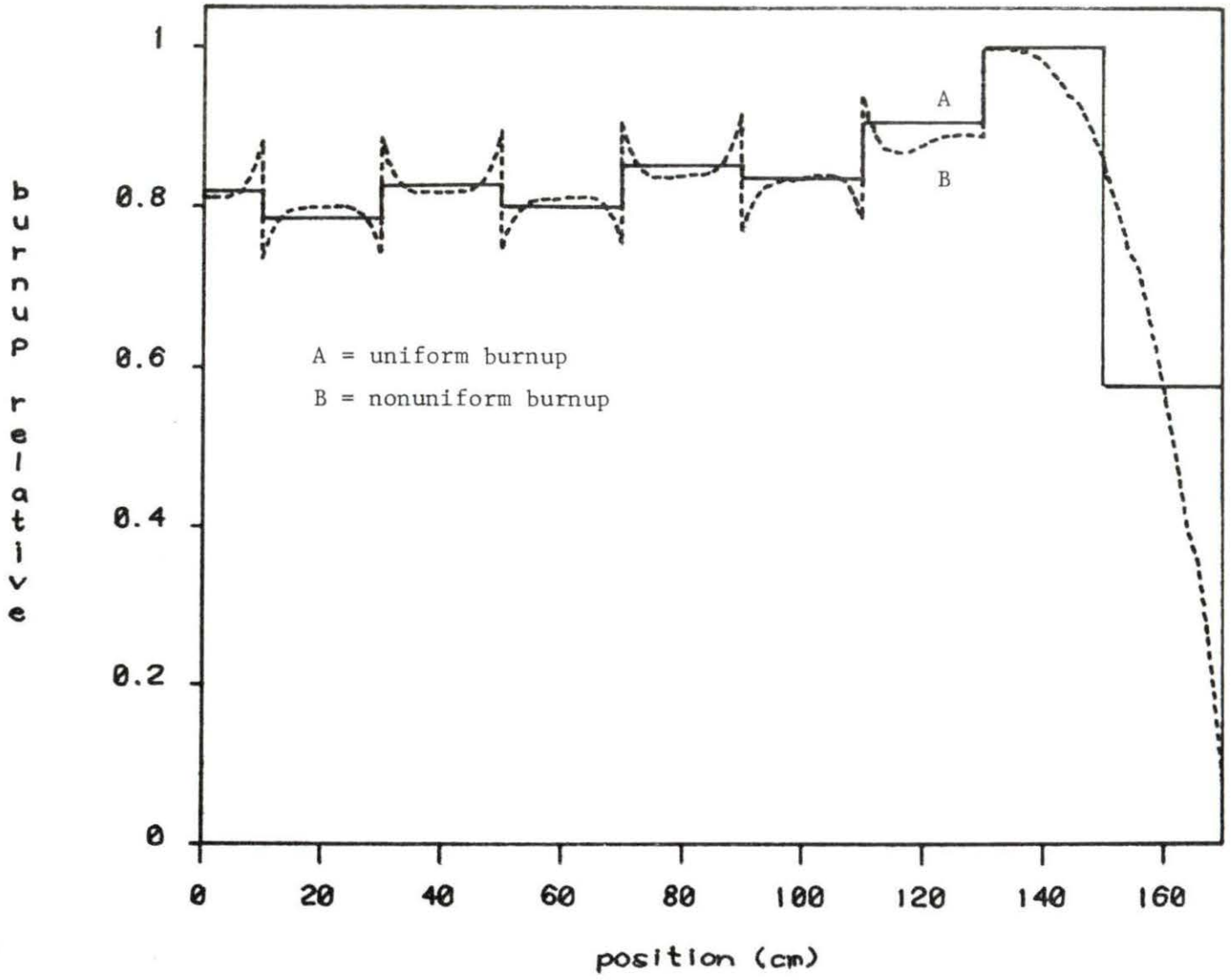

Figure 5-20. The comparison between uniform burnup and nonuniform burnup

calculations, especially in considering a reloading pattern.

Figure 5-21 shows the neutron current distribution at EOC. The continuity of neutron current along the core exists and fits the interface diffusion theory boundary condition. Figures 5-22 and 5-23 show the equation balance at EOC. The equation balance for the fast neutron group is the comparison between Equations (2-68) and (2-65), i.e.

$$\frac{d^2\phi_1(x)}{dx^2} = 2\,a_2 + 6\,a_3x + 12\,a_4x^2 \qquad (2\text{-}68)$$

$$\frac{d^2\phi_1(x)}{dx^2} = -\,C_o - C_1x - C_2x^2 - C_3x^3 - C_4x^4 \qquad (2\text{-}65)$$

The fluxes and group parameters are approximated by the fourth order polynomials. The five conditions and the least-square approximation were used to determine the coefficients of the polynomials. These approximations can be observed in Figures 5-22 and 5-23.

The flux and criticality convergence are shown in Figures 5-24 and 5-25. The log snorm (ℓ_2 norm) and the eigenvalue oscillated at the change of the boron concentration and then converged as the number of iterations increased. One can observe the above results in Figures 5-24 and 5-25.

The vacuum boundary conditions were used for the above calculation. A reflector is very important in reactor operation because it can reduce the critical size of a reactor and the maximum to average flux ratio. A boundary concept which approximates a neutron reflector is the use of an albedo boundary condition. Thus, the albedo boundary

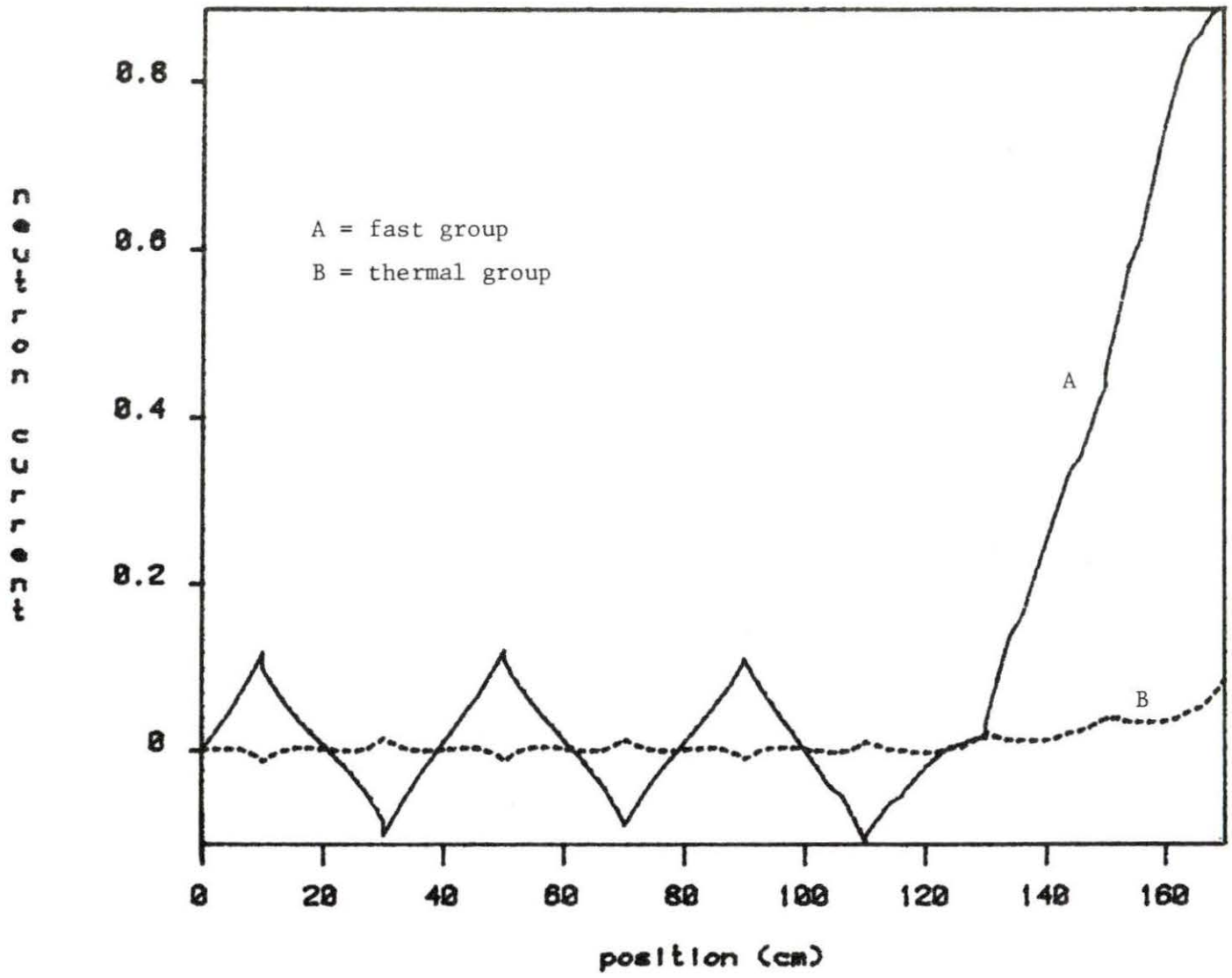

Figure 5-21. The neutron current distribution at EOC

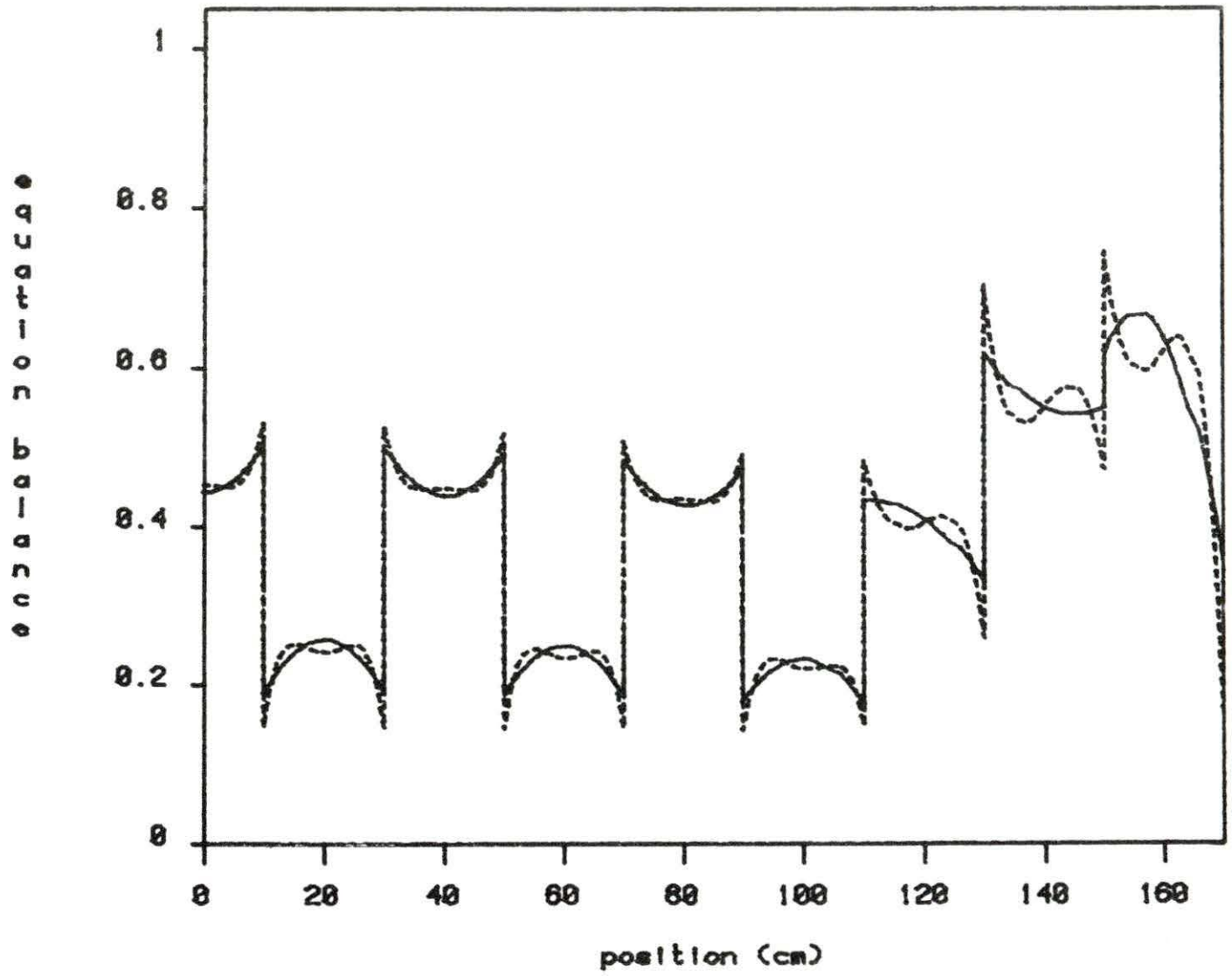

Figure 5-22. The equation balance for fast group neutron

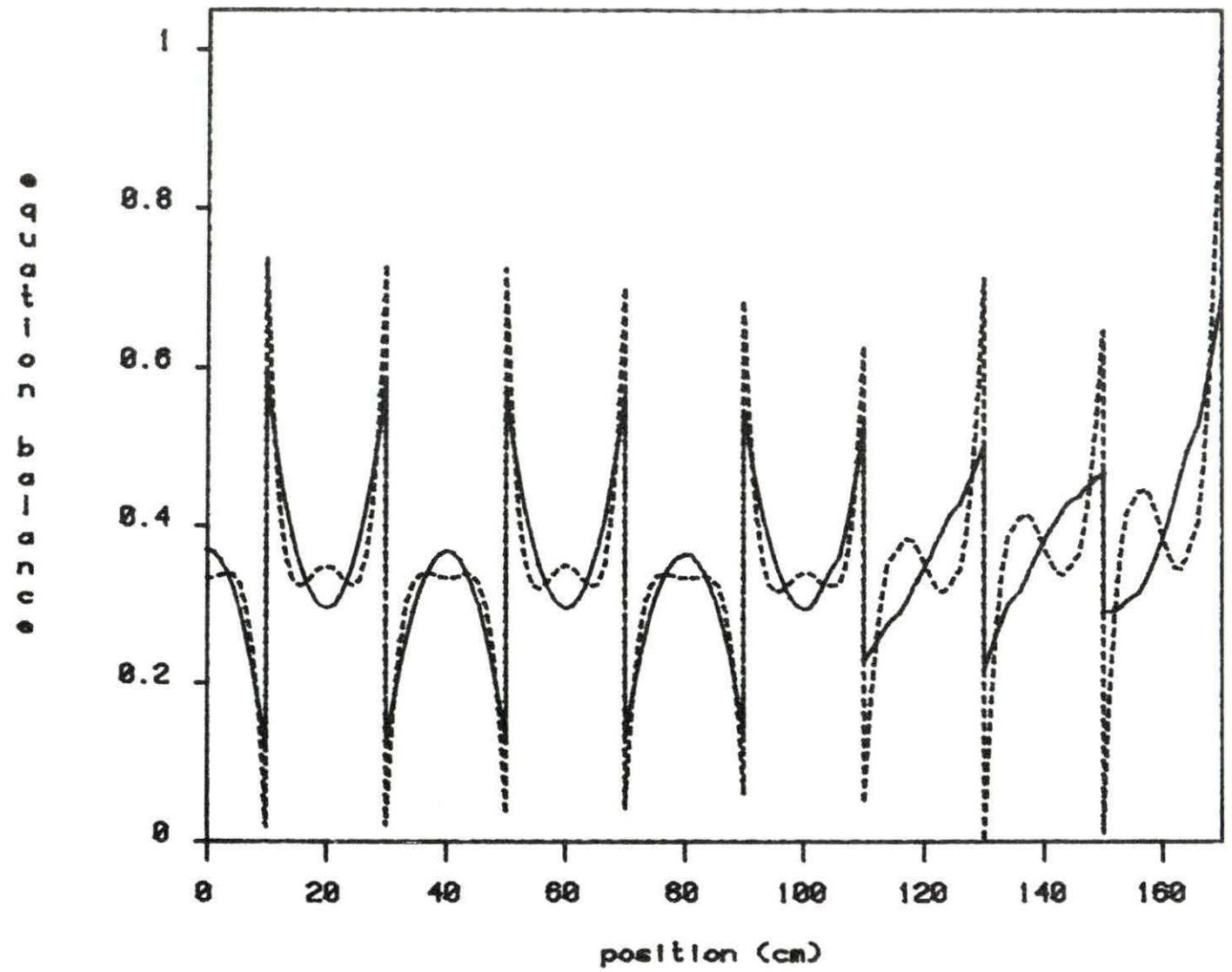

Figure 5-23. The equation balance for thermal group neutron

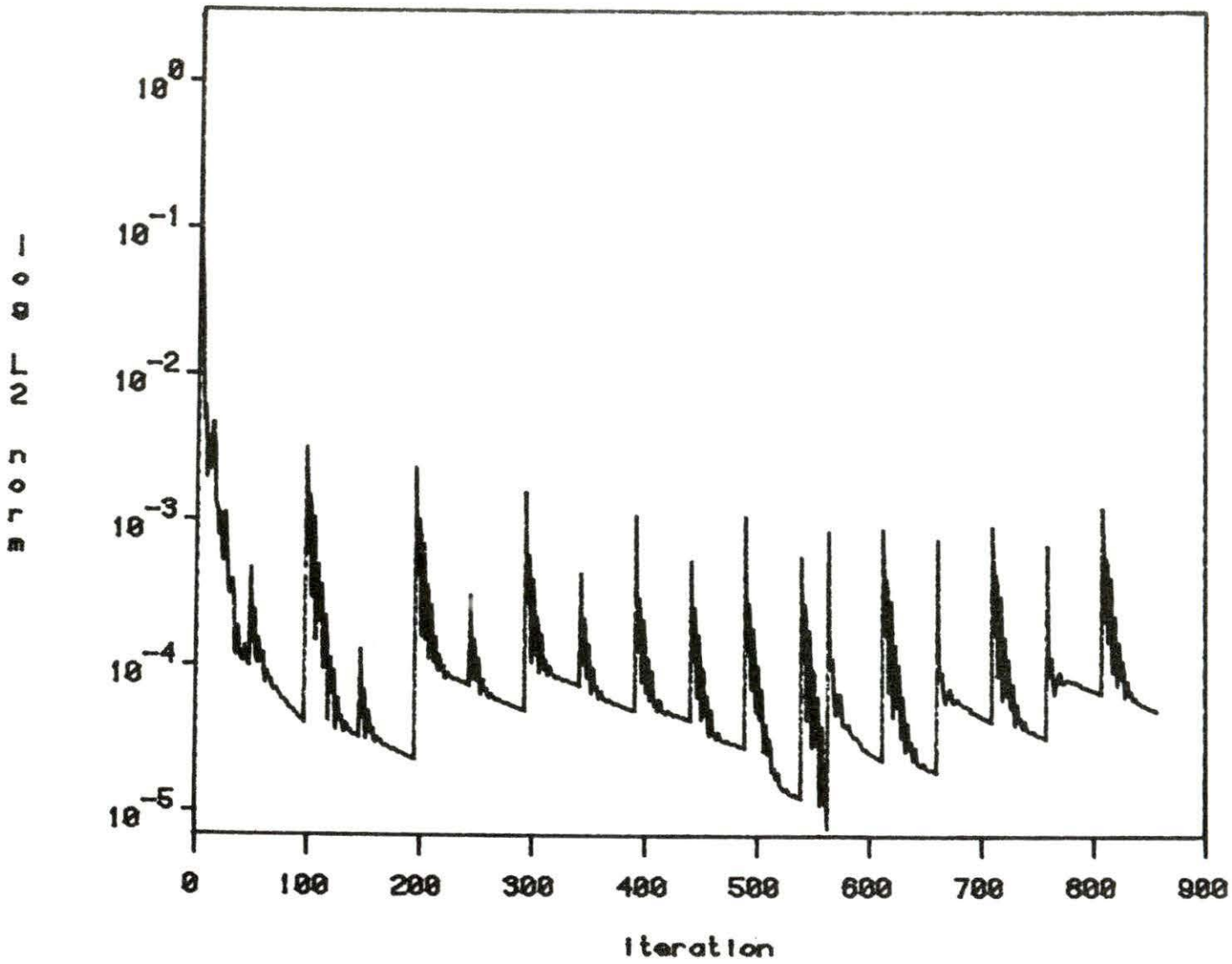

Figure 5-24. The convergence of flux

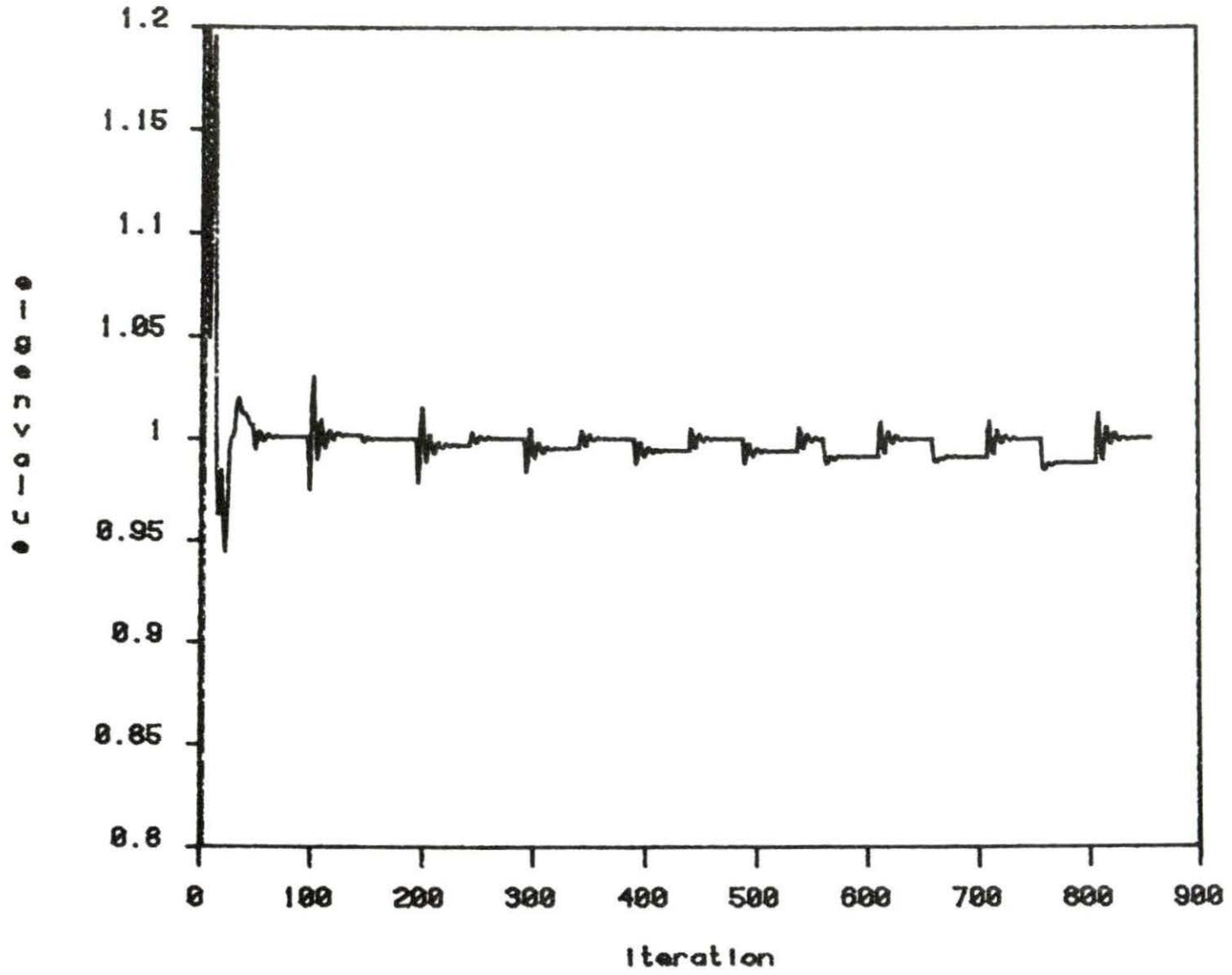

Figure 5-25. The convergence of criticality

condition was used for the following calculations. Another fuel loading pattern B in a one-dimensional model is shown in Figure 5-26. The group parameters for fuel type 7, which are loaded on the periphery of the core, were calculated from the interpolation technique

$$N_7 = N_{I+1} + \frac{(N_{I+1} - N_I)\ (ER_o - ER_{I+1})}{ER_{I+1} - ER_I} \qquad (5\text{-}3)$$

where N_{I+1} = the known group parameters of enrichment ER_{I+1} and

N_I = the known group parameters of enrichment ER_I.

In order to get a flattened power distribution in a core, the enrichment of fuel type 7 needed to be estimated. After several calculations, a 2% enrichment of fuel 7 gave acceptable results. The flux and power distribution at BOC and EOC are shown in Figures 5-27 through 5-30. One can observe that both distributions show some improvements, especially in the outer region of the core, even using the lower enriched fuel. This behavior results from using the albedo boundary condition, i.e. a reflector simulated on the outer side of the core.

Figure 5-31 shows the burnup distribution at EOC. The burnup in the outer region of the core is less than that in the center of the core and has a negative gradient, i.e. the burnup on the left side is greater than that on the right side of these fuel elements. Thus, a fuel reloading plan is also considered in this research.

Many variables and constraints [2] affect a fuel reloading plan in the reactor. Only the multiplication factor K_∞ for each fuel is considered here. The definition of K_∞ is [3]

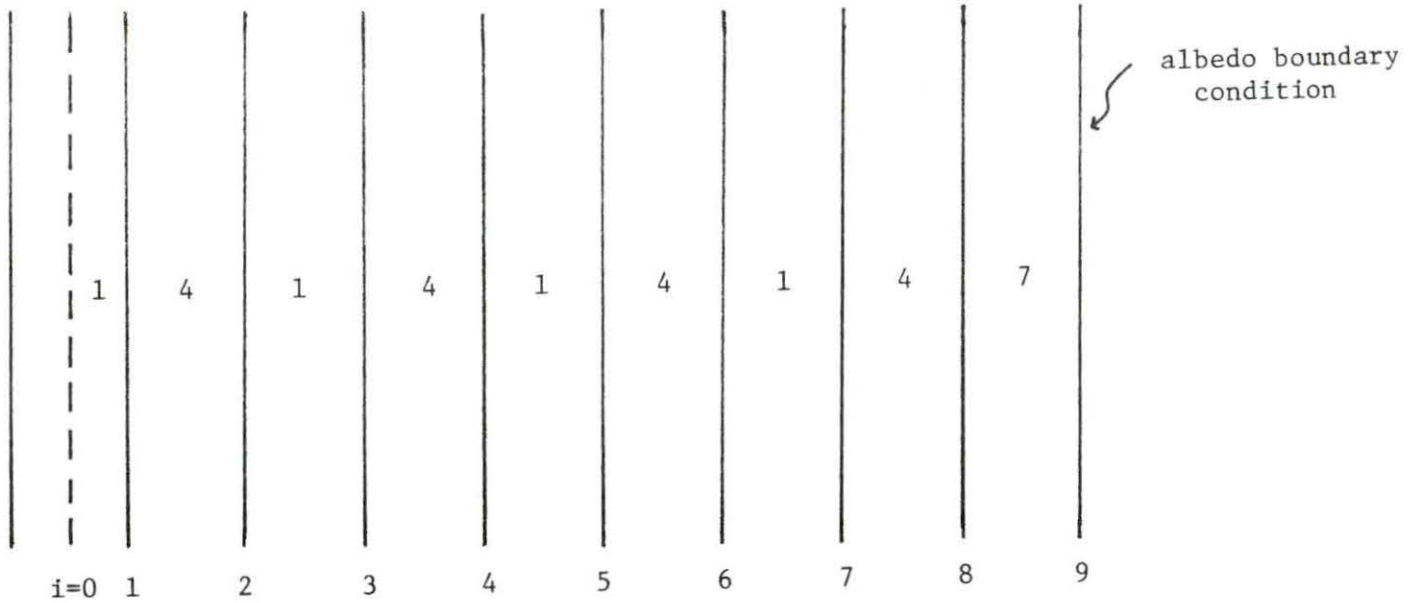

Figure 5-26. The fuel loading pattern B in one-dimensional model with albedo boundary condition

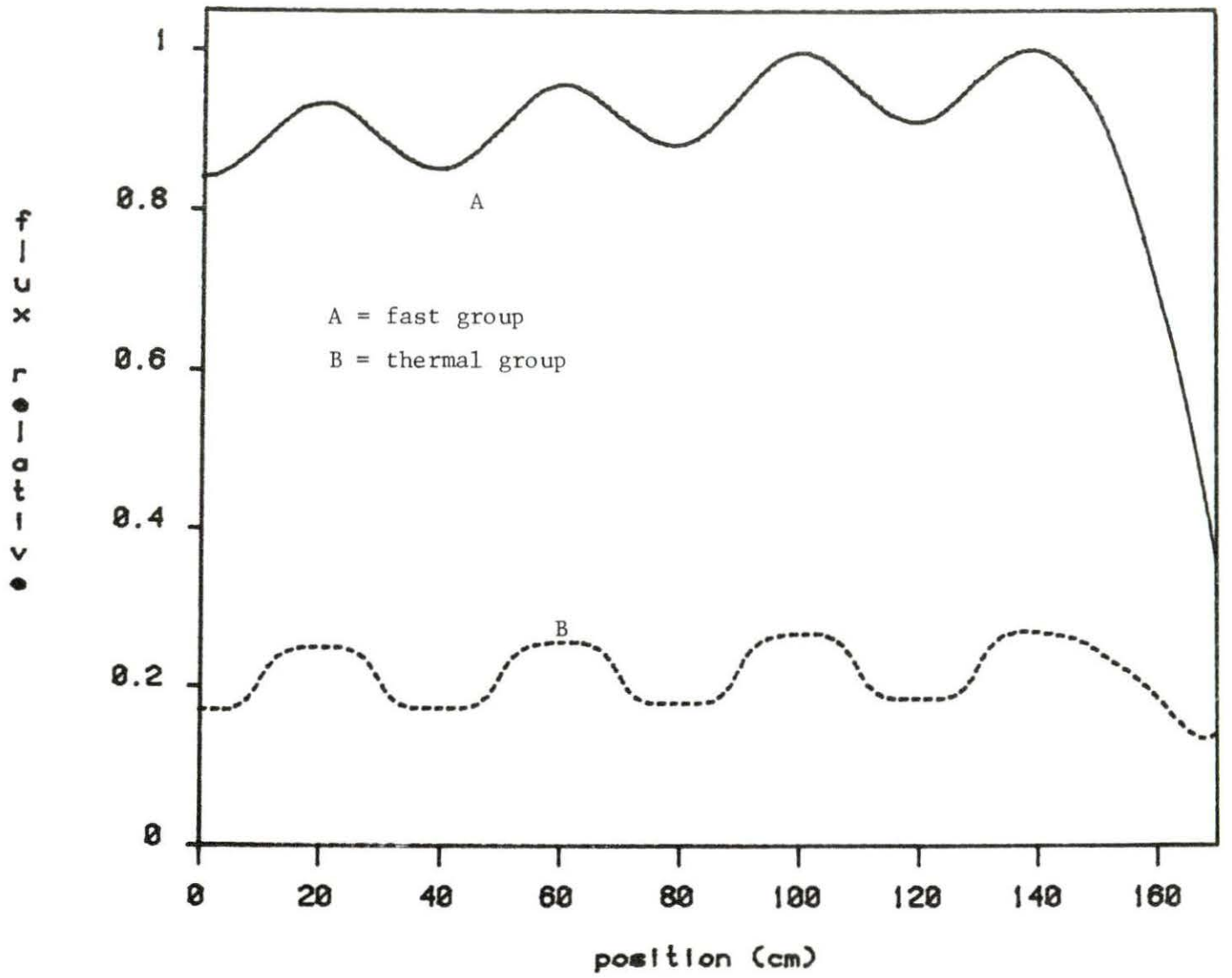

Figure 5-27. The flux distribution at BOC for loading pattern B

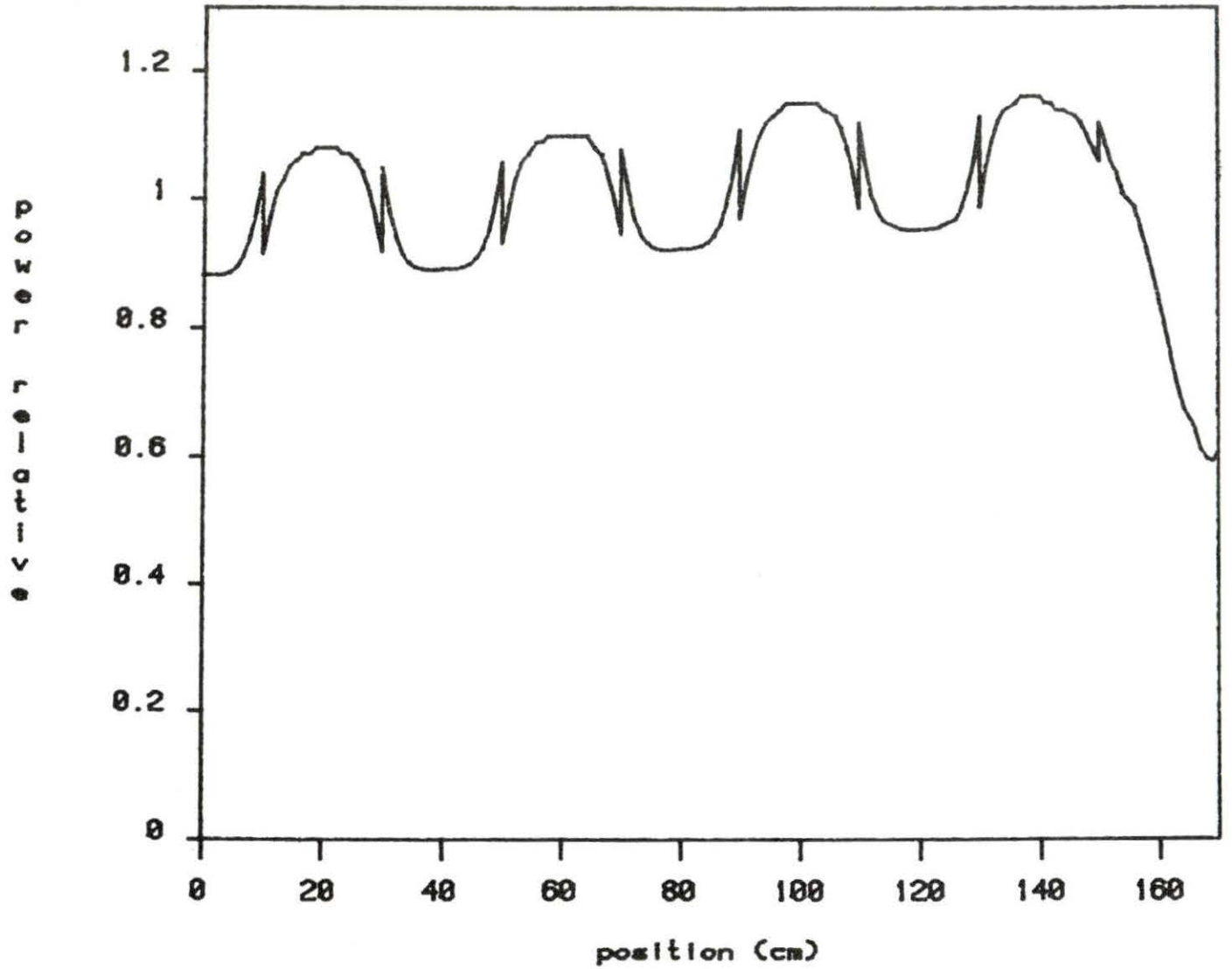

Figure 5-28. The power distribution at BOC for loading pattern B

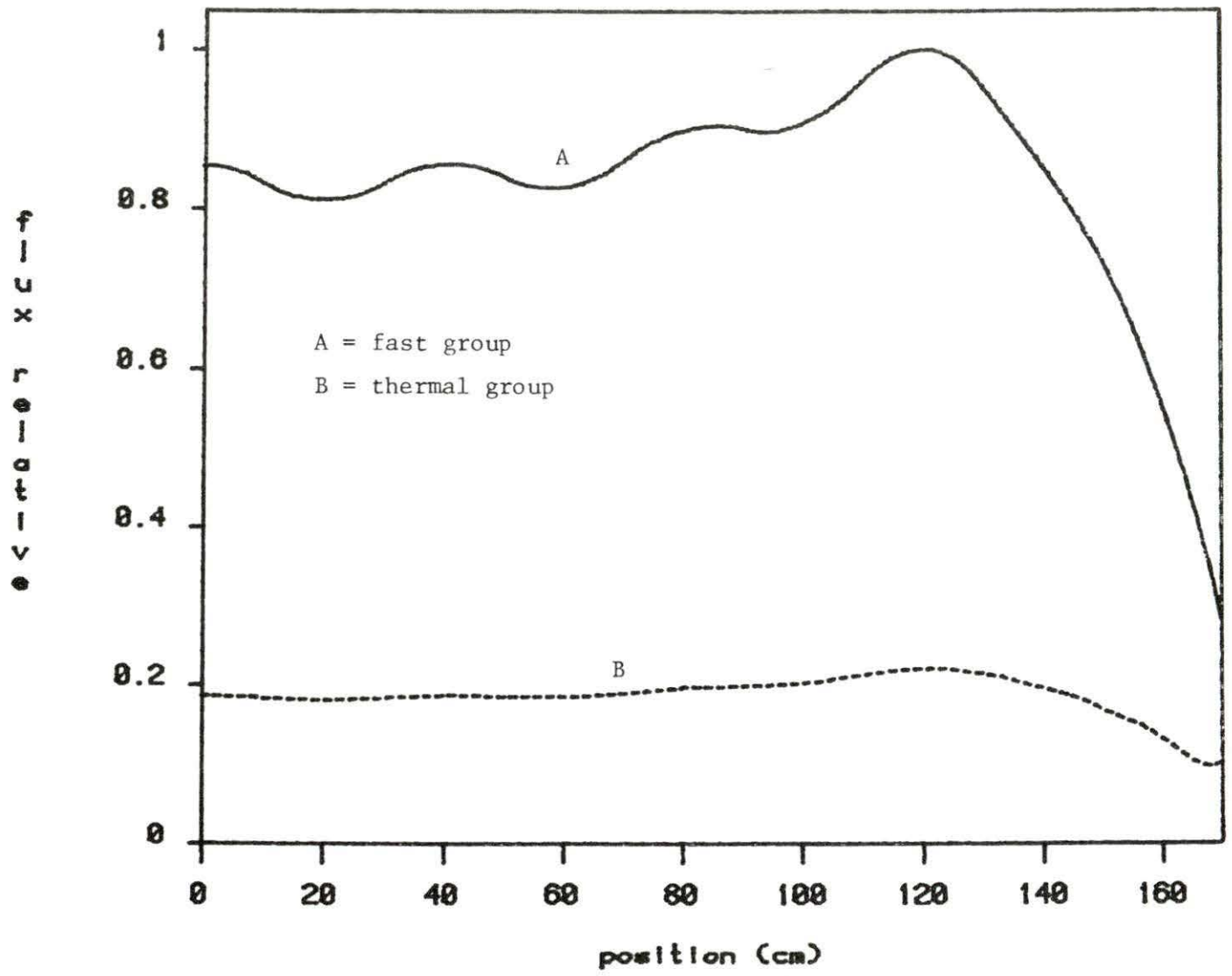

Figure 5-29. The flux distribution at EOC for loading pattern B

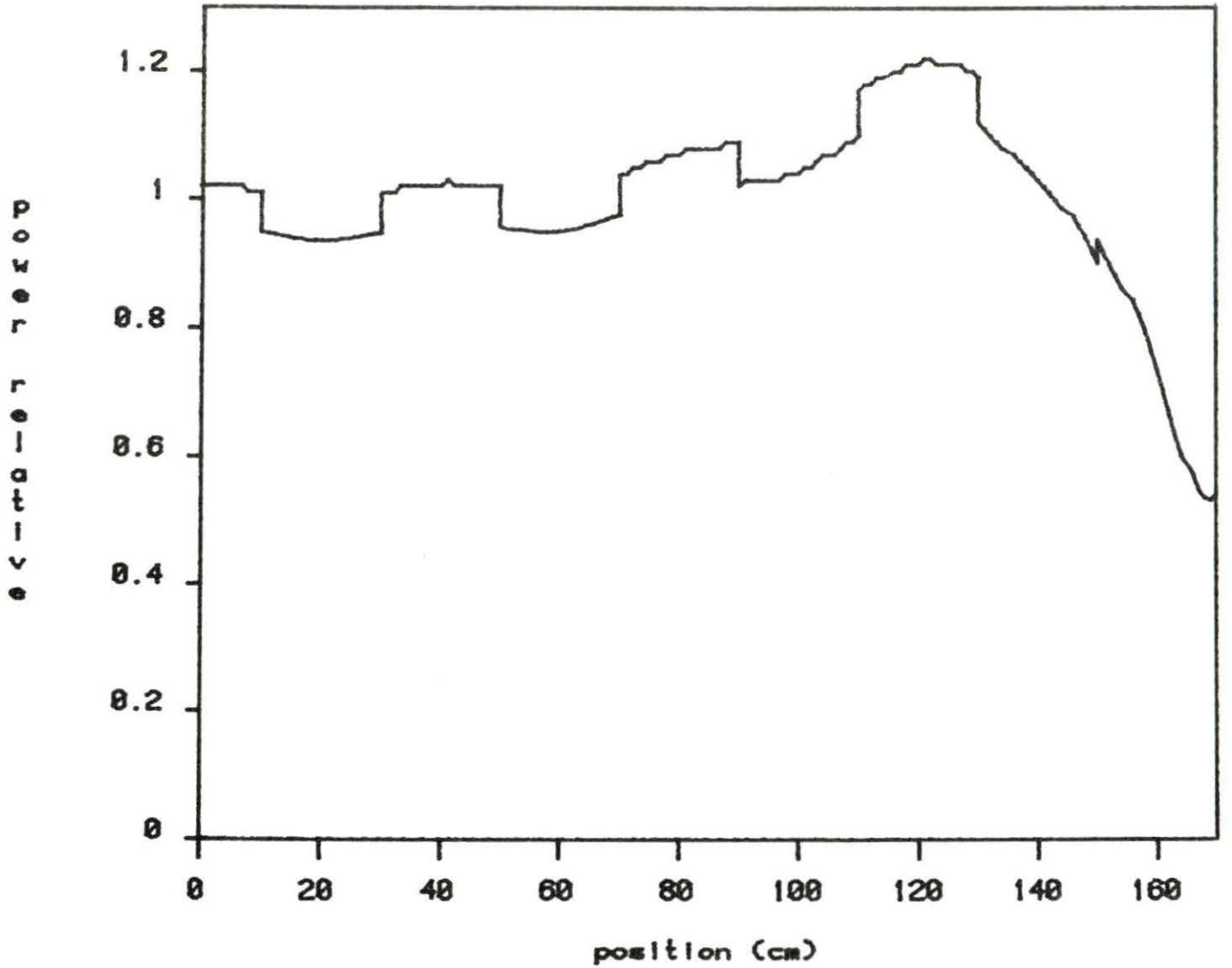

Figure 5-30. The power distribution at EOC for loading pattern B

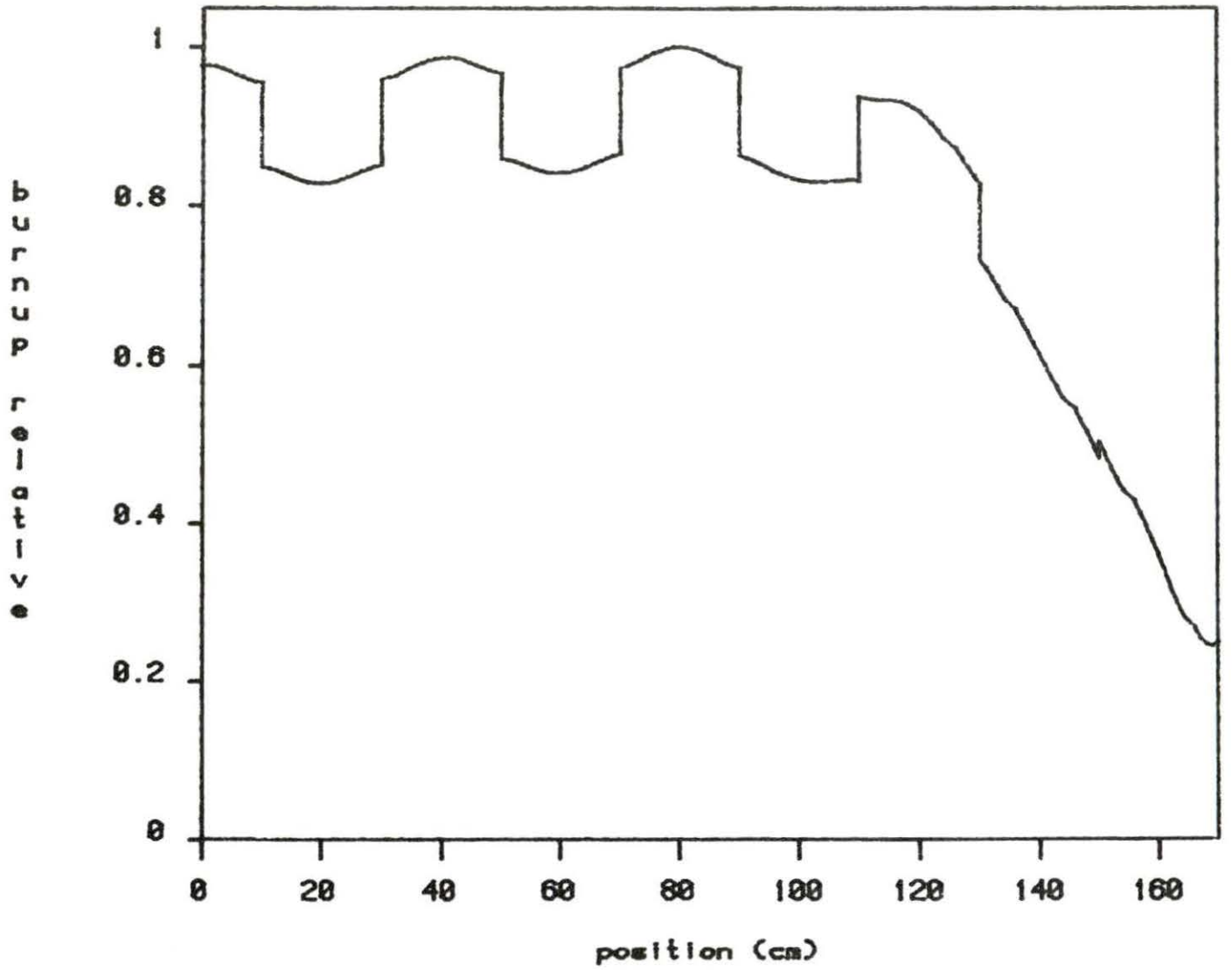

Figure 5-31. The burnup distribution at EOC for loading pattern B

$$K_{\infty} = \frac{\text{Rate of neutron production}}{\text{Rate of neutron loss}} \Big|_{\text{infinite region}}$$

$$= \frac{\sum_{g=1} \nu_g \Sigma_{fg} \phi_g}{\sum_{g=1} \Sigma_{ag} \phi_g} \qquad (5\text{-}4)$$

The K_{∞} at EOC for each fuel is shown in Table 5-2.

Table 5-2. The multiplication factor K_{∞} at EOC for each fuel element

Fuel location	Fuel type	K_{∞}
1	1	1.0279
2	4	0.9741
3	1	1.0252
4	4	0.9721
5	1	1.0216
6	4	0.9738
7	1	1.0462
8	4	1.0122
9	7	1.0844

The K_{∞} of fuel at locations 2, 4 and 6 are less than 1.0. These fuel elements are also the elements which do not contain burnable poison Thus, these fuel elements are replaced by fuel from the outer region (location 9), and a fresh fuel element (type 7) is added to location 9.

The rest of the fuel elements remain in their previous locations. The fuel reloading pattern C is shown in Figure 5-32. The symbol '-' means a once-burnup fuel.

Figures 5-33 and 5-34 show the flux and power distribution at BOSC (beginning of the second cycle). Figure 5-35 shows the burnup distribution at BOSC. One can observe that the burnup at location 9 is zero because of the fresh fuel without burnup. Figures 5-36 through 5-38 show the flux, power and burnup distributions at EOSC (end of the second cycle). One can observe that the distribution at EOSC does not change very much from each distribution at BOSC. This behavior results from a short second cycle. This short second cycle can be improved by using and reloading higher enrichment or burnable poison fuels for the second cycle.

One can recall that the fuel burnup in the outer region of the core has a negative gradient at the end of the first cycle (Figure 5-31) and these fuels were reloaded into the second cycle. For actual reactor operation, uniform burnup of fuel is desirable before it is unloaded from the core. Thus, a loading pattern of rotated fuel is considered. The rotated fuel is such that the side of low burnup is placed opposite the center of the core. Figure 5-32 shows the fuel reloading pattern D. The symbol '-' means that the reloaded fuel is rotated.

The flux, power and burnup distribution at BOSC are shown in Figures 5-39 through 5-41. One can note that the gradient burnup at locations 2, 4, 6 and 8 becomes positive because of the rotated fuel. Figures 5-42 through 5-44 show the flux, power and burnup distribution

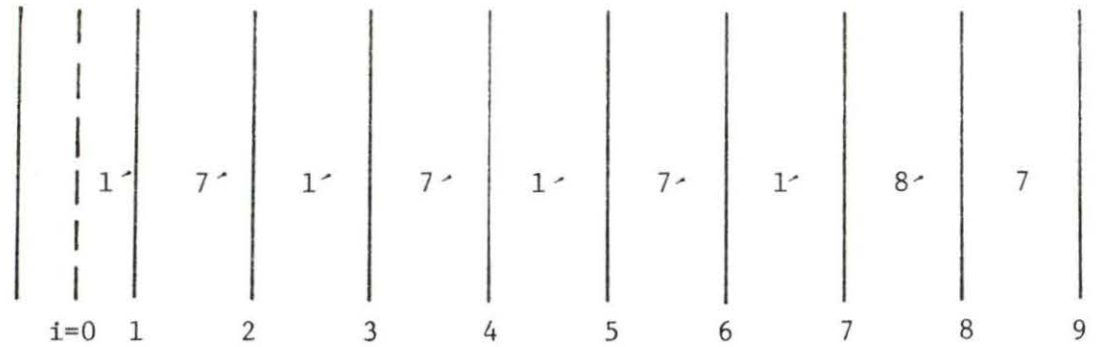

Pattern C

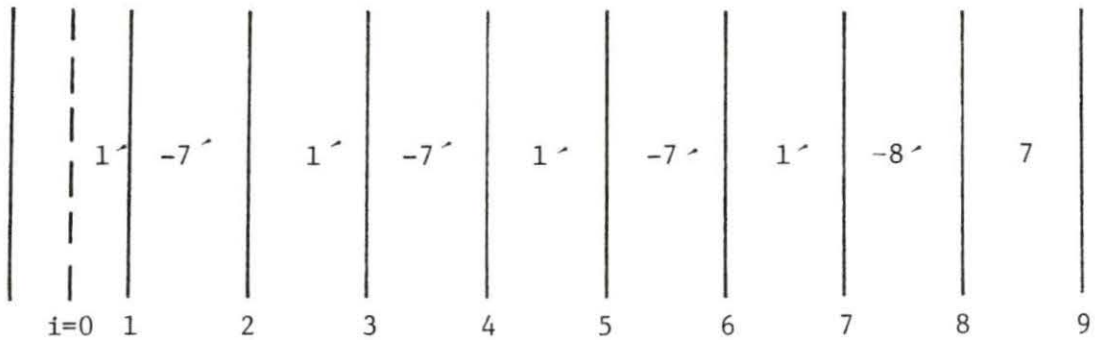

Pattern D

Figure 5-32. Fuel reloading patterns C and D

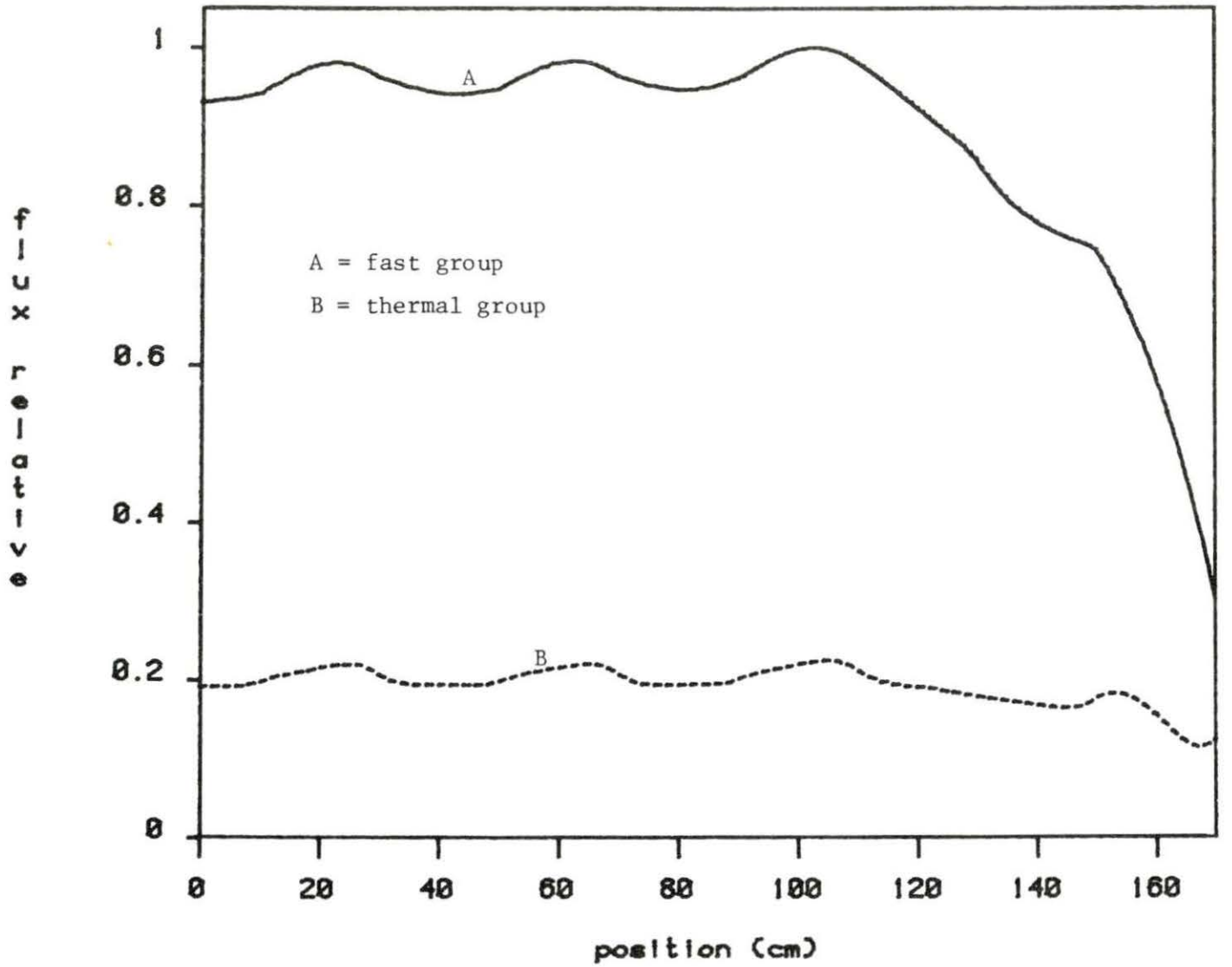

Figure 5-33. The flux distribution at BOSC for reloading pattern C

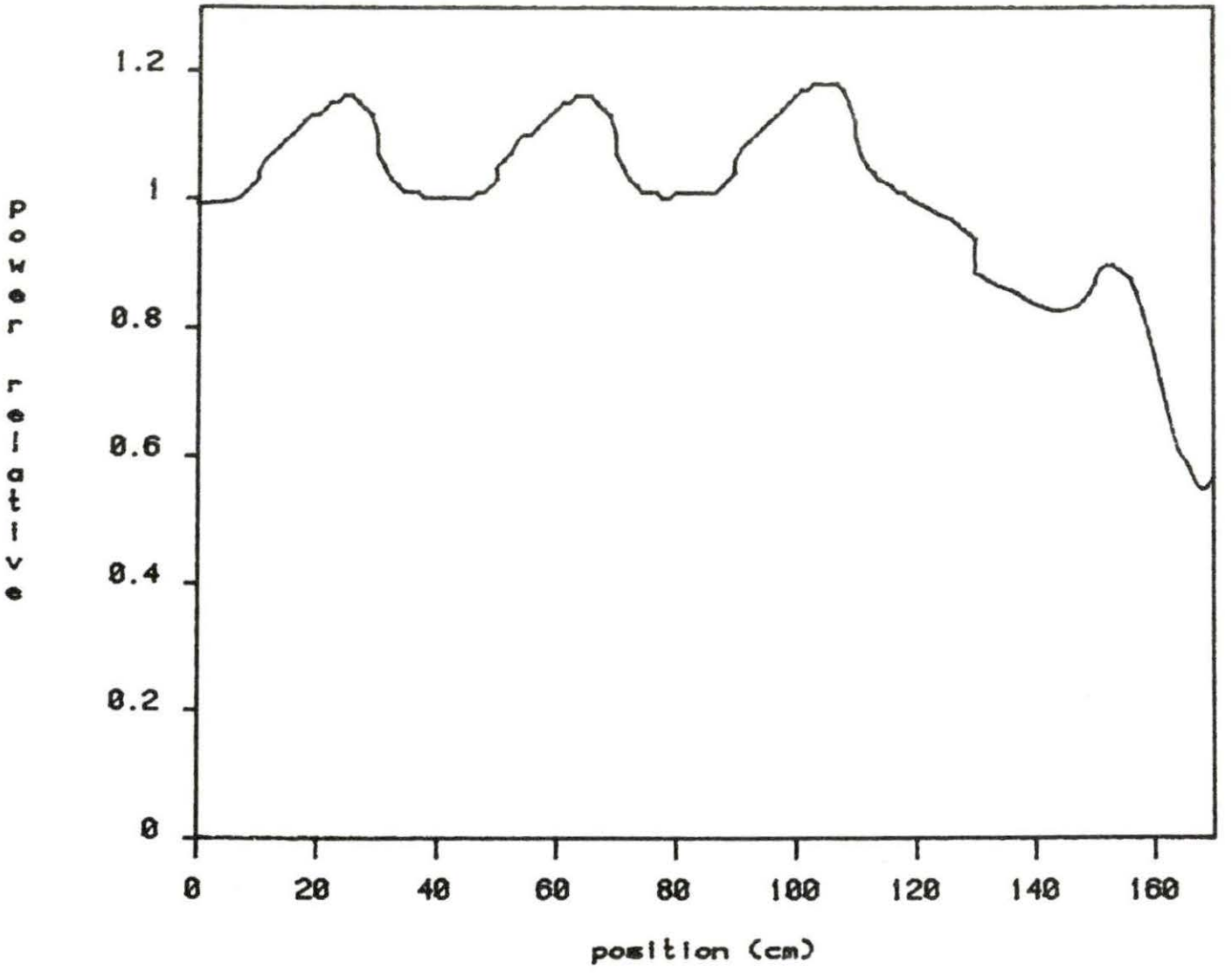

Figure 5-34. The power distribution at BOSC for reloading pattern C

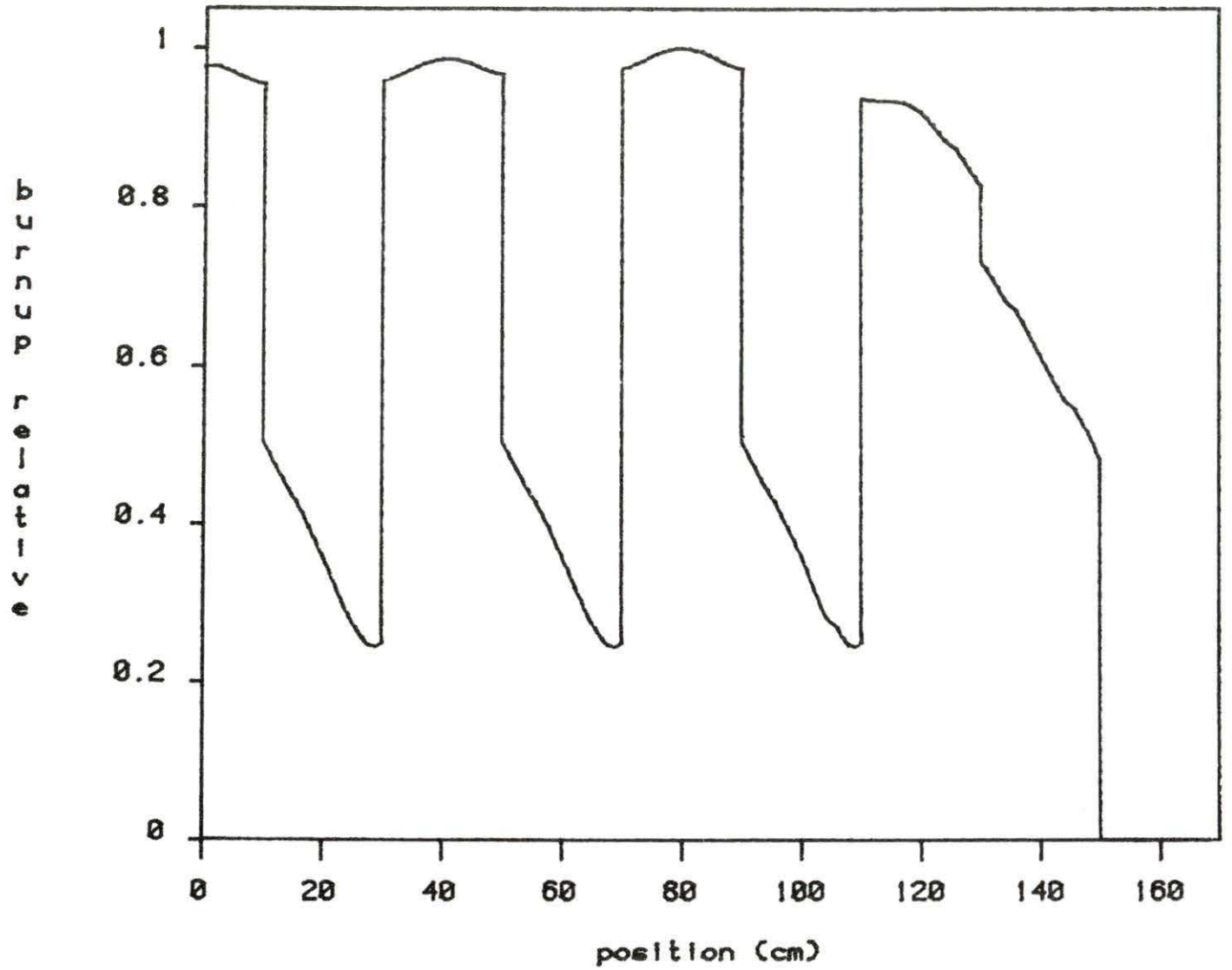

Figure 5-35. The burnup distribution at BOSC for reloading pattern C

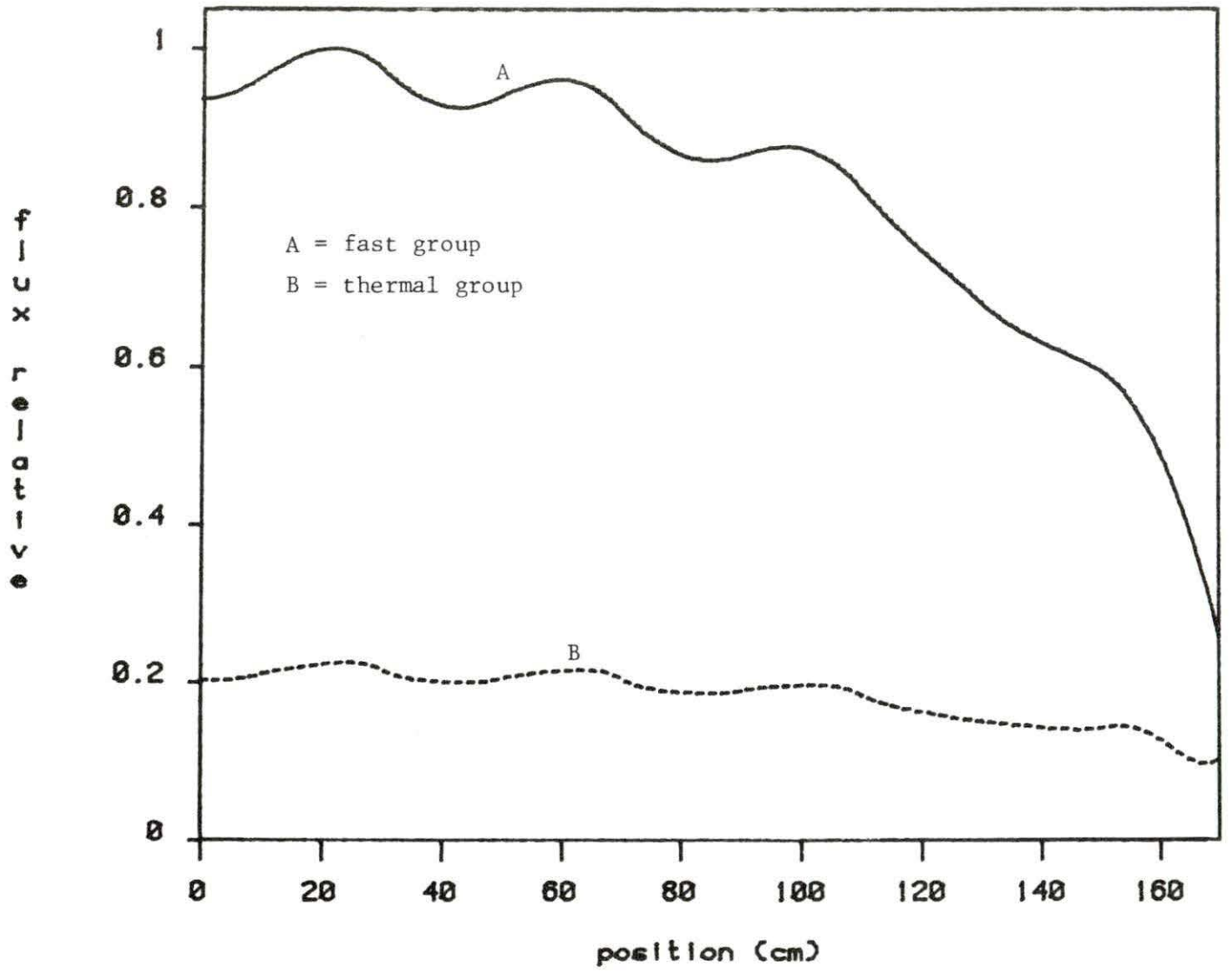

Figure 5-36. The flux distribution at EOSC for reloading pattern C

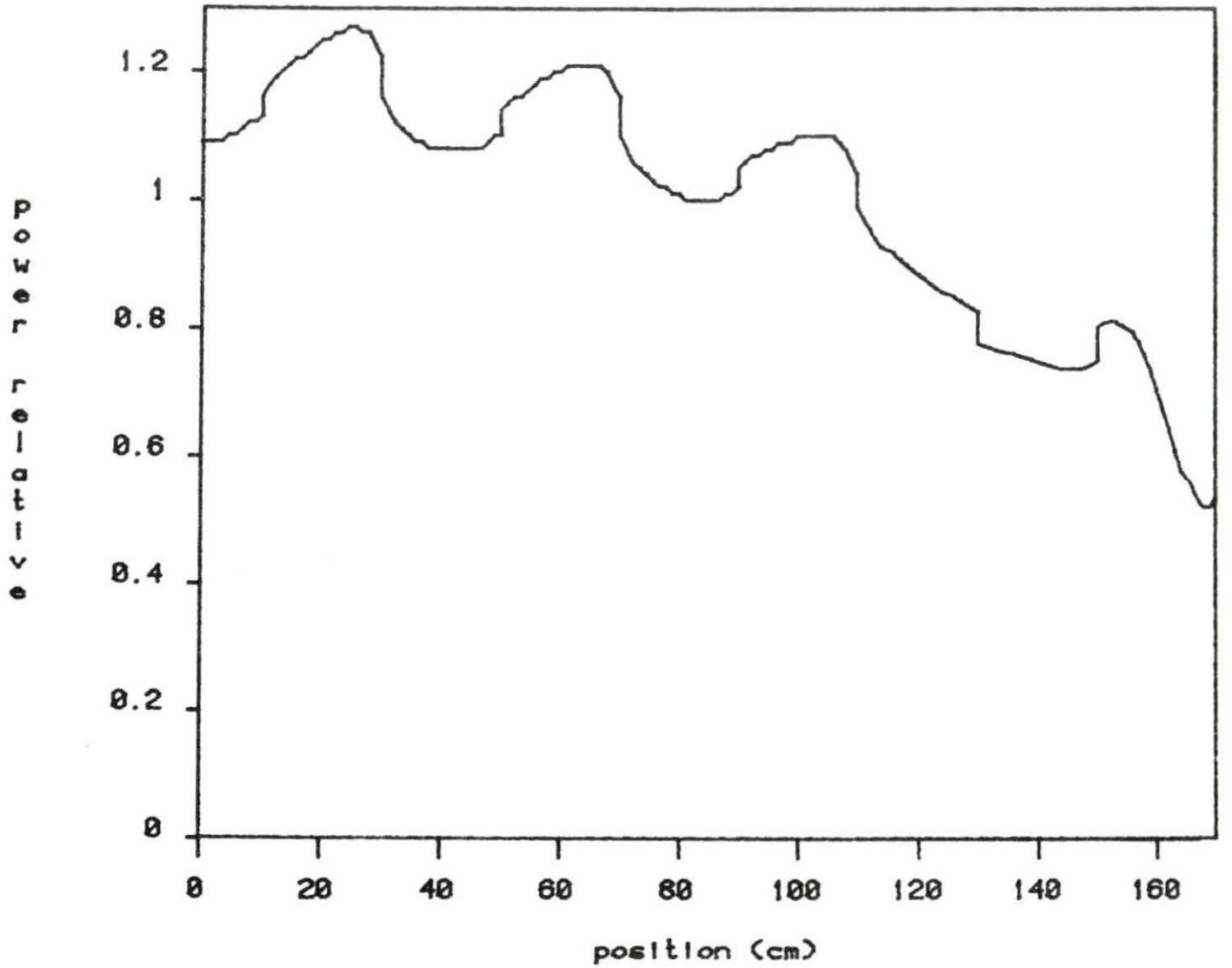

Figure 5-37. The power distribution at EOSC for reloading pattern C

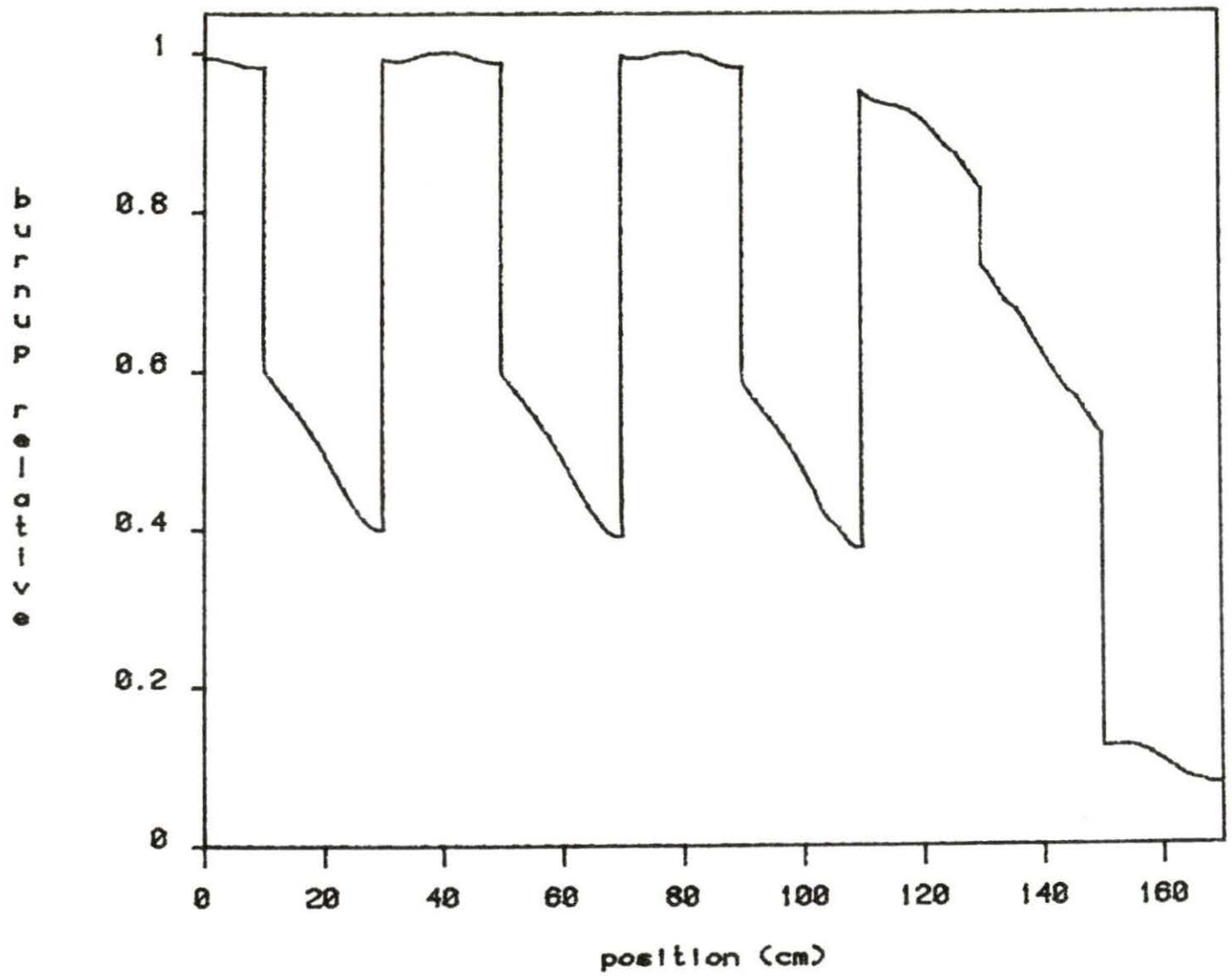

Figure 5-38. The burnup distribution at EOSC for reloading pattern C

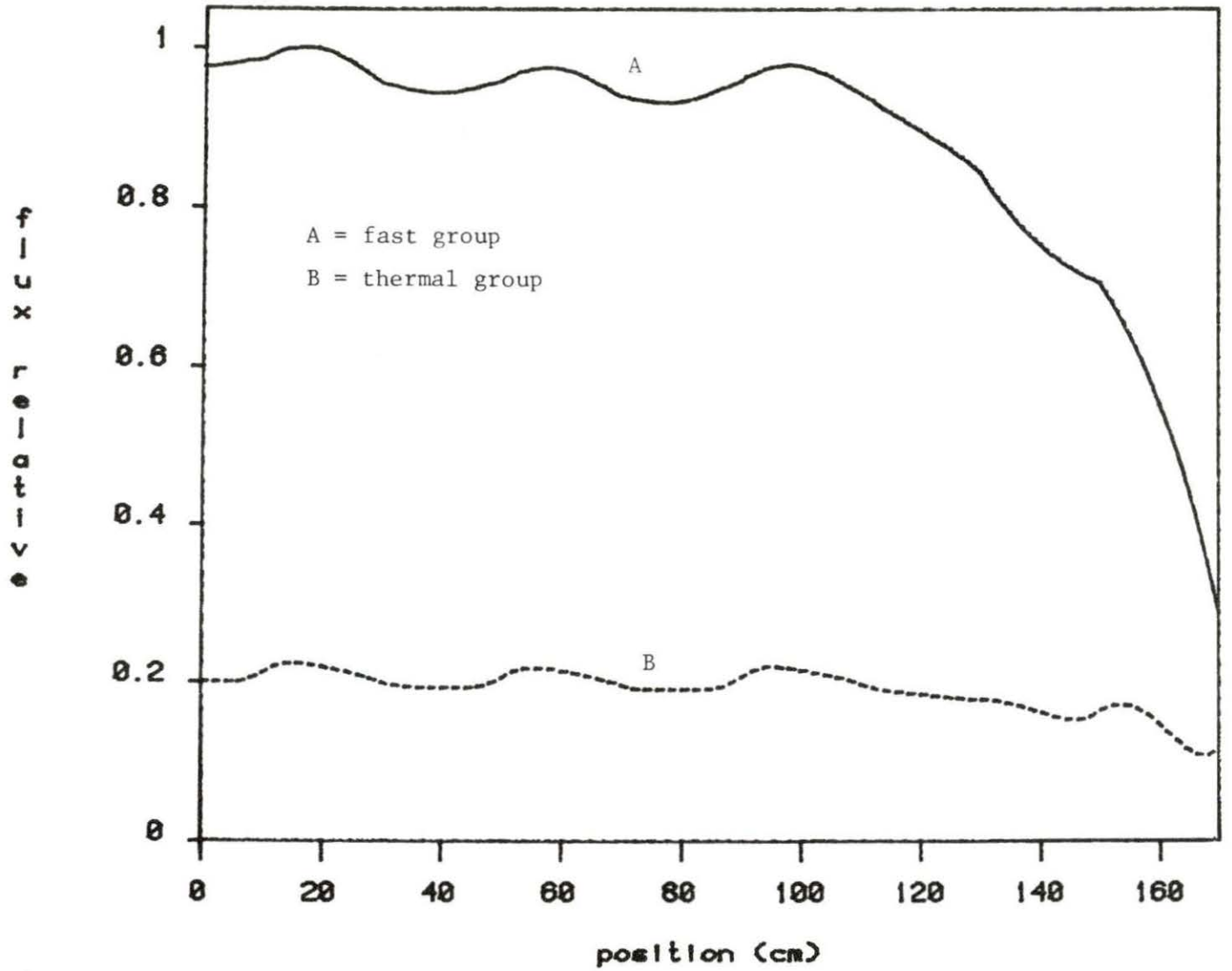

Figure 5-39. The flux distribution at BOSC for reloading pattern D

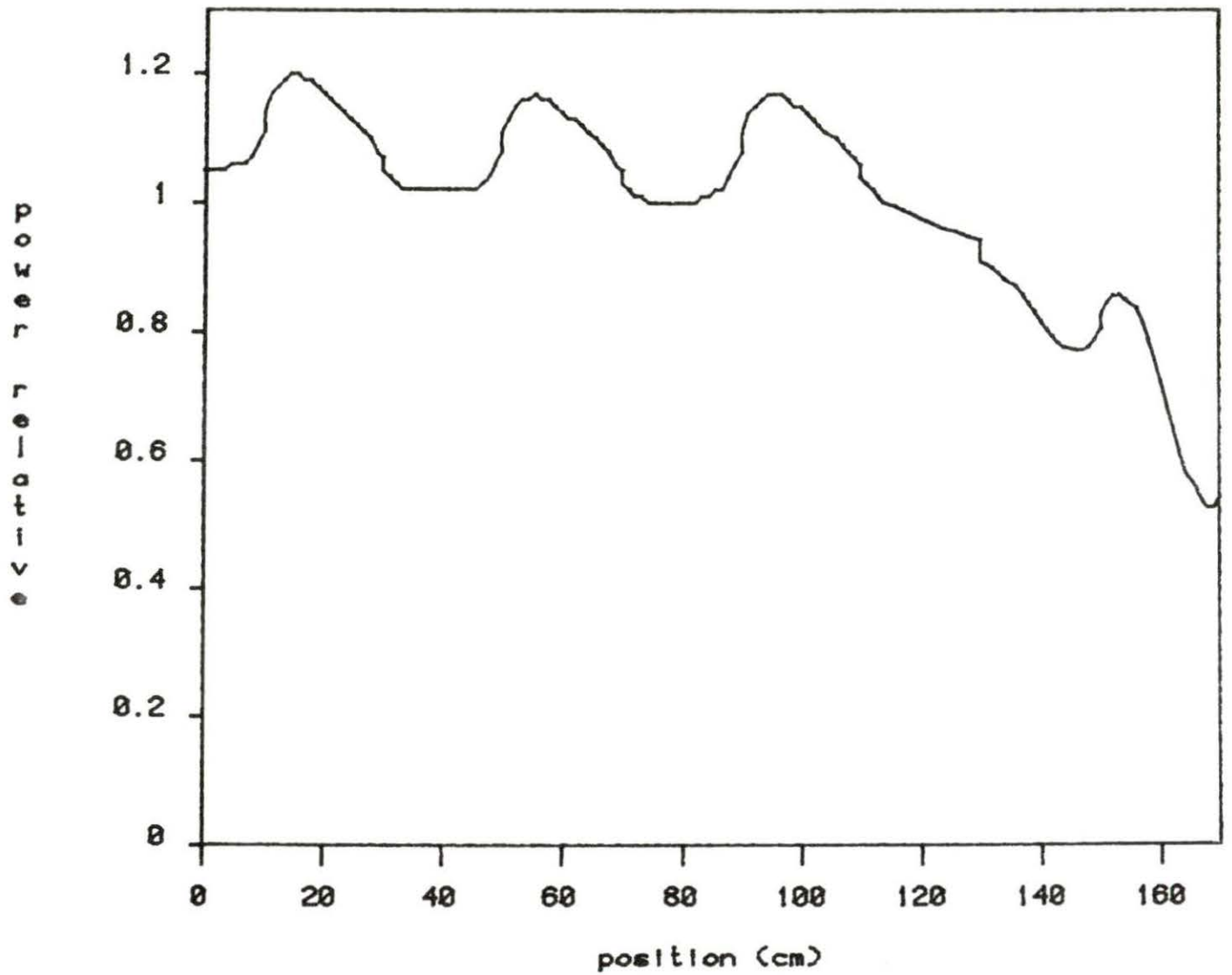

Figure 5-40. The power distribution at BOSC for reloading pattern D

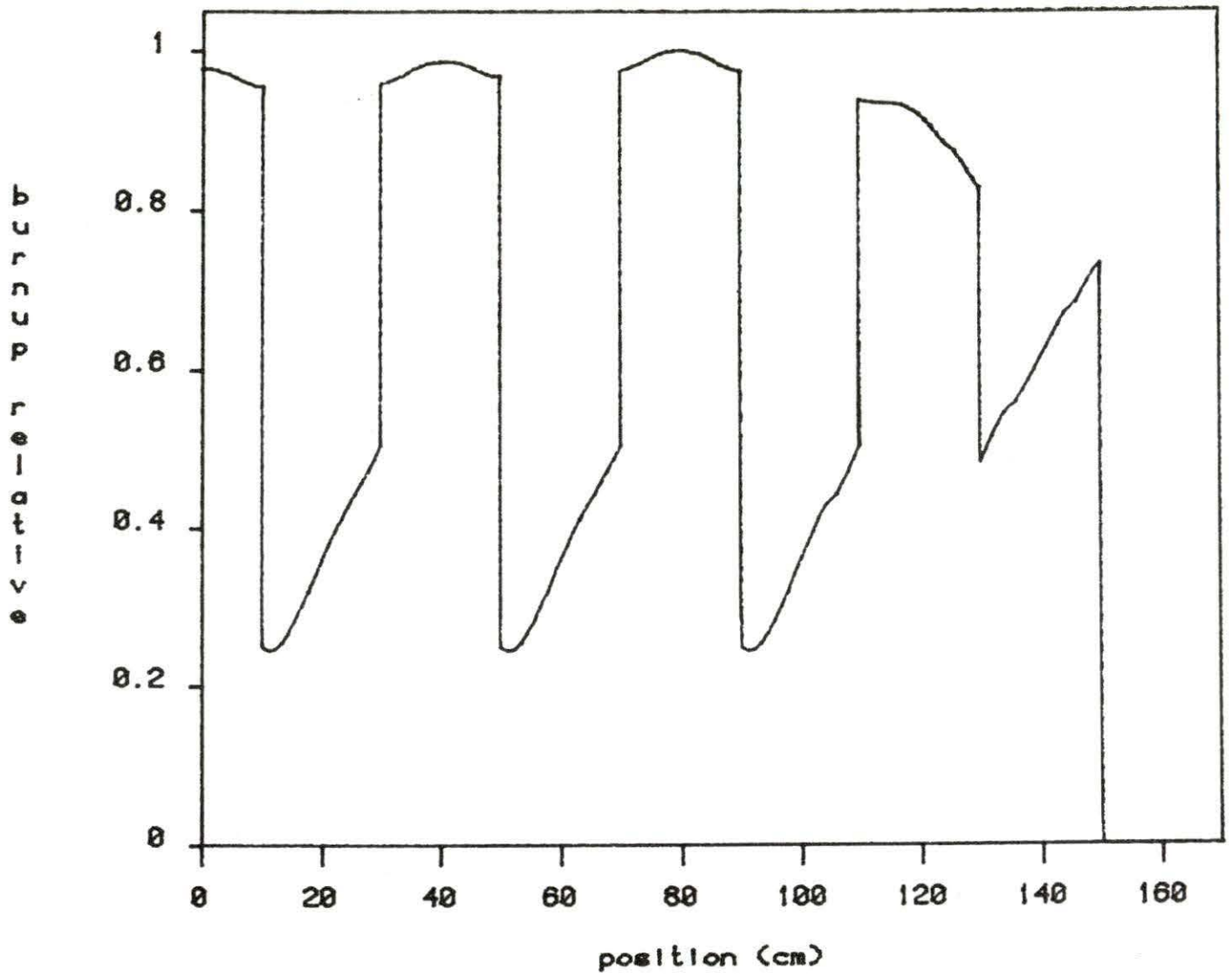

Figure 5-41. The burnup distribution at BOSC for reloading pattern D

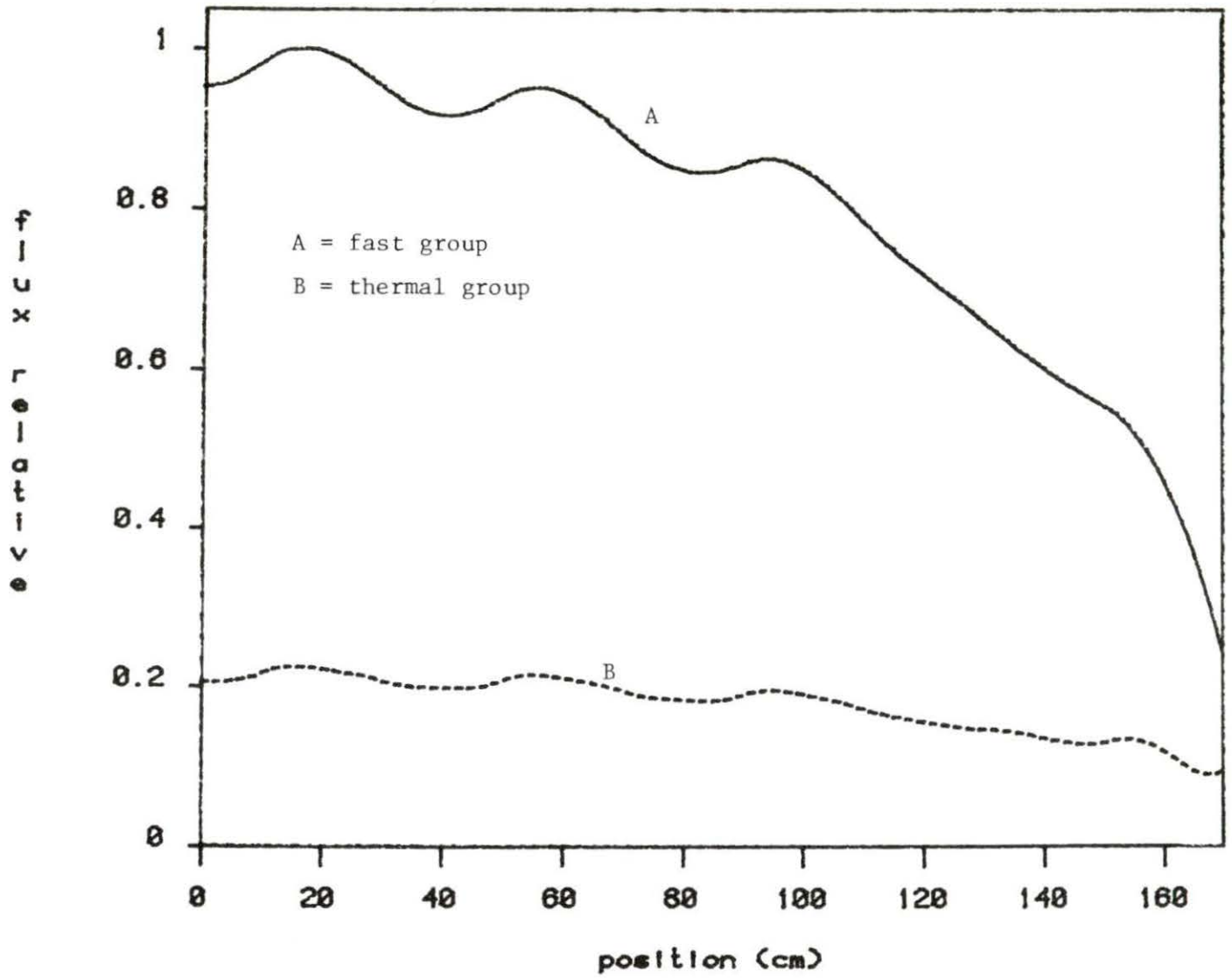

Figure 5-42. The flux distribution at EOSC for reloading pattern D

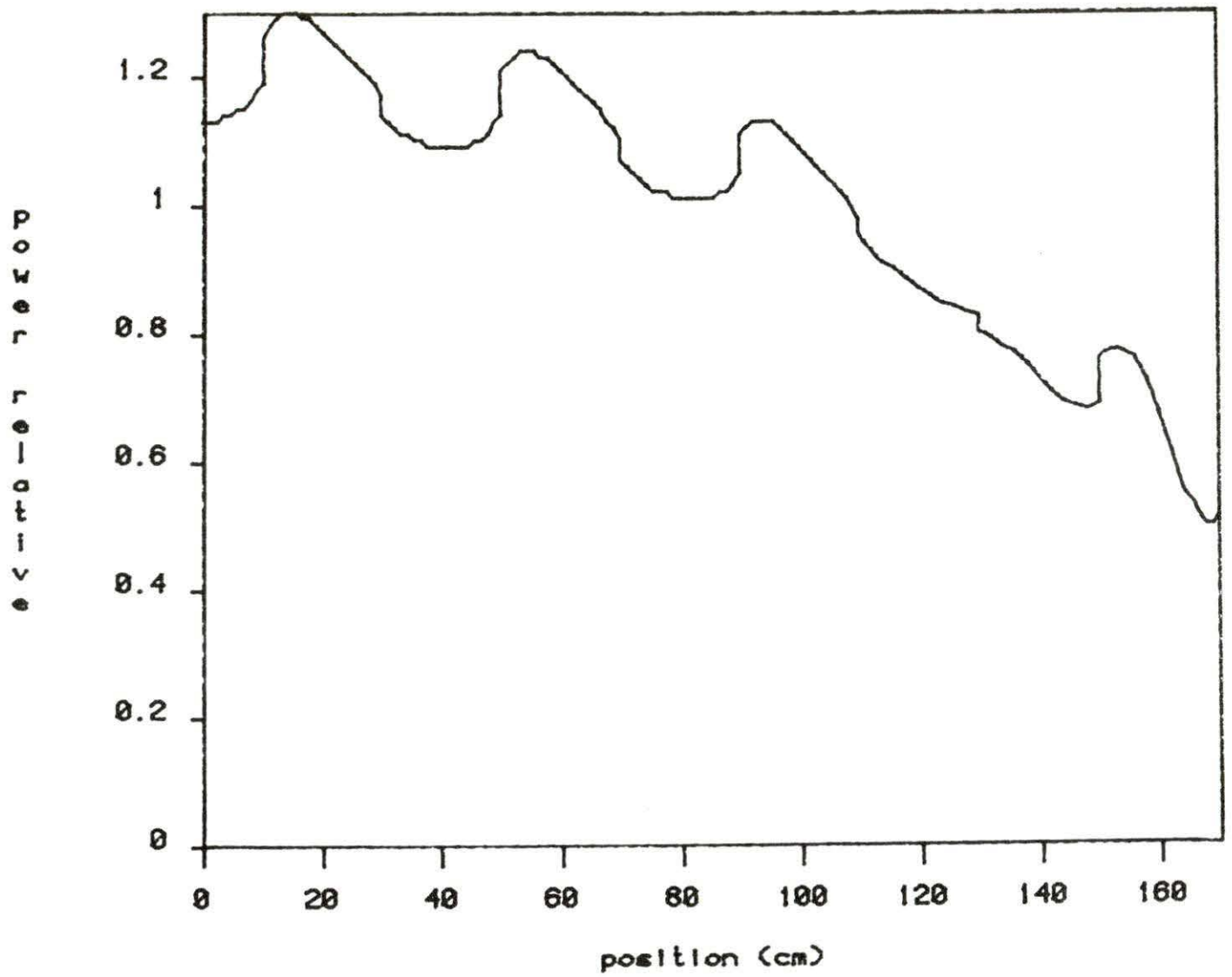

Figure 5-43. The power distribution at EOSC for reloading pattern D

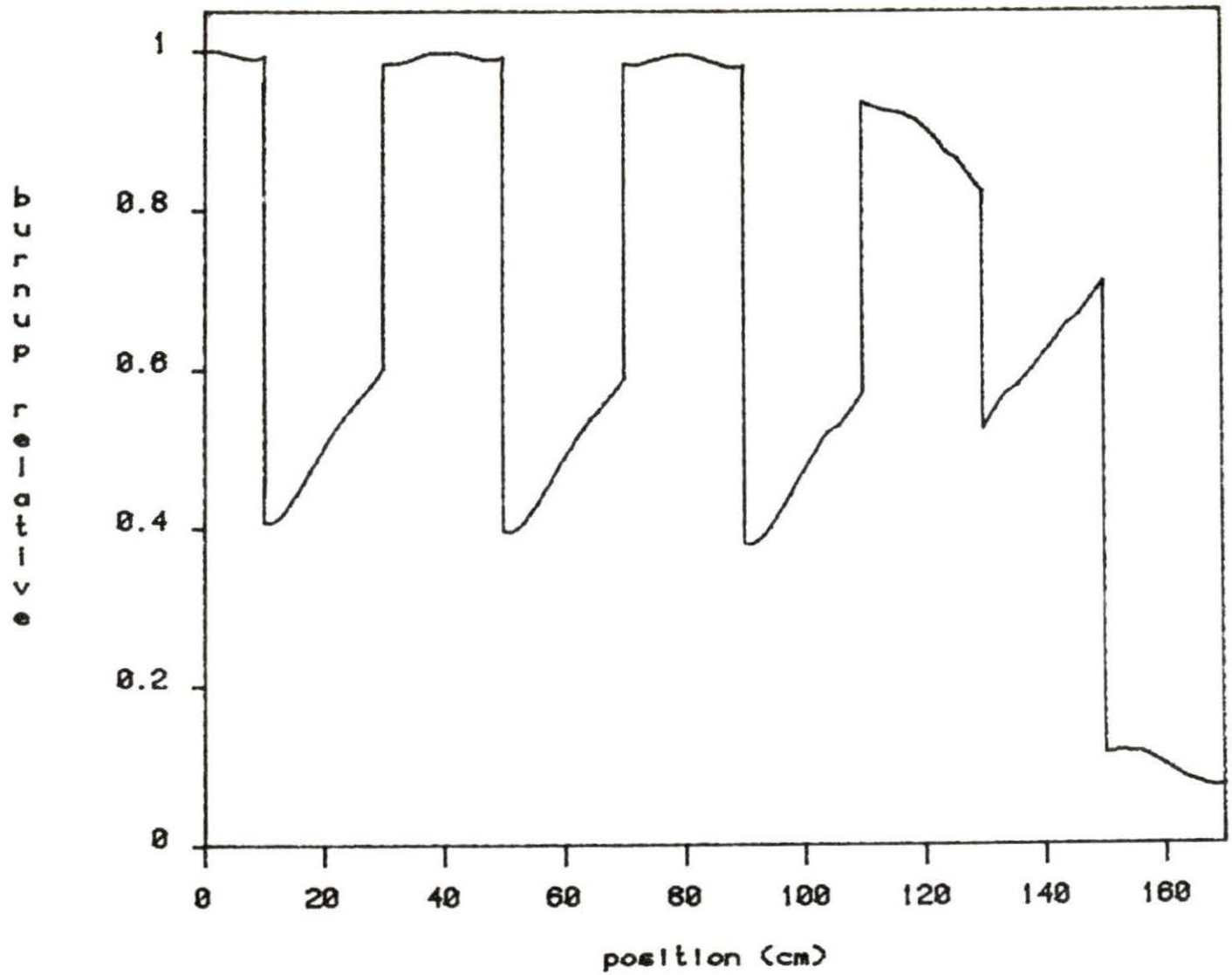

Figure 5-44. The burnup distribution at EOSC for reloading pattern D

at EOSC. The burnup of the rotated fuel does not give a significant improvement. The reason is that the burnup is not large enough during this short life core. If the life of the core was long enough, the burnup of the rotated fuels will become more uniform than before.

Comparing the power distribution between Figures 5-37 and 5-43, one can also note that the rotated fuel affects the power distribution. Thus, one can use this concept to get a more flattened power distribution in a core.

CONCLUSION AND FURTHER STUDIES

The purpose of this research was to develop and test a one-dimensional finite element nodal model for nuclear fuel management by considering the power and burnup of the reactor core. The main idea was to assume that the group parameters are known at five conditions over an assembly and then can be approximated by a polynomial. These five conditions were evaluated for the parameters at the left boundary, center point and right boundary as well as the average parameters over the left half side and right half side of a given node. The power density and burnup were also approximated by polynomials and evaluated by using the known group parameters and fluxes at the five conditions over an assembly for a given time T. Thus, by applying the finite element nodal model and adjusting the critical boron concentration, the power density and burnup were obtained.

For a one-dimensional nuclear fuel management calculation, the method was shown to give acceptable results:

1. When the convergence was in criticality, the flux and power distributions are almost the same as that from a fine mesh calculation.
2. The flux, power and burnup distribution at a certain time can be evaluated by adjustment of the boron concentration window PPM_w. Thus, the above distributions throughout the life of the core can be known. This is very useful for reactor operation.

3. The critical boron concentration as a function of time after startup can be evaluated. Thus, the life of a core is known.
4. The diffusion coefficient can be assumed constant over each node to simplify the neutron diffusion calculations.
5. The K_{∞} of each fuel at EOC can be obtained and used as a reference for a reloading plan.
6. Although the burnup of the rotated fuel does not show any obvious improvement, the concept can be used for further studies.

The theory of this method has not been completely developed for practical use. The recommendations for further studies are as follows:

1. The development of an analytical model for nuclear fuel management is a difficult task because of the large number of variables involved. A one-dimensional model is not enough for practical use. Two- and three-dimensional models should be developed.
2. The convergence rate of flux is slower than that of the source. An accelerated flux convergent technique needs to be developed in order to save computer (CPU) time.
3. Several variables affect a loading plan, e.g. fuel enrichment, the arrangement of the fresh and partially-spent fuels in the core, the fuel cycle length, etc. These variables should be considered in order to get an optimum loading pattern.

VII. REFERENCES

1. Masoud Feiz. "Application of finite element nodal model to multigroup diffusion theory." M.S. Thesis, Iowa State University, Ames, IA, 1983.

2. Harvey W. Graves, Jr. Nuclear Fuel Management. New York: John Wiley and Sons, Inc., 1979.

3. J. J. Duderstadt and L. J. Hamilton. Nuclear Reactor Analysis. New York: John Wiley and Sons, Inc., 1976.

4. Richard L. Burden, J. Douglas Faines and Albert C. Reynolds. Numerical Analysis. Boston: Prindle, Weber & Schmidt, 1978.

5. J. R. Lamarsh. Nuclear Reactor Theory. New York: Addison-Wesley Publishing Company, 1966.

6. H. J. French, A. F. Rohach, C. W. Gahel, W. Stevens and S. P. Wu. "Advanced in-core fuel management optimization methodology for PWRs." Final Research Project RP 1251-1, Electric Power Research Institute, January 1980.

7. A. F. Rohach. Lecture notes for Nuc E 654, Department of Nuclear Engineering, Iowa State University, Ames, IA, 1982.

8. A. F. Rohach. Private communication. Department of Nuclear Engineering, Iowa State University, Ames, IA, 1982.

9. A. F. Rohach. Lecture notes for Nuc E 532, Department of Nuclear Engineering, Iowa State University, Ames, IA, 1983.

VIII. ACKNOWLEDGMENTS

I wish to express my sincere appreciation to Dr. Alfred F. Rohach, my major professor, who provided the freedom, support and suggestions which I needed to complete this research.

I wish to thank all my fellow degree candidates in the Nuclear Engineering Department for their helpful suggestions and discussions, especially Mr. Masoud Feiz and Mr. Mohammed Benghanem.

I express special thanks to the Nuclear Engineering Department for providing the financial assistance, to John Hugg for editing the English in the thesis and to Barbara Dubberke for typing this thesis.

Finally, I wish to express my deepest gratitude to my parents and family for their support and encouragement during my pursuit of this degree.